1995

Macro- and microstructural characterization of organosulfur monolayers adsorbed at gold

Brian Dean Lamp
Iowa State University

INFORMATION TO USERS

This manuscript has been reproduced from the microfilm master. UMI films the text directly from the original or copy submitted. Thus, some thesis and dissertation copies are in typewriter face, while others may be from any type of computer printer.

The quality of this reproduction is dependent upon the quality of the copy submitted. Broken or indistinct print, colored or poor quality illustrations and photographs, print bleedthrough, substandard margins, and improper alignment can adversely affect reproduction.

In the unlikely event that the author did not send UMI a complete manuscript and there are missing pages, these will be noted. Also, if unauthorized copyright material had to be removed, a note will indicate the deletion.

Oversize materials (e.g., maps, drawings, charts) are reproduced by sectioning the original, beginning at the upper left-hand corner and continuing from left to right in equal sections with small overlaps. Each original is also photographed in one exposure and is included in reduced form at the back of the book.

Photographs included in the original manuscript have been reproduced xerographically in this copy. Higher quality 6" x 9" black and white photographic prints are available for any photographs or illustrations appearing in this copy for an additional charge. Contact UMI directly to order.

UMI

A Bell & Howell Information Company
300 North Zeeb Road, Ann Arbor, MI 48106-1346 USA
313/761-4700 800/521-0600

Macro- and microstructural characterization of organosulfur monolayers adsorbed at gold

by

Brian Dean Lamp

A Dissertation Submitted to the

Graduate Faculty in Partial Fulfillment of the

Requirements for the Degree of

DOCTOR OF PHILOSOPHY

Department: Chemistry
Major: Analytical Chemistry

Approved:

Signature was redacted for privacy.

In Charge of Major Work

Signature was redacted for privacy.

For the Major Department

Signature was redacted for privacy.

For the Graduate College

Iowa State University
Ames, Iowa

1995

DEDICATION

This dissertation is dedicated to my parents, Roger and Beverly Lamp, whose love, guidance, and support throughout my life has been invaluable in allowing me to reach this milestone.

This dissertation is also dedicated to the memory of my sister Tracey (1963-1993). Her memory serves as an inspiration in all that I do. Although I would trade all my achievements to bring her back, I can only be sure she is looking on with pride and awaiting the day when we meet again.

TABLE OF CONTENTS

ACKNOWLEDGMENTS v

1. GENERAL INTRODUCTION 1

History 2

Preparation and Characterization 4

Applications 11

Unresolved Issues 18

Dissertation Organization 20

References 21

2. SPONTANEOUSLY ADSORBED MONOLAYERS OF DIALKYL DISULFIDES AND ALKANETHIOLS AT Au(111): STRUCTURAL COMPARISONS BASED ON MACRO- AND MICRO-SCOPIC CHARACTERIZATIONS **27**

Abstract 27

Introduction 28

Experimental 32

Results and Discussion 36

Conclusions 58

References 59

3. AN IN SITU INFRARED SPECTROSCOPIC EXAMINATION OF STRUCTURAL CHANGES AT ALKANETHIOLATE-MODIFIED GOLD ELECTRODES AT DESORPTION POTENTIALS **62**

Introduction 62

Experimental 65

Results and Discussion. 68

Conclusions 78

References 79

4. ELECTROCHEMICAL INVESTIGATIONS OF ADSORPTION AND DESORPTION OF ALKANETHIOLATES AT STEP AND TERRACE SITES ON Au(111) 81

Introduction 81

Experimental 83

Results and Discussion 86

Conclusions 103

References 104

5. CORRELATION OF STRUCTURE AND PERFORMANCE OF PYRIDINETHIOLATE SURFACE MODIFIERS FOR THE FACILITATION OF CYTOCHROME c HETEROGENEOUS ELECTRON-TRANSFER 106

Introduction 106

Experimental 107

Results and Discussion 109

Conclusions 131

Acknowledgments 131

References 133

6. GENERAL CONCLUSIONS 136

ACKNOWLEDGMENTS

I would like to express my gratitude to my major professor, Marc Porter. His enthusiasm for science, and strong support for everyone in his group serve as fine examples for me to strive for. I am grateful for his friendship, guidance and for the many opportunities I have been given during my tenure in the group. I look forward to continuing our friendship in the years to come. To Marc, I can only say one thing...all day long.

I also wish to thank the many friends we've made during our stay in Ames. To all past and present Porter group members, too numerous to mention individually, you have been my second family and I am forever grateful for having the opportunity to know each and every one of you. I wish you all the best and hope that we continue to maintain contact. Special appreciation goes to Scott and Pam Clemons. I don't believe we made it!

Above all, my deepest thanks go to my wife and best friend Amy, and my children Jacob and Nathan (and any others yet to come). Amy's love and support throughout my graduate study has made the difficult times bearable, and the good times better. This dissertation is as much hers as it is mine. To my children, thank you for not really caring whether experiments work or papers are published. You are my anchor to reality. Every day you show me what is truly important in life, I hope you never let me forget.

I would also like to gratefully acknowledge the receipt of a chemistry department FYRST award as well as Noble-Hines and PACE fellowships. This work was conducted at Ames Laboratory under contract no. W-7405-eng-82 with the U. S. Department of Energy. The United States Government has assigned report number IS-T 1760 to this dissertation.

1. GENERAL INTRODUCTION

The tailoring and characterization of chemical interfaces has, in recent years, become an ever growing discipline in analytical chemistry, and chemistry in general. Since the early experiments involving the chemical modification of electrode surfaces [1, 2], effort has focused on the design and function of the electrode itself, as well as the effect on the electrode/electrolyte interface [3-6]. At the center of these explorations are studies that investigate the utility of these tailored interfaces in unraveling information regarding electrochemical reaction kinetics and mechanisms, chemical sensors, as well as the development of techniques which allow characterization of interfacial systems.

As the field has evolved, much emphasis has been put toward the modification of electrodes with thin, structurally robust materials. Most recently, the utility of covalently attached monomolecular films has begun to be exploited in this arena. Their stability, structural coherence, and relative ease of preparation makes these films a promising vein of study [7, 8].

Our group has been interested in the modification of electrode surfaces by the spontaneous adsorption of monolayer films of sulfur-derivatized organic compounds. These systems have become very popular models for the design of tailored interfaces. Primary emphasis in our group has been on the fundamental characterization of these types of materials with interest in both macro- and micro-structural features. Such investigations are

crucial to the implementation of these materials in model systems as well as in analytical applications.

The following section presents a brief review of the literature related to these systems as well as a summary of the current state of understanding of these types of materials. It is divided into three subsections. The first subsection presents a brief look at the landmark studies in the development of sulfur-based monolayer films. A second subsection summarizes the body of characterization data that has been collected. The final subsection describes examples of the efforts to apply these types of systems to several different areas. This introductory chapter is intended to provide a sample of the literature relating to sulfur-based monolayers and is not an exhaustive review.

History

The earliest application in analytical chemistry of sulfur-derivatized layers was in the study of the electron transfer of cytochrome *c* (cyt *c*) at gold electrodes [9-11]. These studies indicated that while electron transfer of cyt *c* is essentially irreversible at bare electrodes, electrodes which were exposed to a solution of 4,4' dipyridyl disulfide exhibited a much more ideal voltammetric response. This observation was attributed to the conditioning of the surface by the disulfide modifier, thus preventing the irreversible unfolding of the protein which occurs at the bare electrode. While not strictly aimed at the covalent modification of electrode surfaces, these initial studies provided indications of the possible utility of organosulfur derivatized electrodes in analytical chemistry.

The immense interest in the modification of a gold surface by a sulfur containing material was triggered in 1983 by Nuzzo and Allara [12]. This communication presented results from the generation and characterization of monomolecular films spontaneously adsorbed from cyclic disulfides at freshly prepared gold electrodes. Characterization by ellipsometry, contact angles, radioisotope labeling, and infrared spectroscopy indicated that these compounds formed stable, monomolecular films at the gold surface, apparently by dissociation of the sulfur-sulfur bond. These data provided the initial evidence into the facility and stability of sulfur derived monomolecular films.

The first report of formation and characterization of monolayers from long-chain alkanethiols at gold electrodes was in 1987. In this study, monolayers were adsorbed from solutions of n-alkyl thiols ($CH_3(CH_2)_nSH$, n = 1, 3, 5, 7, 9, 11, 15, 17, 21) onto evaporated gold electrodes. The resulting films were characterized by ellipsometry, infrared spectroscopy, and electrochemistry. Results indicated that the films formed were monomolecular, comparatively well ordered, and possessed favorable barrier properties to electroactive probe molecules and ions. The combined results of this study, while presenting important characterization data, also presented definitive evidence for the utility of alkanethiolate monolayers as model systems for the study of interfacial processes [13]. A concurrent report examining monolayers formed from octadecanethiol (n = 17) confirmed these assertions [14].

Since these initial landmark endeavors, a host of studies involving the characterization and application of sulfur derivatized monolayer films have been undertaken. The following sections present a brief summary of these studies.

Preparation and Characterization

Sulfur-based monolayer films are typically formed by the immersion of a noble metal (Au, Ag, Pt, Cu) electrode into a dilute (mM) solution of the adsorbate precursor. Although the bulk of the data in the literature presents results from films based on thiol precursors, similar structures form from immersion in solutions of disulfides [9, 11, 12, 15-19] and sulfides [20-22]. Spontaneous adsorption [12] results in the formation of a densely packed monolayer of alkanethiolates, covalently attached to the metal surface *via* cleavage of the S-H, S-S, or S-C bond and formation a metal-sulfur bond, as shown in Scheme 1. The resulting assemblies have been extensively characterized in terms of tail group and chain structure as well as head group chemistry.

$$\begin{matrix} \text{RSH} \\ \text{RSSR} + \text{Au(0)} \rightarrow \text{RSAu} + ? \\ \text{RSR} \end{matrix} \qquad (1)$$

While spontaneous adsorption of alkanethiolates occurs at several noble metals, gold has become the electrode of choice in the study of alkanethiolate films. Gold provides several practical advantages over other noble metals in that it is relatively inert to most

common contaminants, does not readily form a passivating native oxide layer, and does not require elaborate pretreatment methods. The bulk of the present information regarding thiolate monolayers has been gleaned from studies undertaken using gold films that have been evaporated onto silicon, glass, or mica substrates. Evaporated electrodes provide the advantage of a source of reproducible, relatively microscopically smooth substrates which are desirable for these types of fundamental studies. The surface microstructure of evaporated gold films indicates that they are comprised of predominantly Au(111) terraces separated by atomic steps and grain boundaries. The exact surface morphology depends strongly on the substrate and preparation conditions of the electrode itself [23-26]. Given the popularity of gold substrates in the study of alkanethiolate monolayers, the following summary of the characterization data will be concerned primarily with the data collected at these surfaces, examples at other metal electrodes will be included where appropriate.

Several aspects of the monolayer film provide interesting experimental information. Figure 1.1 presents an idealized representation of the electrode/monolayer/solution interface (or monolayer/air in the case of ex situ experiments). For illustrative purposes, the figure divides the monolayer structure into three portions and lists some of the techniques which have been used to probe each region. The three portions are: (1) the interfacial region which consists of the outermost portion of the film as well as any adjacent solution layer; (2) the underlying alkyl chain structure; and (3) the head group region including all aspects of the adsorbate binding chemistry.

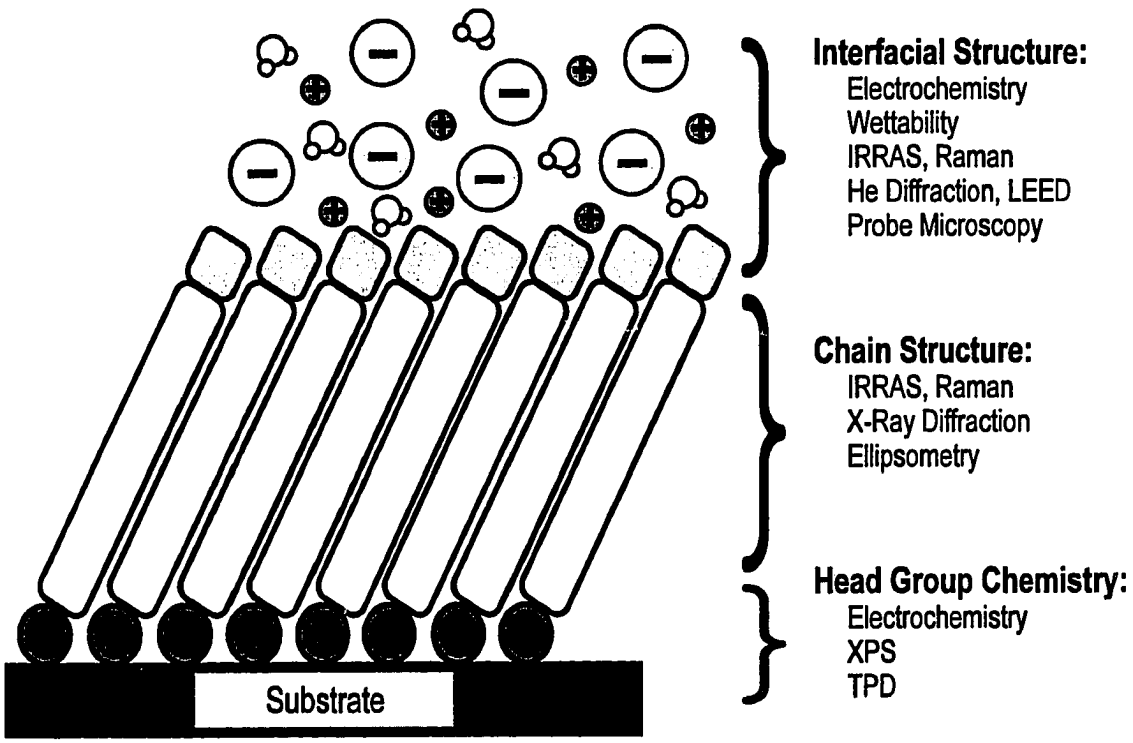

Figure 1.1. Idealized representation of the metal/monolayer/solution interface. Hydration spheres for ions have been omitted for clarity.

A host of characterization methods have been utilized to determine the structure and stability of alkanethiolate monolayers. The earliest studies were concerned primarily with the characterization of the outermost portions of the monolayer structure, primarily in the structure of the alkyl chains and the effect of chain length and terminal group on the barrier properties of the monolayer assembly. Infrared reflection absorption spectroscopy (IRRAS) and ellipsometric thickness measurements indicate that the alkane chains adopt an orientation in which the bulk of the carbon-carbon bonds are in an all trans-configuration. This configuration, combined with maximizing Van der Waals interactions causes the chains to be tilted on the order of 30° from the surface normal [13]. A rigorous examination of the infrared data also provides indications of a twist of ~ 50° about the chain axis for long chain alkanethiolate monolayers [27]. Further experiments with Raman spectroscopy [28], as well as x-ray diffraction [29], corroborate the general features of these descriptions.

Wetting studies [30], as well as IRRAS and helium diffraction data [31-33], also provide information concerning the structure and packing of the terminal functional groups in the monolayer structure. For the methyl-terminated films, a clear dependence is observed for the methyl modes in the IRRAS spectrum depending on whether the number of methylene units in the alkane chain, n, is odd or even [27, 34]. This dependence has been related to the alteration in orientation of the methyl group which results from conservation of the Au-S-C bond angle and the predominantly all trans-chain conformation for all chain lengths. The combination of these two factors causes an oscillation in the orientation of the methyl group

in which, for example, the transition dipole of the symmetric methyl vibration is oriented more normal to the surface when n is odd versus when n is even. Further evidence for this interpretation derives from an investigation of alkanethiolates adsorbed at silver electrodes, where the tilt angle for the polymethylene chain is on the order of 12°, causing the magnitude of the odd-even effect to be somewhat damped. Variation in the carbon-sulfur-metal binding geometry also results in the odd-even effect to be shifted one carbon out of phase [34, 35]

The strength and character of the Au-S bond in these systems is also of great interest. X-ray photoelectron spectroscopic (XPS) investigations indicate that the thiols adsorb as alkanethiolates, apparently by cleavage of the sulfur-hydrogen bond in the thiol precursor. The spectra show the presence of sulfur $2p_{1/2}$ and $2p_{3/2}$ peaks at 163.2 eV and 162.0 eV, respectively, consistent with the positions of sulfur in a thiolate [15-17, 22].

Monolayer coverage, as well as the relative strength of the Au-S bond has also been investigated electrochemically. Application of a cathodic voltage sweep to a thiolate coated electrode exposed to basic aqueous solution results in the cathodic desorption of the intact thiolate [36-38]. The charge consumed during this process can be related to the surface coverage of adsorbates, given the electron stoichiometry of the reaction. Assuming a one electron process, the charge consumed during the desorption of alkanethiolates adsorbed at Au/mica corresponds to a coverage of 9.3×10^{-10} mol/cm^2 [36]. This coverage correlates well with the 7.6×10^{-10} mol/cm^2 coverage predicted from the $(\sqrt{3} \times \sqrt{3})R30°$ adlayer structure determined for these systems (see below) as well as that expected from models based on the other characterization data [39]. The reverse of this desorption process has also

been shown to be a viable method to control the degree of monolayer formation at these electrode surfaces [40].

The microscopic orientation of alkanethiolates at gold has been studied extensively using scanning tunneling (STM) [41, 42] and atomic force microscopies (AFM) [43, 44] as well as with electron diffraction techniques [45-48]. All techniques provide evidence that the long-chain alkanethiolates adopt a predominantly ($\sqrt{3}$ x $\sqrt{3}$)R30° structure at the Au(111) surface in which the sulfur atoms occupy similar adsorption sites, resulting in a sulfur-sulfur nearest neighbor separation distance of 5.0 Å, as shown in Figure 1.2. Consensus is that sulfur resides in the threefold hollow sites on the Au(111) surface. Although awaiting experimental verification, these sites have been predicted to be the most energetically stable of the terrace adsorption sites [49, 50].

Recent studies have also found evidence for a number of other structures, depending on chain length and sample handling method. Some of these structures include: a highly ordered c(4 x 2) superlattice based on the ($\sqrt{3}$ x $\sqrt{3}$) basic structure [51, 52], as well as liquid-like and p x $\sqrt{3}$ phases for short ($n<10$) chain monolayers [53].

A major focus of several recent studies has been the investigation of atomic scale "defects" frequently observed in STM images of most alkanethiolate monolayers. These defects manifest themselves as ~0.23 nm deep depressions in the alkanethiolate structure at the gold terrace. Several groups have examined these structures in detail and have arrived at several explanations regarding their origin, including: defects in the monolayer structure itself, electronic perturbations which result from imaging, or defects in the underlying gold

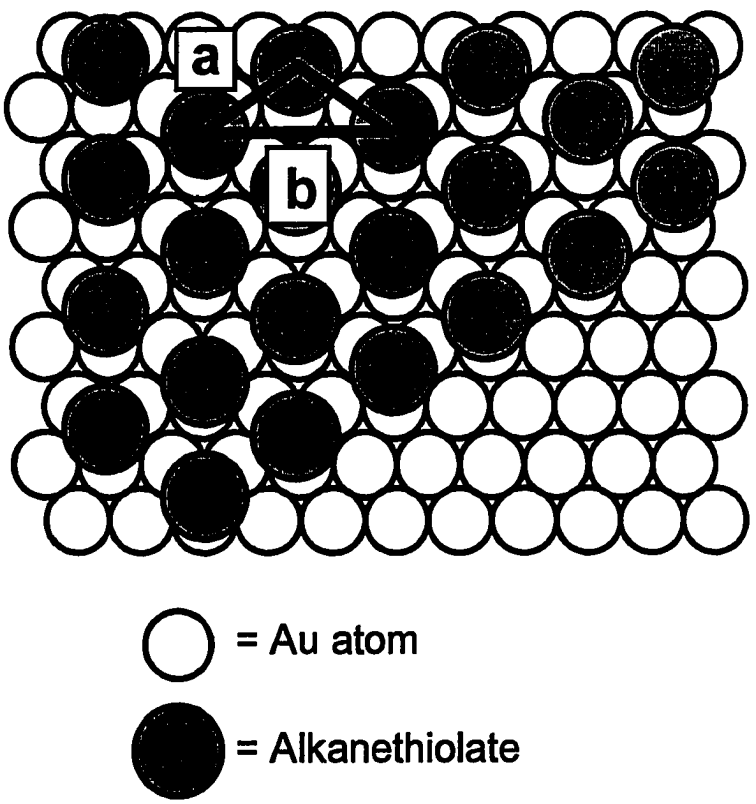

Figure 1.2. Adsorbate structure for alkanethiolate monolayers adsorbed at Au(111). a. nearest neighbor spacing = 5.0 Å, b. next-nearest neighbor spacing = 8.7 Å. Alkyl chains have been omitted for clarity

structure [52-59]. The most plausible to date attributes the depressions to vacancies in the uppermost gold layer which result from an adsorbate driven reconstruction of the gold surface [60]. This assertion is supported by the first observation of these defects by AFM as well as by the observed annealing of the smaller pits due to gold migration and increased ordering in a short chain monolayer [61].

The success of these characterization methodologies has begun to allow the investigation of more complicated monolayer structures. For instance, monolayers containing several adjacent aromatic groups have been successfully characterized, indicating that these precursors also form well ordered monolayer film which behave as substantial barriers to electron-transfer [62]. In another interesting study, monolayer films containing [*n*]staffane rigid rods containing [1,1,1] bicyclopentane spacer units were successfully prepared and characterized for use in electron transfer studies [63].

Applications

Spontaneously adsorbed thiolate monolayers hold promise for applications in an array of settings, ranging from fundamental studies of the properties of interfaces to implementation as chemical sensors. The following section presents a summary of some of these applications.

Electron transfer studies

As previously mentioned, perhaps the earliest use of thiolate monolayer films was in the study of electron transfer of the heme-containing protein cytochrome *c* [9-11]. In this application, pyridine thiolate monolayers were used to condition the electrode surface such that facilitated the electrode reaction of the cytochrome *c*. As speculated, this conditioning prevented the irreversible unfolding or denaturing of the protein which occurs at a bare metal electrode. The result was easily observable, essentially reversible electron transfer for the redox protein. Similar results have been observed when an acid terminated alkanethiolate monolayer is used in place of the pyridinethiolate film [64-66].

The bulk of the interest in electrochemical applications of thiolate monolayers relates to studies of the fundamentals of electron transfer across an interface. The well defined structure of alkanethiolate films makes them ideal model systems for studies of the effects of such things as interfacial structure, separation distance, and overpotential on the kinetics of long-range electron transfer.

The first work presenting the possibilities for utilizing alkanethiolate-based monolayers as models for these types of studies employed a monolayer of a ferrocene-terminated alkanethiolate [67, 68]. With appropriate dilution using shorter chain methyl-terminated alkanethiols, the ferrocene moieties behaved as kinetically homogeneous electron transfer sites. With these conditions, it was possible to measure the forward and reverse rate constants over a wide range of potentials and thus determine the reorganizational energy and electron tunneling parameters for the system.

Similar studies have utilized various other combinations of electroacitve terminal groups and chain lengths to further test these systems. A electroactive thiol with a pendant ruthenium pentamine group has been shown to behave less ideally [69]. This system [70], as well as the ferrocene terminated system [71] have also been used to examine the temperature and electrolyte effects on the electron transfer of the pendant group. Other studies have focused on the effect of chain length of the diluent alkanethiol [72,73], temperature [74] and solvent and double layer effects [75-77] on the formation and behavior of electroactive assemblies.

Electroactive monolayers have also been employed as models for the characterization of the potential distribution across a dielectric film [78, 79]. These models have been used to describe the dependence of the voltammetry of such electroactive films on the thickness of the underlying monolayer film, as well as the separation distance between adjacent electroactive moieties.

Sensors

Toward the goal of the utilization of thiolate monolayers in sensor systems, a great deal of effort has been focused on the investigation of structure-reactivity relationships in monolayer films. These studies have focused on problems which attempt to correlate bulk properties and reactivity with those at the monolayer interface, as well as specific interactions between adsorbates and solution and gas phase probe molecules. For example, the surface pK_a of single [80, 81] and multicomponent monolayers [82] has been measured, with

particular interest in its potential and chain length dependence as well as its relation representative bulk values provide background for surface derivatization and sensor transduction studies.

Other studies have focused on the surface reactivity of several monolayer systems in terms of electrostatic binding interactions between the monolayer film and charged probe molecules. For instance, one study examined the interaction of poly-L-lysine (PL) with an adsorbed monolayer of 11-mercaptoundecanoic acid (MUA). At 6.5<pH<12, the ammonium moieties in the PL can form ion pairs with the carboxylic acid functionaities at the electrode surface [83]. Structural characterization of the resulting bilayer system indicates that the lysine chains adsorb onto the MUA surface in an extended fashion. There remain, however, free lysine sites which afford the binding of a third layer consisting of an iron phthalocyanine. The presence of exposed and reactive lysine sites suggests the possible implementation of a MUA-PL based sensor.

Another study has examined the pH dependence on the adsorption and electrochemical response of anthraquinone-based adsorbates interacting with monolayers formed from isomers of mercaptopyridine [84]. The results indicate that the structure of both the adsorbate and the monolayer film play crucial roles in the adsorption process. Monolayer films where the pH dependent component of the monolayer structure is readily exposed to the adsorbate provide the strongest retention of adsorbates in all cases.

The ability to alter monolayer composition and reactivity after adsorption provides a host of interesting possibilities in terms of sensor design and construction. The initial

investigation of monolayer reactivity involved the conversion of an acid terminated monolayer to a corresponding amide or ester [85]. After initial assembly from dilute solution of 11-mercaptoundecanoic acid (MUA), the MUA monolayer was exposed briefly to gaseous thionyl chloride to convert the acid functionality to the corresponding acid chloride. Upon conversion, further reaction with gas phase primary amines or alcohols resulted in conversion to the corresponding amide or ester. Infrared and X-ray photoelectron spectroscopic analysis confirmed the reaction.

Comparable investigations have been conducted for vapor phase adsorbed monolayers. In an extensive study, the interactions between monolayer sample and gas-phase probes has been examined. These experiments have been concerned with hydrogen bonding interactions [86], acid-base interactions [87], reactivity [88], and film structure [89] of thiolate monolayers adsorbed from the gas phase and interacting with gas phase probes.

One direct attempt at application of thiolate based films in sensor design involves the construction of a pH microsensor consisting of two terminals, a sensor electrode coated with a two component electroactive thiolate monolayer, and a large counter electrode [90]. The sensor electrode is coated with a mixed monolayer of a hydroquinone terminated thiol (HQ) and ferrocene terminated thiol (FC). Solution pH is determined by comparison of the voltammetrically determined formal reduction potential, $E^{o\prime}$, for the pH dependent hydroquinone redox couple (E_{HQ}) with the $E^{o\prime}$ for the pH independent ferrocene couple (E_{FC}). In this proof-of-concept experiment, the correlation of the E_{HQ} - E_{FC} with pH presents a viable method for pH sensing, independent of external reference electrodes.

Microfabrication

Given their relative stability and inherently small dimensions in terms of both thickness and lateral size, thiolate monolayer films are ideal prospects for utilization in the fabrication of micro- and nanoscopically small architectures. The bulk of such experiments to date have been concerned with the preparation and characterization of microscopically small structures using lithographic techniques which result in micron-sized structures. A popular method for the creation of patterned surfaces involves the irradiation of a masked substrate with UV light which results in conversion the exposed chemisorbed alkanethiolates to weakly physisorbed alkanesulfonates. The resulting sulfonates can be removed by rinsing the electrode in ethanol, and replaced by immersion of the electrode into a solution of a second thiol precursor. Secondary ion mass spectrometric (SIMS) and XPS data were used to validate the conversion and removal of the alkanesulfonates. Features on the order of 20 μm were readily observable in the SIMS imaging [91]. An analog of this photolithographic method has been successfully used to create patterns with alkanethiolate monolayers having photoreactive end group, achieving resolution on the order of 200 nm, as observed with lateral force microscopy (LFM) [92].

A second method of pattern formation on monolayer surfaces is microcontact printing (μCP) which involves the use of a thiolated stamp which generates the patterned surface [93, 94]. With μCP, an elastomeric stamp is formed which contains the pattern of interest, this mask is then wetted with alkanethiol and brought into contact with the gold electrode. Upon

contact, local regions of monolayer are formed where the stamp contacted the bare gold electrode. Upon removal, the electrode is then briefly immersed in a solution of a second thiol to coat the remainder of the electrode, rinsed, and dried. The resulting patterned surfaces have resolution on the order of 1 μm, as observed by AFM and lateral force microscopy (LFM) [95]. A related technique, microwriting, involves the use of micron-sized "pen" filled with neat alkanethiolate which can be used to create micron-sized lines and structures on the electrode surface. Once the initial lines are drawn, samples are treated essentially as in μCP [96].

Yet another technique involves lithography of an alkanethiolate-coated electrode by etching with the tip of an STM. With this technique, structures can be created with dimensions ranging from 50 nm to 5.0 μm [97]. Refilling of the etched portions of the film *via* low temperature chemical vapor deposition of copper confirms the etching process and reinforces the reported resolution [98].

The highest lithographic resolution to date results from an adaptation of the STM-induced lithography. This method takes advantage of atomic force microscopy (AFM) to create patterns in bilayer or monolayer surfaces [99, 100]. In these studies, a large normal force applied to the AFM cantilever results in selective etching of the outer component of a bilayer [99] or selective hydrolysis of an ester [100]. The highest resolution reported is on the order of 10 nm.

In what may lead to the development of lithographically small structures with linewidths approaching that of single molecules, recent studies have examined the

polymerization of monomeric monolayer films [101-103]. These studies indicate that monolayers terminated with pyrrole functionalities can be electropolymerized, likely forming arrays of end-to end polymers. In addition, these pyrrole monolayer films can be used to enhance and control the deposition of bulk polypyrrole films on electrode surfaces. One could envision a case where a microelectrode such as an STM tip could result in the creation of extremely small polypyrrole structures which could have a large impact on techniques for microfabrication.

Unresolved Issues

Although a large volume of data has been gathered concerning spontaneously adsorbed thiolate monolayers, several issues still remain unsettled. While listed separately, studies into any of these issues will have direct impact and will provide useful information on many of the others. Common to all of the studies will continue to be the improvement and modification of existing techniques as well as development of new methods which provide the sensitivity required to unravel these important issues.

First, details on the influence of the identity of the adsorbate precursor on the structure and stability of the resulting monolayer have yet to be fully resolved. Special interest has been and will continue to be placed on the elucidation of processes which lead to defects in the monolayer film. One aspect of these studies will be the delineation of the various types of defect structures and their effect on the properties of the monolayer. An understanding of the mechanisms, as well as the driving forces for the formation of various

types of defect structures is crucial to the implementation of these materials in many analytical applications.

A second point of emphasis will continue to be on investigation of the factors which influence interactions between neighboring chains in the monolayer film. Apart from fundamental characterization and quantitation of these properties, several other avenues will likely continue to be explored. Such studies will include topics such as the role of interchain interactions in driving film nucleation and growth, as well as influence on possible phase segregation of multicomponent films which will likely be utilized in applications of these materials.

Aside from the role of the alkyl chains in monolayer formation, much remains to be understood regarding the binding chemistry of the head group at the metal surface. Of primary interest is the mechanism by which thiolate monolayers form and any reaction byproducts which result from formation. Further attempts will be aimed at elucidation of the preferred binding sites for the thiolate moieties at several crystal faces of the substrate electrode. Continued efforts will also investigate an dependencies on adsorbate structure and oxidation state on the resulting binding chemistry.

Additionally, most of the structural characterizations have been performed *ex-situ* or under reduced pressure. Since most applications of these types of films as sensors will require the introduction of the film into a solution or gas-phase sample matrix, an extensive set of *in situ* characterization data needs to be compiled. A data set of this type would allow for more judicious choice of materials for new sensor applications. Collection of this type of

data will require refinement in or adaptation of many typical existing in situ techniques to afford the sensitivity required to examine these films.

The work which comprises this dissertation is aimed at addressing some of the above issues. The following chapters are concerned with fundamental characterization of thiolate-based monomolecular films, with particular interest in examination of head group reactivity, as well as structural characterization. These studies seek to relate topics such as surface morphology, precursor identity, and applied potential to general monolayer structure and reactivity.

Dissertation Organization

The body of the dissertation is divided into four chapters. Chapter 2 consists of a paper which presents the results of a study which provides a comparison into the macro- and microscopic structure of monolayers assembled from *n*-alkanethiols and di-*n*-alkyldisulfides. Chapter 3 provides some preliminary results of a study of the in situ structural characterization of alkanethiolate monolayers near and beyond desorption potentials. Chapter 4 presents the an investigation of the thermodynamic and kinetic aspects of thiolate binding at the various adsorption sites present on gold electrodes which have been evaporated on glass substrates. Chapter 5 is a paper which describes the structure, coverage, and the interesting instability in monolayers formed from sulfur-derivatized pyridines and related compounds. Finally, a section is included which provides an overall summary and presents a prospectus for future studies.

References

1 . Lane, R. F.; Hubbard, A. T. *J. Phys. Chem.* **1973**, *77*, 1401-1410.

2 . Moses, P. R.; Wier, L.; Murray, R. W. *Anal. Chem.* **1975**, *47*, 1882-1886.

3 . Murray, R. W. In *Electroanalytical Chemistry, Vol. 13*; Bard, A. J., Ed.; Marcel Dekker: New York, 1984, and references therein.

4 . Murray, R. W.; Ewing, A. G.; Durst, R. A. *Anal. Chem.* **1987**, *59*, 379A-390A, and references therein.

5 . Bard, A. J.; Abruna, H. D.; Chidsey, C. E.; Faulkner, L. R.; Feldberg, S. W.; Itaya, K.; Majda, M.; Melroy, O.; Murray, R. W.; Porter, M. D.; Soriaga, M. P.; White, H. S. *J. Phys. Chem.* **1993**, *97*, 7147-7173, and references therein.

6 . Zhong, C. J.; Porter, M. D. *Anal. Chem.* **1995**, in press.

7 . Ulman, A. *An Introduction to Ultrathin Organic Films: From Langmuir-Blodgett to Self-Assembly*, Academic: Boston, 1991.

8 . Dubois, L. H.; Nuzzo, R. G. *Annu. Rev. Phys. Chem.* **1992**, *43*, 437-463.

9 . Taniguchi, I.; Toyosawa, K.; Yamaguchi, H.; Yasukouchi, K. *J. Electroanal. Chem.* **1982**, *140*, 187-193.

10 . Taniguchi, I.; Iseki, M.; Yamaguchi, H.; Yasukouchi, K. *J. Electroanal. Chem.* **1984**, *175*, 341-348.

11 . Taniguchi, I.; Iseki, M.; Yamaguchi, H.; Yasukouchi, K. *J. Electroanal. Chem.* **1985**, *186*, 299-307.

12 . Nuzzo, R. G.; Allara, D. L. *J. Am. Chem. Soc.* **1983**, *105*, 4481-4483.

13 . Porter, M. D.; Bright, T. B.; Allara, D. L.; Chidsey, C. E. D. *J. Am. Chem. Soc.* **1987**, *109*, 3559-3568.

14 . Sabatini, E.; Rubinstein, I.; Maoz, R.; Sagiv, J. *J. Electroanal. Chem.* **1987**, *219*, 365-371.

15 . Bain, C. D.; Biebuyck, H. A.; Whitesides, G. M. *Langmuir* **1989**, *5*, 723-727.

16 . Nuzzo, R. G.; Zegarski, B. R.; Dubois, L. H. *J. Am. Chem. Soc.* **1987**, *109*, 733-740.

17 . Nuzzo, R. G.; Fusco, F. A.; Allara, D. L. *J. Am. Chem. Soc.* **1987**, *109*, 2358-2368.

18 . Whitesides, G. M.; Laibinis, P. E. *Langmuir*, **1990**, *6*, 87-96.

19 . Biebuyck, H. A.; Bain, C. D.; Whitesides, G. M. *Langmuir* **1994**, *10*, 1825-1831.

20 . Troughton, E. B.; Bain, C. D.; Whitesides, G. M.; Nuzzo, R. G.; Allara, D. L.; Porter, M. D. *Langmuir* **1988**, *4*, 365-385.

21 . Zhang, M.; Anderson, M. R. *Langmuir* **1994**, *10*, 2807-2813.

22 . Zhong, C. J.; Porter, M. D. *J. Am. Chem. Soc.* **1994**, *116*, 11616-11617.

23 . Chidsey, C. E. D.; Loiacono, D. N.; Sleator, T.; Nakahara, S. *Surf. Sci.* **1988**, *218*, 108-124.

24 . Golan, Y.; Margulis, L.; Rubinstein, I. *Surf. Sci.* **1992**, *264*, 312-326.

25 . Creager, S. E.; Hockett, L. A.; Rowe, G. K.; *Langmuir*, **1992**, *8*, 854-860.

26 . Walczak, M. M.; Alves, C. A.; Lamp, B. D.; Porter, M. D. *J. Electroanal. Chem.* **1995**, *396*, 103-114.

27 . Nuzzo, R. G.; Dubois, L. H.; Allara, D. L. *J. Am. Chem. Soc.* **1990**, *112*, 558-569.

28 . Bryant, M. A.; Pemberton, J. E. *J. Am. Chem. Soc.* **1991**, *113*, 8284-8293.

29 . Fenter, P.; Eisenberger, P.; Liang, K. S. *Phys. Rev. Lett.* **1993**, *70*, 2447-2450.

30 . Whitesides, G. M.; Laibinis, P. E. *Langmuir* **1990**, *6*, 87-96.

31 . Camillone, N.; Chidsey, C. E. D.; Liu, G.; Scoles, G. *J. Chem. Phys.* **1993**, *98*, 4234-4245.

32 . Chidsey, C. E. D.; Liu, G.-Y.; Rowntree, P.; Scoles, G. *J. Chem. Phys.* **1989**, *91*, 4421-4423.

33 . Camillone, N.; Chidsey, C. E. D.; Liu, G.; Putvinski, T. M.; Scoles, G. *J. Chem. Phys.* **1991**, *94*, 8493-8502

34 . Laibinis, P. E.; Whitesides, G. M.; Allara, D. L.; Tao, Y. T.; Parikh, A. N.; Nuzzo, R. G. *J. Am. Chem. Soc.* **1991**, *113*, 7152-7167.

35 . Walczak, M. M.; Chung, C.; Stole, S. M.; Widrig, C. A.; Porter, M. D. *J. Am. Chem. Soc.* **1991**, *113*, 2370-2378.

36 . Widrig, C. A.; Chung, C.; Porter, M. D. *J. Electroanal. Chem.* **1991**, *310*, 335-359.

37 . Schneider, T.; Buttry, D. A. *J. Am. Chem. Soc.* **1994**, *115*, 12391-12397.

38 . Walczak, M. M; Popenoe, D. D.; Deinhammer, R. S.; Chung, C.; Porter, M. D. *Langmuir*, **1991**, *7*, 2687-2693.

39 . A similar coverage results from considerations of the average molecular area given the 30° average tilt of the alkyl chains observed in infrared spectroscopic and ellipsometric data.

40 . Weisshaar, D. E.; Lamp, B. D.; Porter, M. D. *J. Am. Chem. Soc.* **1992**, *114*, 5860-5862.

41 . Widrig, C. A.; Alves, C. A.; Porter, M. D. *J. Am. Chem. Soc.* **1991**, *113*, 2805-2810.

42 . McCarley, R. L.; Kim, Y.-T.; Bard, A. J. *J. Phys. Chem.* **1993**, *97*, 211-215.

43 . Alves, C. A.; Smith, E. L.; Porter, M. D. *J. Am. Chem. Soc.* **1992**, *114*, 1222-1227.

44 . Butt, H.-J.; Seifert, K.; Bamberg, E. *J. Phys. Chem.* **1993**, *97*, 7316-7320.

45 . Strong, L.; Whitesides, G. M. *Langmuir* **1988**, *4*, 546-558.

46 . Chidsey, C. E. D.; Liu, G.-Y.; Rowntree, P.; Scoles, G. *J. Chem. Phys.* **1989**, *91*, 4421-4423.

47 . Chidsey, C. E. D.; Loiacono, D. N. *Langmuir* **1990**, *6*, 682-691.

48 . Dubois, L. H.; Zegarski, B. R.; Nuzzo, R. G. *J. Chem. Phys.* **1993**, *98*, 678-688.

49 . Sellers, H.; Ulman, A.; Schnidman, Y.; Eilers, J. E. *J. Am. Chem. Soc.* **1993**, *115*, 9389-9401.

50 In fact, a recent x-ray diffraction study (Fenter, P.; Eberhardt, A.; Eisenberger, P. *Science* **1994**, *266*, 1216-1218.) suggests that alkanethiols assemble as disulfides and not alkanthiolate, although this is yet to be independently confirmed.

51 . Camillone, N.; Chidsey, C. E. D.; Liu, G.; Scoles, G. *J. Chem. Phys.* **1993**, *98*, 3503-3511.

52 . Poirier, G. E.; Tarlov, M. J. *Langmuir* **1994**, *10*, 2853-2856.

53 . Poirier, G. E.; Tarlov, M. J.; Rushmeier, H. E. *Langmuir* **1994**, *10*, 3383-3386.

54 . Sun, L.; Crooks, R. M. *J. Electrochem. Soc.* **1991**, *138*, L23-L25.

55 . Schonenberger, C.; Sondag-Huethorst, J. A. M.; Jorritsma, J.; Fokkink, L. G. J. *Langmuir* **1994**, *10*, 611-614.

56 . Han, T.; Beebe, T. P., Jr. *Langmuir* **1994**, *10*, 2705-2709.

57 . Delamarche, E.; Michel, B.; Kang, H.; Gerber, C. *Langmuir* **1994**, *10*, 4103-4108.

58 . Sondag-Huethorst, J. A. M.; Schonenberger, C.; Fokkink, L. G. L. *J. Phys. Chem.* **1994**, *98*, 6826-6834.

59 . McCarley, R. L.; Dunaway, D. J.; Willicut, R. L. *Langmuir* **1993**, *9*, 2775-2777.

60 . McDermott, C. A.; McDermott, M. T.; Green, J.-B.; Porter, M. D. *J. Phys. Chem.* **1995**, *99*, 13257-13267.

61 . Poirier, G. E.; Tarlov, M. J. *J. Phys. Chem.* **1995**, *99*, 10966-10970.

62 . Sabatini, E.; Cohen-Boulakia, J.; Bruening, M.; Rubinstein, I. *Langmuir* **1993**, *9*, 2974-2981.

63 . Obeng, Y. S.; Laing, M. E.; Friedli, A. C.; Yang, H. C.; Wang, D.; Thulstrup, E. W.; Bard, A. J.; Michl, J. *J. Am. Chem. Soc.* **1992**, *114*, 9943-9952.

64 . Tarlov, M. J.; Bowden, E. F. *J. Am. Chem. Soc.* **1991**, *113*, 1847-1849.

65 . Song, S.; Clark, R. A.; Bowden, E. F.; Tarlov, M. *J. Phys. Chem.* **1993**, *97*, 6564-6572.

66 . Nahir, T. M.; Clark, R. A.; Bowden, E. F. *Anal. Chem.* **1994**, *66*, 2595-2598.

67 . Chidsey, C. E. D.; Bertizzi, C. R.; Putvinski, T. M.; Mijsce, A. M. *J. Am. Chem. Soc.* **1990**, *112*, 4301-4306.

68 . Chidsey, C. E. D. *Science* **1991**, *251*, 919-922.

69 . Finklea, H. O.; Hanshew, D. D. *J. Am. Chem. Soc.* **1992**, *114*, 3173-3181.

70 . Finklea, H. O.; Ravenscroft, M. S.; Snider, D. A. *Langmuir* **1993**, *9*, 223-227.

71 . Rowe, G. K.; Carter, M. T., Richardson, J. N.; Murray, R. W. *Langmuir* **1995**, *11*, 1797-1806.

72 . Rowe, G. K.; Creager, S. E. *Langmuir* **1991**, *7*, 2307-2312.

73 . Rowe, G. K.; Creager, S. E. *Langmuir* **1994**, *10*, 1186-1192.

74 . Richardson, J. N.; Peck, S. R.; Curtin, L. S.; Tender, L. M.; Terrill, R. H.; Carter, M. T.; Murray, R. M.; Rowe, G. K.; Creager, S. E. *J. Phys. Chem.* **1995**, *99*, 766-772.

75 . Rowe, G. K.; Creager, S. E. *J. Phys. Chem.* **1994**, *98*, 5500-5507.

76 . De Long, H. C.; Donohoue, J. J.; Buttry, D. A. *Langmuir* **1991**, *7*, 2196-2202.

77 . De Long, H. C.; Buttry, D. A. *Langmuir* **1992**, *8*, 2491-2496.

78 . Smith, C. P.; White, H. S. *Anal. Chem.* **1992**, *64*, 2398-2405.

79 . Creager, S. E.; Weber, K. *Langmuir* **1993**, *9*, 844-850.

80 . Bain, C. D.; Whitesides, G. M. *Langmuir* **1989**, *5*, 1370-1378.

81 . Bryant, M. A.; Crooks, R. M. *Langmuir* **1993**, *9*, 385-387.

82 . Creager, S. E.; Clarke, J. *Langmuir* **1994**, *10*, 3675-3683.

83 . Jordan, C. E.; Frey, B. L.; Kornguth, S.; Corn, R. M. *Langmuir* **1994**, *10*, 3642-3648.

84 . Jones, T. A.; Perez, G. P.; Johnson, B. J.; Crooks, R. M. *Langmuir* **1995**, *11*, 1318-1328.

85 . Duevel, R. V.; Corn, R. M. *Anal. Chem.* **1992**, *64*, 337-342.

86 . Sun, L.; Kepley, L. J.; Crooks, R. M. *Langmuir* **1992**, *8*, 2101-2103.

87 . Sun, L.; Crooks, R. M.; Ricco, A. J. *Langmuir* **1993**, *9*, 1775-1780.

88 . Xu, C.; Sun, L.; Kepley, L. J.; Crooks, R. M.; Ricco, A. J. *Anal. Chem.* **1993**, *65*, 2102-2107.

89 . Chailapakul, O.; Sun, L.; Xu, C.; Crooks, R. M. *J. Am. Chem. Soc.* **1993**, *115*, 12459-12467.

90 . Hickman, J. J.; Oder, D.; Laibinis, P. E.; Whitesides, G. M.; Wrighton, M. S. *Science* **1991**, *252*, 688-691.

91 . Tarlov, M. J.; Burgess, D. R. F., Jr.; Gillen, G. *J. Am. Chem. Soc.* **1993**, *115*, 5305-5306.

92 . Frisbie, C. D.; Rozsnyai, L. F.; Noy, A.; Wrighton, M. S.; Lieber, C. M. *Science* **1994**, *265*, 2071-2074.

93 . Kumar, A.; Whitesides, G. M. *Appl. Phys. Lett.* **1993**, *63*, 2002-2004.

94 . Kumar, A.; Biebuyck, H. A.; Whitesides, G. M. *Langmuir* **1994**, *10*, 1498-1511.

95 . Wilbur, J. L.; Biebuyck, H. A.; MacDonald, J. C.; Whitesides, G. M. *Langmuir* **1995**, *11*, 825-831.

96 . López, G. P.; Biebuyck, H. A.; Frisbie, D. C.; Whitesides, G. M. *Science* **1993**, *260*, 647-649.

97 . Ross, C. B.; Sun, L.; Crooks, R. M. *Langmuir* **1993**, *9*, 632-636.

98 . Schoer, J. K.; Ross, C. B.; Crooks, R. M.; Corbitt, T. S.; Hampden-Smith, M. J. *Langmuir* **1994**, *10*, 615-618.

99 . Green, J.-B. D.; McDermott, M. T.; Porter, M. D.; Siperko, L. M. *J. Phys. Chem.* **1995**, *99*, 10960-10965.

100 . McDermott, M. T.; Green, J.-B. D.; Porter, M. D., manuscript in preparation.

101 . Willicut, R. J.; McCarley, R. L. *J. Am. Chem. Soc.* **1994**, *116*, 10823-10824.

102 . Willicut, R. J.; McCarley, R. L. *Langmuir* **1995**, *11*, 296-301.

103 . Sayre, C. N.; Collard, D. M. *Langmuir* **1995**, *11*, 302-306.

2. SPONTANEOUSLY ADSORBED MONOLAYERS OF DIALKYL DISULFIDES AND ALKANETHIOLS AT Au(111): STRUCTURAL COMPARISONS BASED ON MACRO- AND MICRO-SCOPIC CHARACTERIZATIONS

A paper to be submitted to *Langmuir*

Brian D. Lamp, Joe E. Franek, Carla A. Alves, and Marc D. Porter

Abstract

Spontaneously adsorbed monolayers from dialkyl disulfides were studied by infrared reflectance absorbance spectroscopy (IRRAS), electrochemical capacitance, scanning tunneling microscopy (STM), atomic force microscopy (AFM), and electrochemically-induced desorption measurements. These results were compared to those obtained for monolayers generated from alkanethiols with analogous chain lengths. Both precursors form a surface adsorbed thiolate species, as judged by the comparability of the positions of the waves for the voltammetrically induced desorption of the two types of layers. The chain structure, based on IRRAS spectra, however, reveal that the disulfide monolayers are less well ordered than those from the corresponding alkanethiols. Images of the disulfide monolayers obtained by STM and AFM are representative of a $(\sqrt{3}x\sqrt{3})R30°$ adlayer structure of thiolate molecules on Au(111); nearest- and next-nearest neighbor distances, as well as the average domain sizes, are indicative of an adlayer with less long range order than

those formed from alkane thiol precursors. As a result, the disulfide layers have increased permeability causing the reductive desorption of the disulfide monolayers occurs at slightly more positive potentials than for the corresponding thiol layers. This result is consistent with our model of these layers and with the results of electrochemical capacitance measurements. Coverage determined from reductive desorption experiments is $(7.7 \pm 0.2)\times10^{-10}$ mol/cm^2 for disulfide monolayers compared to $(9.3 \pm 0.7)\times10^{-10}$ mol/cm^2 previously determined for thiol monolayers. Taken together, our findings indicate that both thiols and disulfides form the same surface adsorbed thiolate species but that steric limitations for the disulfide precursors inhibit the formation of an adlayer as tightly packed as that from alkanethiols.

Introduction

Spontaneously adsorbed monolayers of sulfur-containing compounds have been extensively applied as models in explorations of a host of interfacial phenomena [1-3]. Of the many possibilities (*e.g.*, thiols, disulfides, sulfides, and thiones), monolayers from long chain alkanethiols ($X(CH_2)_nSH$) at Au(111) have been the most extensively studied. The interest in this particular system derives largely from the definition of the resulting organic surface structure. Long chain alkanethiols chemisorb at gold as densely packed $(\sqrt{3}\times\sqrt{3})R30°$ layers of the corresponding thiolates with an average chain tilt of ~30° from the surface normal as idealized in Figure 2.1 [4]. In contrast to alkanethiolate monolayers, details concerning the formation, structure, and interfacial properties of the layers derived from dialkyl disulfides $(CH_3(CH_2)_nS)_2$ at gold are much less developed [5-11]. This paper focuses on extending insights in the latter system.

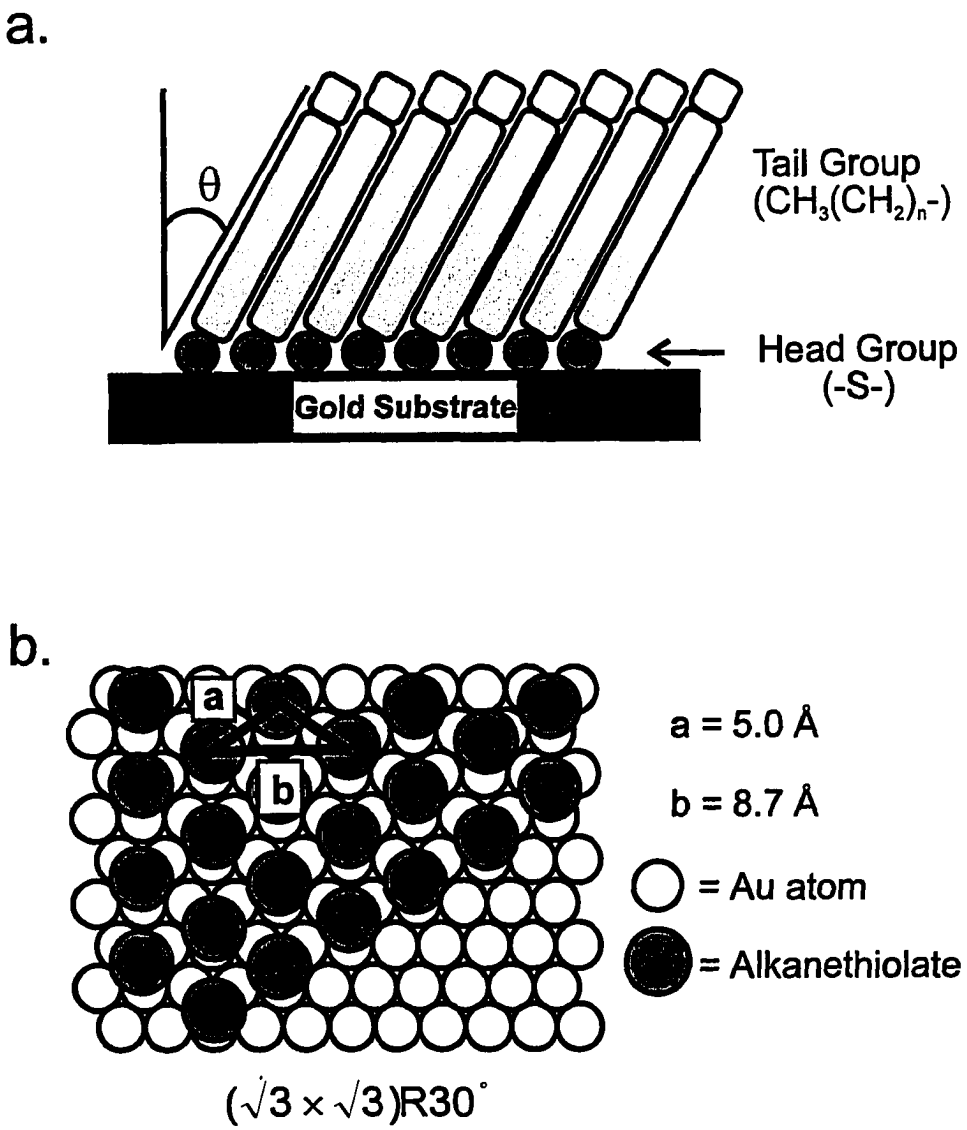

Figure 2.1. Idealized description of alkanethiolates bound at Au(111). a. chain orientation, b. headgroup geometry.

In earlier efforts, studies utilizing surface enhanced Raman spectroscopy (SERS) [12] failed to detect the presence of an intact S-S bond for the layer formed from bis(4-pyridyl)disulfide (PySSPy) at a roughened gold electrode. The strong similarities with the spectrum of a layer from 4-mercaptopyridine further argues that PySSPy chemisorbs at gold *via* S-S cleavage as the corresponding thiolate. The same conclusions have been put forth in SERS studies of these [13] and analogous [14, 15] compounds chemisorbed at silver.

The findings in more recent efforts support the conclusions of the SERS studies. Temperature programmed desorption mass spectrometry has shown that the adlayer formed at gold from dimethyl disulfide desorbs as methanethiolate [6]. A study using transmission electron microscopy has found that the nearest-neighbor separation distances are indistinguishable for monolayers prepared from docosanethiol and didocosyl disulfide [16]. The similarity of the interactions for the two types of head groups is also supported by the strong similarities of the features in the S(2p) region of the x-ray photoelectron spectroscopy of the two systems. Further, the reaction of asymmetric disulfides at gold (*e.g.*, $HO(CH_2)_{10}SS(CH_2)_{10}CH_3$) resulted in a surface structure of close to equal amounts of thiolates of each side chain, a structural composition consistent with the formation of gold-thiolate bonds through S-S cleavage [5]. Secondary ion mass spectrometric studies have also observed no indication for intact S-S bonds in monolayers formed from disulfide precursors [11].

Although the above results indicate that gold-supported monolayers from alkanethiols and dialkyl disulfides have strong structural similarities, two pieces of information suggest that there are subtle, but important differences. In an early preliminary screening of the structures and properties of monolayers formed at gold from the two types of precursors, dialkyl disulfide-derived monolayers were found to be less effective as barriers to heterogeneous electron transfer [17]. A difference in structure was also detected in a recent wettability study [10], with the hydrophobicity as measured with hexadecane as the probe liquid slightly lower at a layer from diundecyl disulfide in comparison to that at a layer from undecanethiol. Both observations are diagnostic of a less ordered interfacial structure for the layers from dialkyl disulfide precursors.

This paper reports the results of a multitechnique study that examined and compared the structural details of monolayers prepared from the spontaneous adsorption of dialkyl disulfides and alkanethiols at gold. Monolayers were formed and characterized from both types of precursors with short (number of methylene carbons, n, = 3), intermediate (n = 6-9), and long (n = 17) alkyl chains. X-ray photoelectron spectroscopy (XPS) was used to probe general details concerning the mode of interaction between the sulfur head groups and gold substrate, whereas infrared reflection spectroscopy was applied to assess the packing and orientation of the alkyl chains. Electrochemical, contact angle, and scanning probe microscopic techniques (*i.e.*, scanning tunneling (STM) and atomic force microscopies (AFM)) were used to examine more subtle details of the interfacial structure. Together, these results serve as a basis for a comparison of the structure and interfacial properties of the two

different precursor-derived systems as well as for an assessment of possible differences in their formation mechanisms.

Experimental

Substrate Preparation. Gold substrates were prepared by the resistive evaporation of 300 nm thick gold films onto freshly cleaved (75 mm x 25 mm) green mica sheets (Asheville-Schoonmaker Mica Co., Newport News, VA). The pressure in a cryopumped Edwards E306A coater was less than 1 x 10^{-6} torr during evaporation. Evaporation rates were 0.3-0.4 nm/s. After ~40 min cooling time, the evaporator was backfilled with dry N_2 and the substrates were removed and annealed in a muffle furnace (Jelrus, Ossining, NJ), at 300° C for 3 h in the laboratory ambient. Upon cooling to ambient temperature, the substrates were cleaned in an O_2-plasma system (Harrick Scientific) at a pressure of ~20 mtorr for 1 min. The substrates were then immersed into the disulfide- or thiol-containing solutions.

As prepared, the above films consist primarily (>99%) of Au(111) crystallites separated by grain boundaries of varying width [18]. The roughness factor (1.1 ± 0.1 [19]) of these films was determined voltammetrically by iodide adsorption/desorption. This value that corresponds to the division of the surface area determined voltammetrically by the geometric area of the electrode. For the purposes of this discussion, we will denote the gold surface simply as Au(111).

Substrates for the STM and AFM characterizations were further treated by heating mica in the evaporation chamber for 1 h at 250 to 300° C immediately prior to metal deposition. Subsequent to deposition, the gold-coated mica was allowed to cool radiatively to below 70° C, removed from the vacuum chamber, and immersed immediately into the solutions containing the adsorbate precursors. This preparation yields substrates that facilitate characterization by STM and AFM and electrochemical coverage determination (see below); however, we have not detected differences in the results from infrared reflection spectroscopic and wettability characterizations.

Monolayer Preparation. The following precursors were used in this study: diethyl disulfide (Aldrich), di-*n*-butyl disulfide (Aldrich), di-*n*-heptyl disulfide (Alfrebo, Monroe, OH), di-*n*-decyl disulfide (TCI American, Portland, OR), di-*n*-octyl disulfide, di-*n*-nonyl disulfide, and di-*n*-octadecyl disulfide (Lancaster Synthesis, Windham, NH), *n*-butanethiol, *n*-heptanethiol, *n*-octanethiol, *n*-nonanethiol, *n*-octadecanethiol (Aldrich) and *n*-decanethiol (Kodak). The octadecyl disulfide and octadecanethiol were recrystallized from ethanol. All other chemicals were used as received.

Monolayer formation resulted from immersion of Au(111) substrates in precursor solutions with nominal concentrations between 0.5 and 1.0 mM in chloroform (HPLC grade, Fisher) or absolute ethanol (Quantum Chemical Corp., Tuscola , IL). Immersion times ranged from 6 to 24 h with no observable difference in the structure and interfacial properties of the layers. Emmersed electrodes were rinsed with ethanol and/or hexane and dried on a Headway Research Inc. (Garland, TX) spin coater.

X-Ray Photoelectron Spectroscopy. XPS spectra were acquired using a Physical Electronics model 5500 multitechnique surface analysis system equipped with a hemispherical analyzer, torroidal monochrometer, and a multichannel detector. 300 W aluminum Kα radiation was used for excitation, with detection at 45°.

Infrared Spectroscopy. Infrared spectra were obtained with a Nicolet 740 FT-IR Spectrometer. Reflectance spectra were acquired with p-polarized light incident at 80° from the surface normal and liquid N_2 cooled HgCdTe or InSb detection [20]. The spectra are presented as $-\log(R/R_0)$ where R is the reflectance of the sample and R_0 is the reflectance of a reference octadecanethiolate-d_{37} monolayer on Au. Details concerning the preparation and handling of reference substrates have been given previously [21].

Contact Angle Measurements. Contact angle measurements were made using a Ramé-Hart model 100-00115 goniometer with hexadecane (Aldrich), glycerol (Fisher), methylene iodide (Aldrich), and deionized water as probe liquids. The measurements were taken by forming a small (~2 μL) droplet on the surface and slowly increasing or decreasing the volume for the advancing (θ_a) and receding (θ_r) contact angle measurements, respectively.

Scanning Probe Microscopies. All STM and AFM images were obtained using a Digital Instruments Nanoscope II or Nanoscope III (Santa Barbara, CA) equipped with a 0.7 μm STM or AFM scan head. The instrument was operated under ambient conditions. After loading the samples, the instrument was allowed to equilibrate thermally for ~30 min. All

images were acquired at a rate of 14 to 28 lines/s, which requires about 15 to 25 s per image, and were lightly filtered with an XY spectrum filter.

The STM tips were made by etching 0.25 mm tungsten wire (Aldrich) in 1M KOH (99.99%, Aldrich) at 30 V ac. After etching, the tips were rinsed with deionized water and used immediately. Images were scanned in constant height mode. A tip was discarded if, after scanning several regions of a sample, no well defined images were obtained. Horizontal displacements of the tip were calibrated against a sample of highly ordered pyrolytic graphite. Bias voltage was typically 100 to 200 mV with tunneling current on the order of 500 pA.

All AFM images were collected with the AFM tip in contact with the sample in a constant force mode. Samples were scanned at forces ranging from 5 nN to 100 nN using 100 μm triangular silicon nitride cantilevers (Digital Instruments) with a force constant of 0.58 N/m. Horizontal tip displacements were calibrated against samples of freshly cleaved mica.

Electrochemistry. Samples were mounted in a conventional three electrode cell with a working electrode area of 0.62 cm^2, as defined by the opening in an inert elastomer gasket. A platinum coil counter electrode and Ag/AgCl/sat'd KCl reference electrode were used in these experiments. All potentials herein are reported with respect to this reference. Electrolyte solutions were 0.5 M KOH (99.99%, Aldrich) and were prepared with water passed through a Milli-Q purification system. Prior to cycling, solutions were purged for at least 15 min. with water saturated Ar or N_2 (Air Products). Voltammograms were recorded

using either a CV-27 potentiostat (Bioanalytical Systems) and x-y recorder (Houston Instruments) or a computer controlled potentiostat (Cypress Systems, Inc.) at a scan rate of 100 mV/s.

Results and Discussion

X-Ray Photoelectron Spectroscopy. The interactions of the head groups of the two types of monolayers with Au(111) were first probed using XPS. Data in the S(2p) region for the monolayers from di-decyl disulfide and the analogous alkanethiol are presented in Figure 2.2a and b, respectively, and summarized in Table 2.1.

As found previously [5, 6, 8], the positions of the $S(2p_{3/2})$ and $S(2p_{1/2})$ bands are representative of sulfur present on the electrode surface as a gold-bound alkanethiolate. It follows, in view of the close correspondence of the positions and intensities of the bands in the two spectra and the sensitivity of the positions of the XPS features to the relative electronic density surrounding the emitting atom [22], that the interactions between sulfur and gold in both systems are similar. By extension, the formation of a monolayer at Au(111) from the dialkyl disulfide results in S-S bond cleavage to yield the corresponding gold-bound thiolate. The lack of detectable bands for other more extensively oxidized or reduced forms of sulfur further indicates that the gold-bound thiolate is the dominant form of sulfur in both systems.

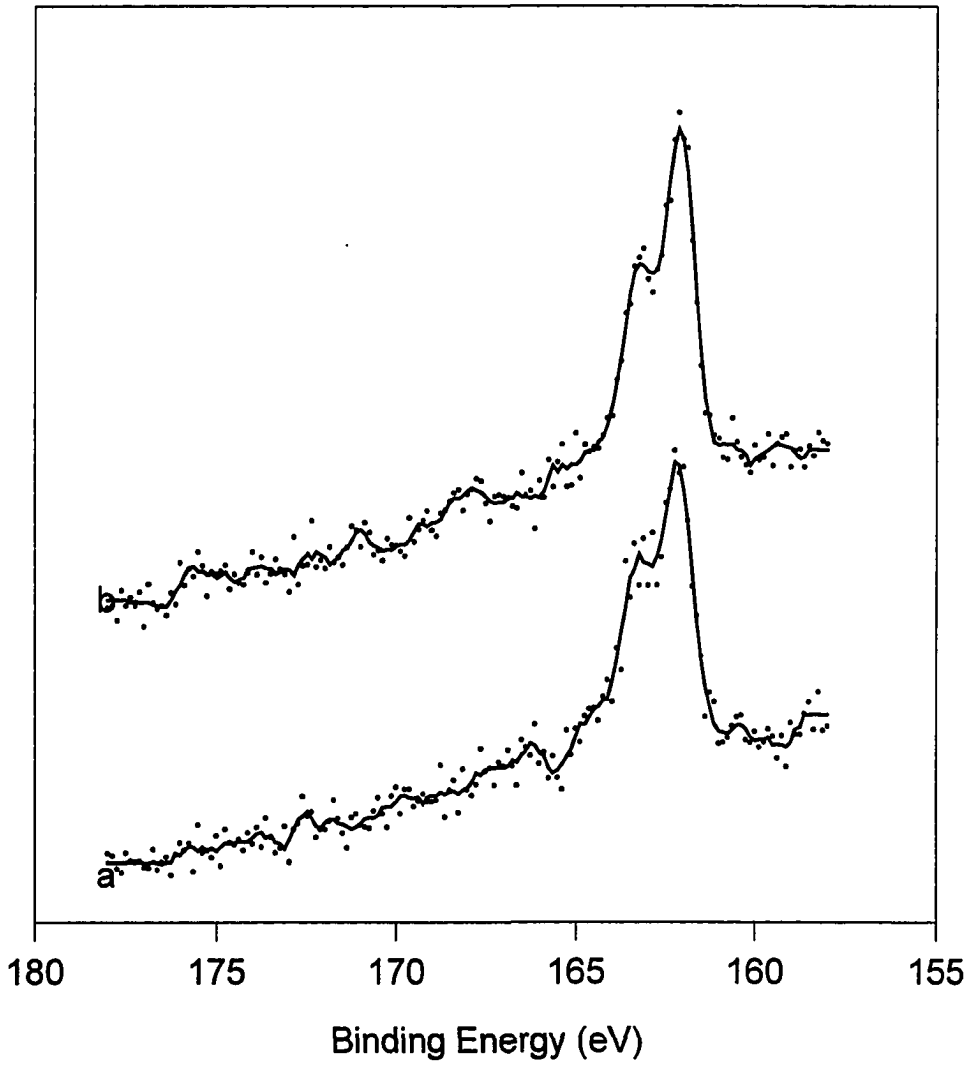

Figure 2.2. XPS spectra in the sulfur 2p region for monolayers formed from: a. di-n-decyl disulfide, and b. decanethiol.

Table 2.1. Binding energies and compositional assignments for the XPS spectra of monolayers formed from $CH_3(CH_2)_9SH$ and $(CH_3(CH_2)_9S)_2$ at gold.

	Position (eV)	
Band	$CH_3(CH_2)_9SH$	$(CH_3(CH_2)_9S)_2$
$Au(4f_{7/2})$	84.1	84.1
$Au(4f_{5/2})$	87.9	87.8
$S(2p_{3/2})$	162.1	162.2
$S(2p_{1/2})$	163.1	163.1
C(1s)	284.9	285.0

Electrochemistry. Electrochemical measurements were also used to characterize the monolayers formed from the dialkyl disulfides. This characterization is based on our series of explorations of the electrode reactions of alkanethiolate monolayers [23-27]. These studies have shown that alkanethiolates can be desorbed into alkaline solution through the reductive pathway in Reaction 1.

$$RS\text{-}Au + e^- \rightarrow Au(0) + RS^- \qquad [1]$$

Driving the reaction by a linear voltage sweep produces a well-defined cathodic desorption wave (*e.g.* Figure 4 in ref. 23) at annealed, mica-supported gold [28]. This type of experiment provides diagnostic information related to the energetics of the interaction between sulfur and gold from the position of the desorption wave, and to the surface coverage of the monolayer from the charge (Q_{rd}) under the desorption wave.

Figure 2.3 presents linear sweep voltammograms (LSVs) for the desorption of the monolayers formed at gold from each of the dialkyl disulfides (curves a-f). Table 2.2 summarizes key features of the results, along with comparative data for the layers from the analogous alkanethiols. Sweeps were initiated at -0.2 V and scanned at -100 mV/s to just below the solvent limit; 0.5 M KOH was used as the supporting electrolyte. A single cathodic wave is present in each of the curves that shifts to more negative values as the length of the alkyl chain increases. The shapes of these are diagnostic of a surface-bound electrochemical process, as expected for Reaction 1. Importantly, the positions of the waves are, in general, similar to those for the adlayers formed from the corresponding alkanethiols (Table 2.2), indicating that the sulfur-gold interactions for the monolayers from the two different precursors are strongly similar.

Table 2.2. Peak potential (V vs Ag/AgCl/Sat'd KCl), charge ($\mu C/cm^2$), and coverage ($moles/cm^2$) values from reductive desorption measurements of dialkyl disulfides and alkyl thiol[a] adsorbed at Au(111).

	$-E_{rd}$		Q_{rd}[b]		Γ_{rd}[b] $x10^{10}$	
n	disulfide	thiol	disulfide	thiol	disulfide	thiol
1	0.774	0.749	75±9	82±6	7.8±0.9	8.5±0.6
3	0.846	0.920	72±4	82±6	7.6±0.4	8.5±0.6
6	0.990	0.986	80±6	82±6	7.6±0.5	8.5±0.6
7	0.995	1.004	81±8	82±6	8.0±0.8	8.5±0.6
8	1.001	1.022	79±8	82±6	7.8±0.7	8.5±0.6
9	1.027	1.040	78±5	82±6	7.4±0.5	8.5±0.6
17	1.144	1.202	76±7	82±6	7.9±0.7	8.5±0.6

[a]The data from the monolayers from alkanethiols are from reference 23.
[b]These values are reported after account for the roughness factor (1.1) the annealed gold at mica substrates

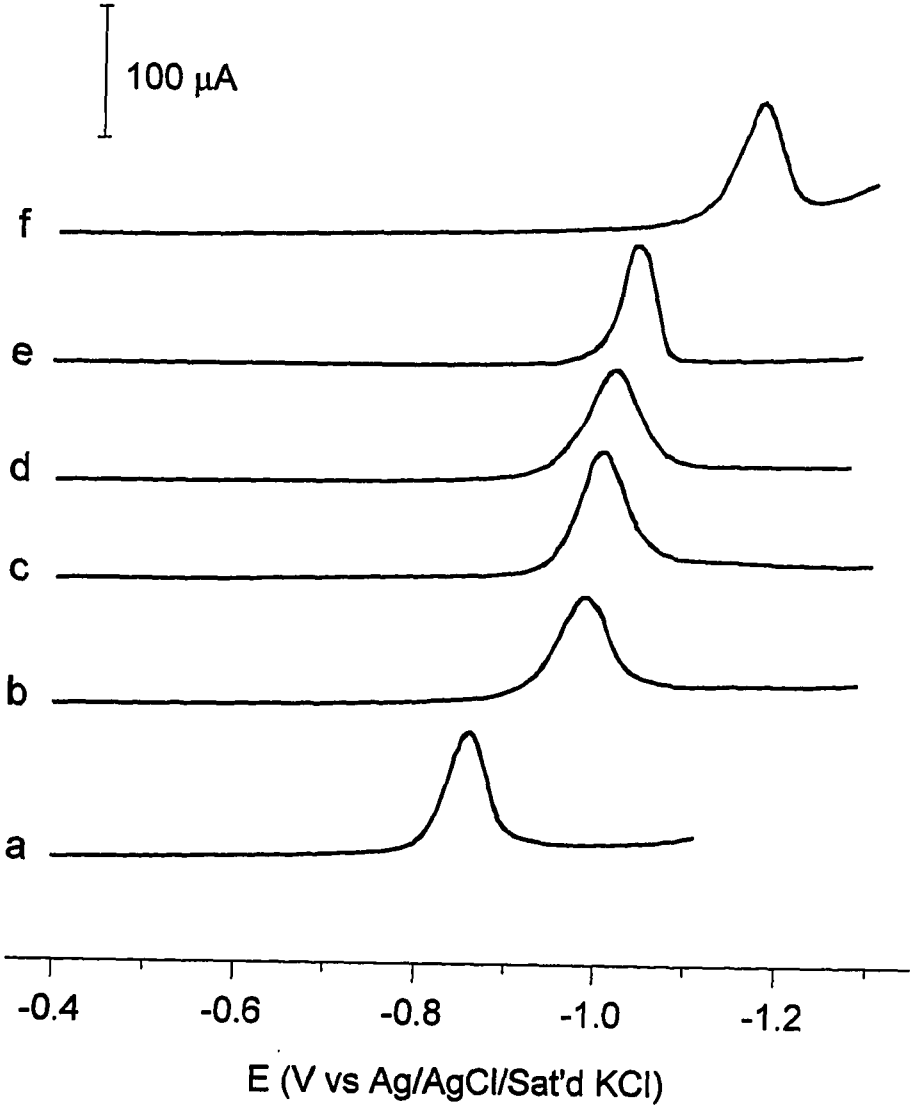

Figure 2.3. Electrochemical desorption of monolayers assembled from $(CH_3(CH_2)_n)_2$ solutions. Values for n are a. 3, b. 6, c. 7, d. 8, e. 9, f. 17. Electrode area: 0.62 cm^2, sweep rate: 100 mV/s, electrolyte: 0.5M KOH(aq).

The above conclusion is also consistent with the shift of E_p to more negative values as the length of the alkyl chain increases. In earlier studies of alkanethiolate monolayers [23], we found that value of E_p becomes increasingly more negative (20 mV per CH_2 group) as the length of the alkyl chain increased. We have interpreted this dependence to the combination of two effects: a decrease in the fractional drop of the applied voltage across the sulfur head group as the length of the alkyl chain increases [23] and an increase in the cohesive interactions between the polymethylene chains as the alkyl chain increases. With increasing length of the alkyl chain, the fraction of the applied potential dropped across the sulfur head group decreases, which, along with the increase in attractive interactions of the chains, results in the observed cathodic shift in the desorption wave. The general comparability of the shifts in the values of E_p for the layers formed form the two types of precursors (see below) further supports the similarities of the structure of the layers.

An analysis of the charge passed under the desorption wave provides additional insight into the structural details of the monolayers from dialkyl disulfides. In this analysis, the surface coverage (Γ) of the monolayer is related to Q_{rd} *via* Equation 2,

$$\Gamma = \frac{Q_{rd}}{nFA} \qquad [2]$$

where n is the number of electrons involved in the electron-transfer process, F is the Faraday, and A is the surface area of the electrode after accounting for surface roughness (see Experimental Section). The value of Q_{rd} is determined by integrating the area under the desorption wave after a straight capacitive -baseline approximation of the double layer

charging current [29]. As summarized in Table 2.2, the values of Q_{rd} for the layers from the disulfide precursors are largely independent of chain length; values range from 72±4 $\mu C/cm^2$ to 81±8 $\mu C/cm^2$, with an average of 77±3 $\mu C/cm^2$. These values are close to (within 15% or less), but slightly lower than those for the layers from the alkanethiol precursors, indicating that the surface coverage of the layers from dialkyl disulfides is lower than that from the alkanethiols. Interestingly, the lower average value of Γ for the layers from the disulfide precursors is also reflected by the small differences in the values of E_p, which in most of the cases are slightly more positive than those from the thiol precursors. We attribute this difference, as is discussed in a more detailed structural perspective in subsequent sections, to a slightly larger value of the capacitance with the disulfide-based monolayers. The larger capacitance results in a smaller drop in the voltage across the alkyl chains, and in turn, a greater drop of the applied potential across the sulfur head group.

Infrared Spectroscopy. Infrared spectra for both types of monolayers are given the C-H stretching region in Figure 2.4 and in a few isolated cases in the C-H bending region in Figure 2.5. These spectra were obtained in an external reflectance (IRRAS) mode. Band assignments and peak positions are summarized in Table 2.3.

These spectra support the general similarities of the structures of the two types of monolayers. As discussed [3], the polymethylene chains for alkanethiolate monolayers exhibit an average tilt of ~30° from the surface normal. The strong similarities in the magnitudes of the spectra for thiol and disulfide monolayers are supportive of a comparable structural orientation of the chains in the two systems.

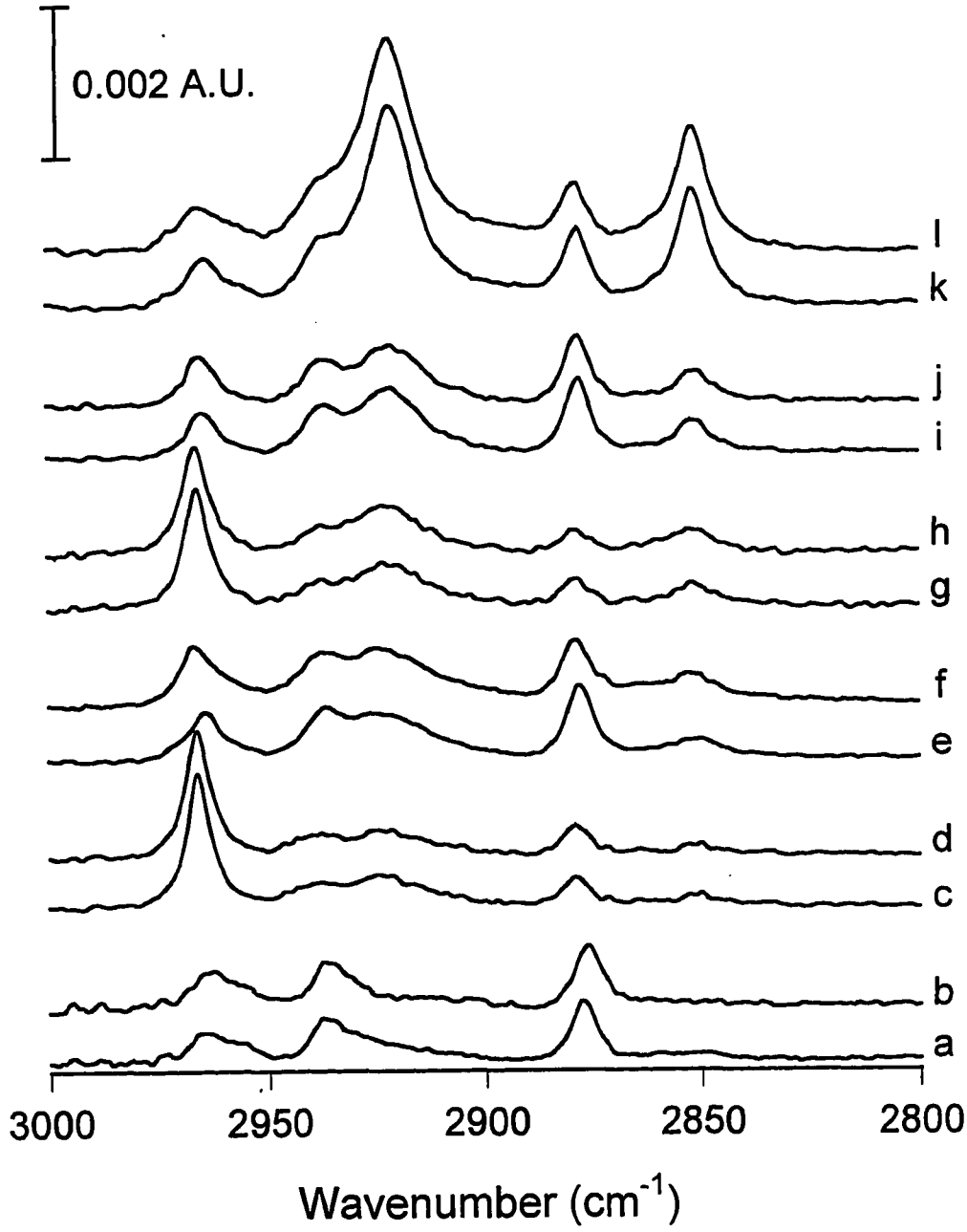

Figure 2.4. Infrared spectra in the C-H stretching region for a series monolayers adsorbed from alkanethiols and dialkyl disulfides. a. $(C_4H_9S)_2$, b. C_4H_9H, c. $(C_7H_{15}S)_2$, d. $C_7H_{15}SH$, e. $(C_8H_{17}S)_2$, f. $C_8H_{17}SH$, g. $(C_9H_{19}S)_2$, h. $C_9H_{19}SH$, i. $(C_{10}H_{21}S)_2$, j. $C_{10}H_{21}SH$, k. $(C_{17}H_{35}S)_2$, l. $C_{17}H_{35}SH$.

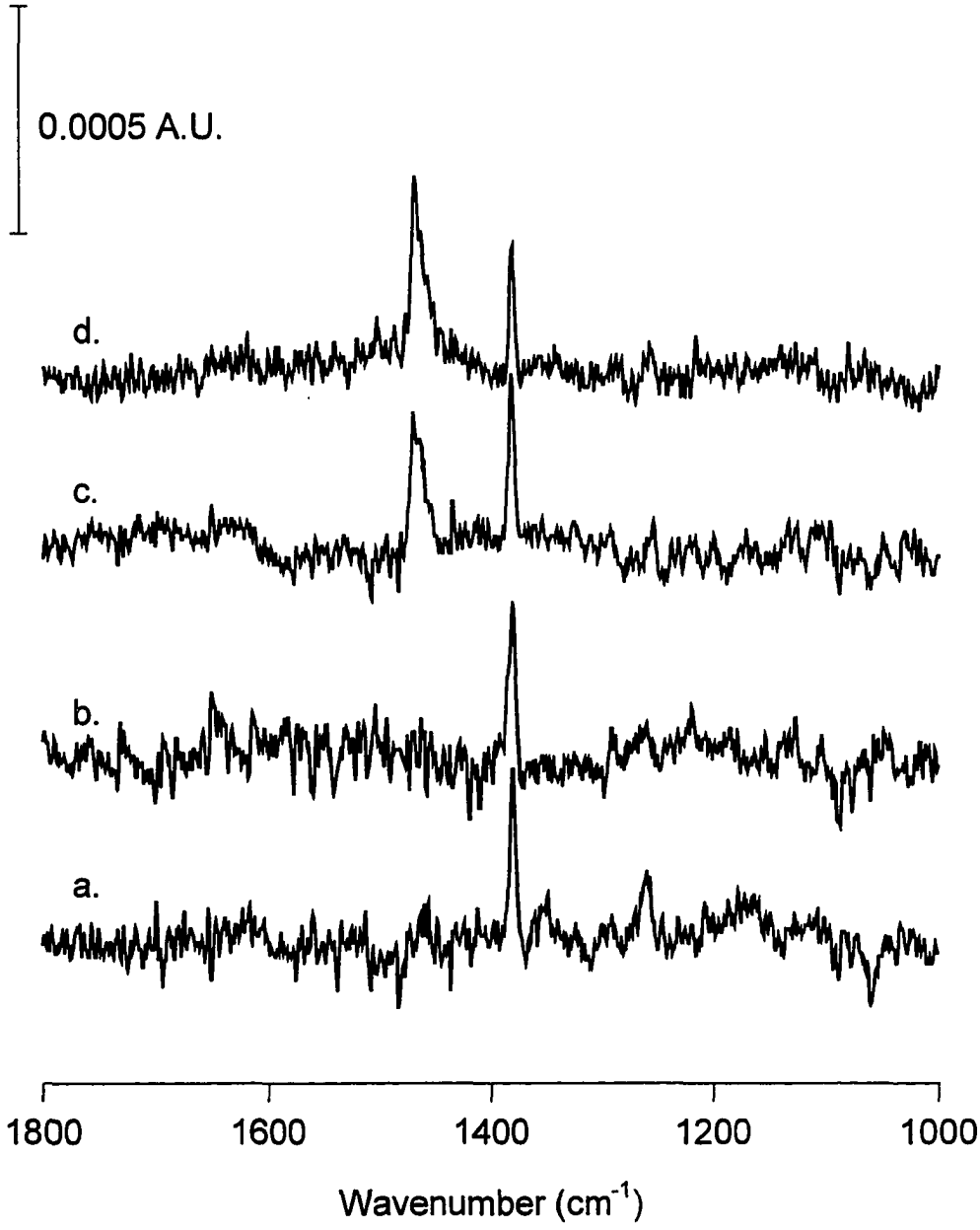

Figure 2.5. Infrared spectra in the C-H bending region for monolayers formed from: a. $(C_4H_9S)_2$, b. C_4H_9SH, c. $(C_{17}H_{35}S)_2$, d. $C_{17}H_{35}SH$.

Table 2.3. Peak positions (values in paranthesees are for $CH_3(CH_2)_nSH$) and mode assignments for the C-H stretching and bending modes for monolayers formed from $(CH_3(CH_2)_nS)_2$ and $CH_3(CH_2)_nSH$ at Au(111)

Structural	C-H	Peak Position (cm^{-1})													
Group	Mode	n = 17		n = 9		n = 8		n = 7		n = 6		n = 3		n = 1	
$-CH_2-$	ν_a	2921	(2919)	2922	(2921)	2922	(2921)	2922	(2922)	2921	(2921)	*b*	(*b*)	*b*	(*b*)
	ν_S	2851	(2850)	2851	(2850)	2850	(2851)	2850	(2850)	2848	(2848)	*b*	(*b*)	*b*	(*b*)
	δ_S	1470	(1471)	1469	(1463)	1464	(1470)	1461	(1463)	1465	(1466)	*b*	(*b*)	*b*	(*b*)
CH_3-	ν_a(ip)	2964	(2963)	2965	(2964)	2966	(2965)	2965	(2964)	2966	(2965)	2964	(2965)	*b*	(*b*)
	ν_S(FR)	*a*	(2934)	2936	(2935)	2936	(2936)	2936	(2936)	2940	(2938)	2936	(2936)	2919*c*	(2918*c*)
	ν_S(FR)	2878	(2877)	2878	(2878)	2879	(2878)	2878	(2878)	2878	(2878)	2876	(2876)	2866*c*	(2863*c*)
	δ_S	1383	(1383)	1383	(1382)	*b*	(*b*)	1381	(1381)	*b*	(*b*)	1381	(1381)	1372	(1372)

a Peak position not determined because of overlap of $\nu_a(CH_2)$ band.

*b*Peak position could not be determined because of low signal to noise ratio

*c*In the ethyl disulfide and ethanethiol spectra, we attribute the bands in the high energy region to methyl and not methylene modes. This assignment is in correlation with modes seen with sum-frequency-generation spectroscopy for methyl thiolate on Ag(111) [28] as well as IR and raman spectra of bulk ethyl iodide [29].

The positions of the features for the methylene modes are also very comparable, indicating a comparability in the microscopic environment for the polymethylene chains for each value of n for both types of monolayers. The increased magnitude of the methylene modes is indicative of either an increase in average chain tilt or a decrease in order in the film. It would be expected, however, that such a tilt change would also result in a shift in the position of the features due to increased crystallinity throughout the film. The absence of such a shift suggests instead, that a change in the average orientation of the alkyl chainsresults when the monolayer is formed from a disulfide. This increase in the methylene intensity is also seen in the low energy spectra in Figure 2.5a and c.

As expected, methylene band intensity in both the low and high energy regions increases with increasing chain length while maintaining peak position, as illustrated in Figure 2.6. This trend reflects similar structure for both long and short chain disulfide monolayers. If the structure of long and short chain layers is indeed similar, the barrier properties of the monolayer film should be controllable by simply altering the chain length of the alkyl group.

In contrast to the similarities of the polymethylene chains, an in depth comparison of the methyl stretching modes reveals a subtle difference in the structure at the chain terminus of the thiol and disulfide monolayers. The positions and widths of these bands, as evident from Figure 2.6 and Table 2.3, are comparable for the two types of monolayers. The spectra for both types also exhibit a clear dependence on whether the number of methylene carbons,

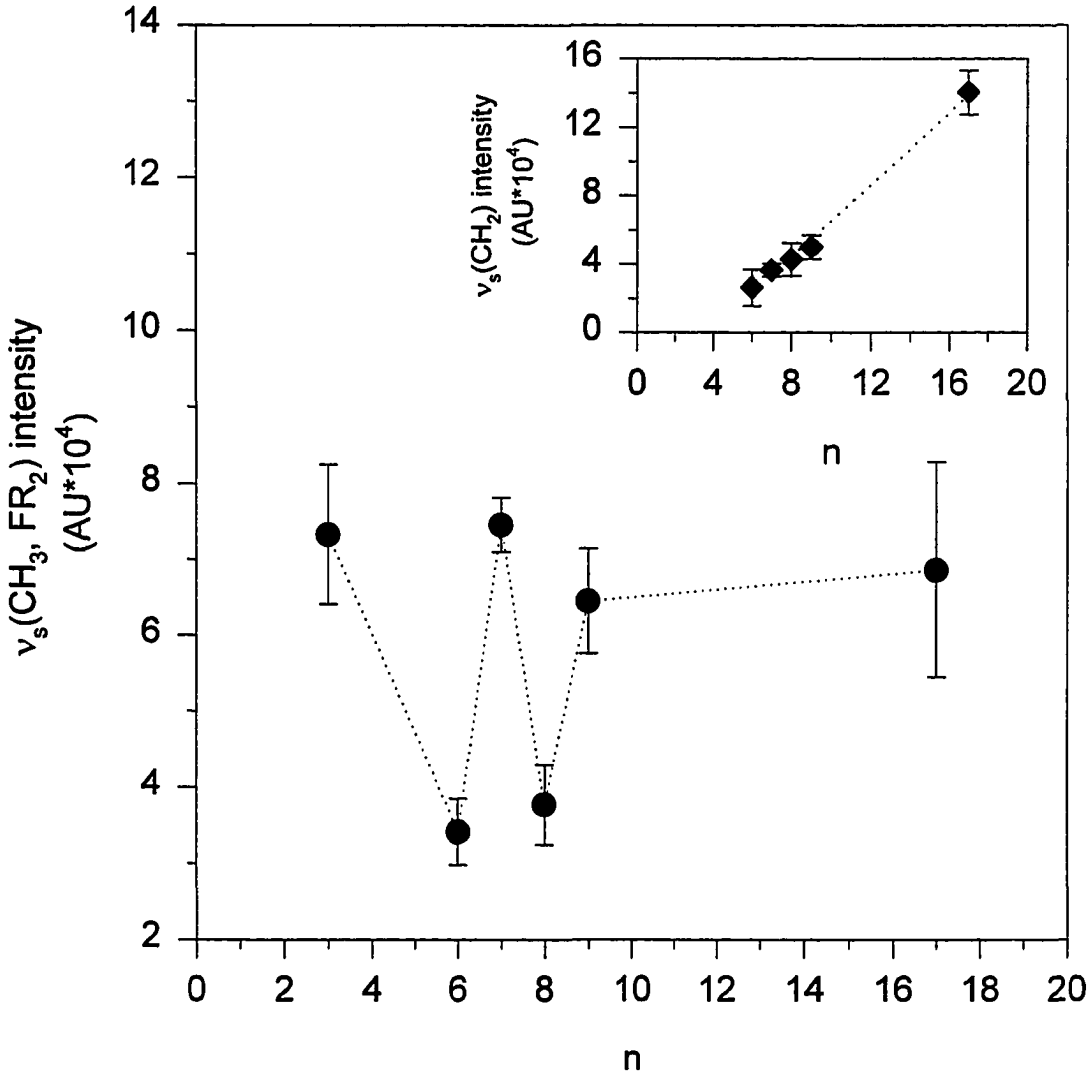

Figure 2.6. Intensities for the symmetric methyl (•) and methylene (♦) modes for a series of disulfide monolayers.

n, is an odd or an even number. This effect has been previously described for thiols on Au(111) [32] and Ag(111)/(110) [33]. As in thiol spectra, while methylene modes are essentially linear in n, methyl intensities exhibit a marked odd-even effect as shown in Figure 2.6. This effect has been attributed to the differing structural relationships between the methyl mode and the surface with reference to the surface selection rule and is evident for all methyl modes in the spectra. Although this effect is observed in both precursor's spectra, the maximum absorbance is less in the disulfide spectra. This suggests that the average orientation of the $\nu_s(CH_3)$ is less perpendicular to the surface for the odd chains in the disulfide monolayers, relative to the thiol monolayers. This result is indicative of the increased "disordering" of the alkyl chains which results in an apparent increased chain tilt.

Wettability. The wetting characteristics of the dialkyl disulfide monolayers were assessed by measurements of advancing (θ_a) and receding (θ_r) contact angles using water, glycerol, methylene iodide, and hexadecane as probe liquids. The results are presented in Figure 2.7, along with comparative data for alkanethiol monolayers for comparison. The values for θ_a have an uncertainty of $\pm 1°$, whereas those for θ_r, are $\pm 2°$. With both types of monolayers, the values of θ_a and θ_r increase as n increases. However, the values for both sets of measurements are consistently larger for the monolayers from the alkanethiols than those at the monolayers from the dialkyl disulfides, with larger differences in the θ_r values. These differences, in view of conventional descriptions of wetting, therefore support the presence of a more disordered chain structure for the systems formed from the dialkyl disulfides.

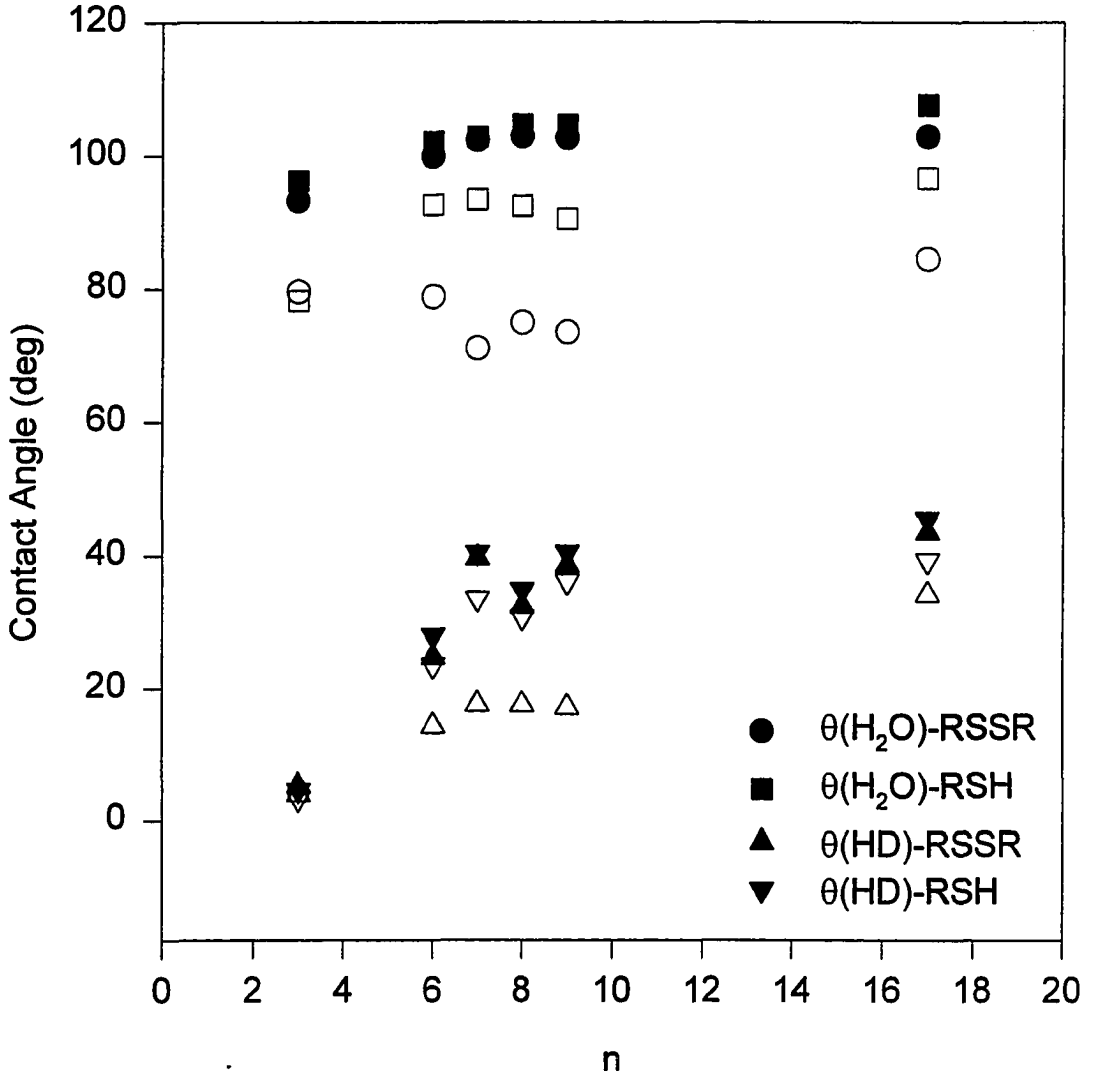

Figure 2.7. Advancing (filled symbols) and receding (open symbols) contact angles for a series of monolayers formed from alkanethiols and dialkyl disulfides.

A qualitative approach to a structural assessment of these systems can be developed from the hysteresis of the contact angle data using Cassie's equation [34, 35, 36]. The basis of this approach, which is clearly an oversimplification of the underlying physical basis of wetting, follows from considering the monolayer as a two-component interfacial structure where the observed contact angle, θ, is given as:

$$\cos\theta = \sigma_1\cos\theta_1 + \sigma_2\cos\theta_2. \qquad [2]$$

In this equation, σ_1 is the fraction of the surface having contact angle θ_1 and σ_2 is the fraction of the surface having contact angle θ_2. If the σ_2- portion of the interface is attributed to defects that give rise to a void volume in the chain structure of the monolayer, then these voids will be filled with the probe liquid during retraction of the droplet in determinations of receding contact angles. In such an instance, θ_2 becomes zero. Assigning θ_1 and σ_1 to the portion of the interfacial structure that is defect free, the following expressions can be developed for θ_a and θ_r

$$\cos\theta_r = \sigma_1\cos\theta_1 + \sigma_2 \qquad [3]$$

$$\cos\theta_a = (\sigma_1 + \sigma_2)\cos\theta_1. \qquad [4]$$

Combining Equations 3 and 4 and solving for σ_2 yields

$$\sigma_2 = \frac{\cos\theta_r - \cos\theta_a}{1 - \cos\theta_a} \qquad [5]$$

Using this general approach, we can develop a rough assessment of the structural differences in the two types of layers.

A comparison of σ_2 for alkane thiol and dialkyl disulfide-derived layers, shown for all four probe liquids in Figure 2.8, reveals that disulfide films exhibit a larger fractional coverage of defects, 0.40±0.15, compared to 0.22±0.07 for thiol monolayers. The more polar probe liquids (*i.e.*, H_2O and glycerol) give the smallest values for σ_2 since they only probe the outermost portion of the monolayer and are thus blind to underlying defects. Less polar probe liquids (*i.e.*, hexadecane and CH_2I_2) give larger values for σ_2. Since these liquids penetrate further into the film one can infer that the difference in the σ_2 values results from defects that extend past the end groups and into the chain structure itself [37].

Also, the contact angle data for both the disulfide and thiol films with hexadecane as probe liquid indicate an odd-even effect as previously seen for thiols on Ag(111) surfaces [19]. The similarity in the odd even effect is indicative of similar structural orientation in the thiol and disulfide films, that is, ordered regions of both films behave similarly. Although the specific reason for this effect is not definitively known, the fact that the trend follows for both precursors is strong evidence for similar structure in the monolayers.

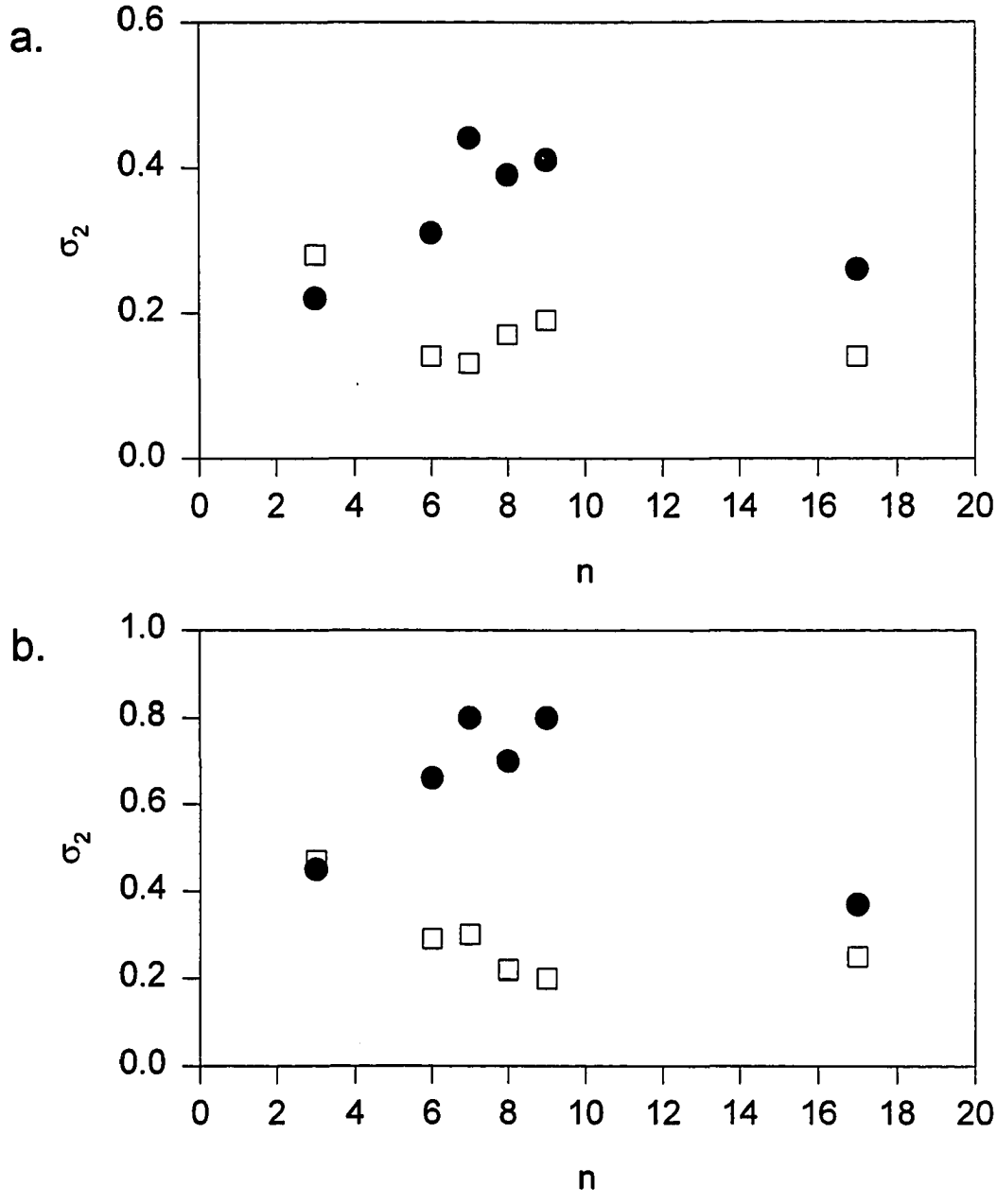

Figure 2.8. Fractional coverage of defects (σ_2) for monolayers assembled from dialkyl disulfides (●) and alkanethiols (□). Probe liquid: a. water, b. hexadecane.

Scanning Tunneling and Atomic Force Microscopy. The microscopic structure of disulfide monolayers was probed using both STM and AFM. Images using STM were obtained for several (n = 1, 3, 6, 7, 9, 17) disulfide monolayers with similar results for all values of n. Figure 2.9 shows a representative STM image of a monolayer formed from di-*n*-heptyl disulfide. Most prominent is the presence of a large number of single-atom deep depressions in the terrace regions of the image. These depressions have been previously observed for monolayers made from alkanethiols, and arise largely from an adsorbate-induced reconstruction of the underlying substrate [38]. Interestingly, while the average diameter (2.4 nm) and depth (0.24 nm) of the depressions observed for monolayers formed from disulfides correlates well with the values noted for analogous thiol monolayers, the number density of the depressions (58±15 depressions/2500 nm^2) is about a factor of two larger than the density seen for monolayers assembled from alkane thiols.

Also present in Figure 2.9 are several regions of molecular order. Box A encloses a region of order corresponding to the c(4 x 2) superlattice of the ($\sqrt{3}$ x $\sqrt{3}$)R30° adlayer of thiolate adsorbates on the Au(111) surface which has been recently noted for monolayers formed from thiols [39]. Also present in the image are rotationally equivalent domains of the (p x $\sqrt{3}$) structure also observed for thiol monolayers [40].

While the short range order and structure for disulfide monolayers is similar to that seen for monolayers formed from thiols, the respective long range order and domain sizes exhibit some differences. Typical areas of order for disulfide monolayers are 100 nm^2 at best compared to as much as 600 nm^2 for thiol monolayers.

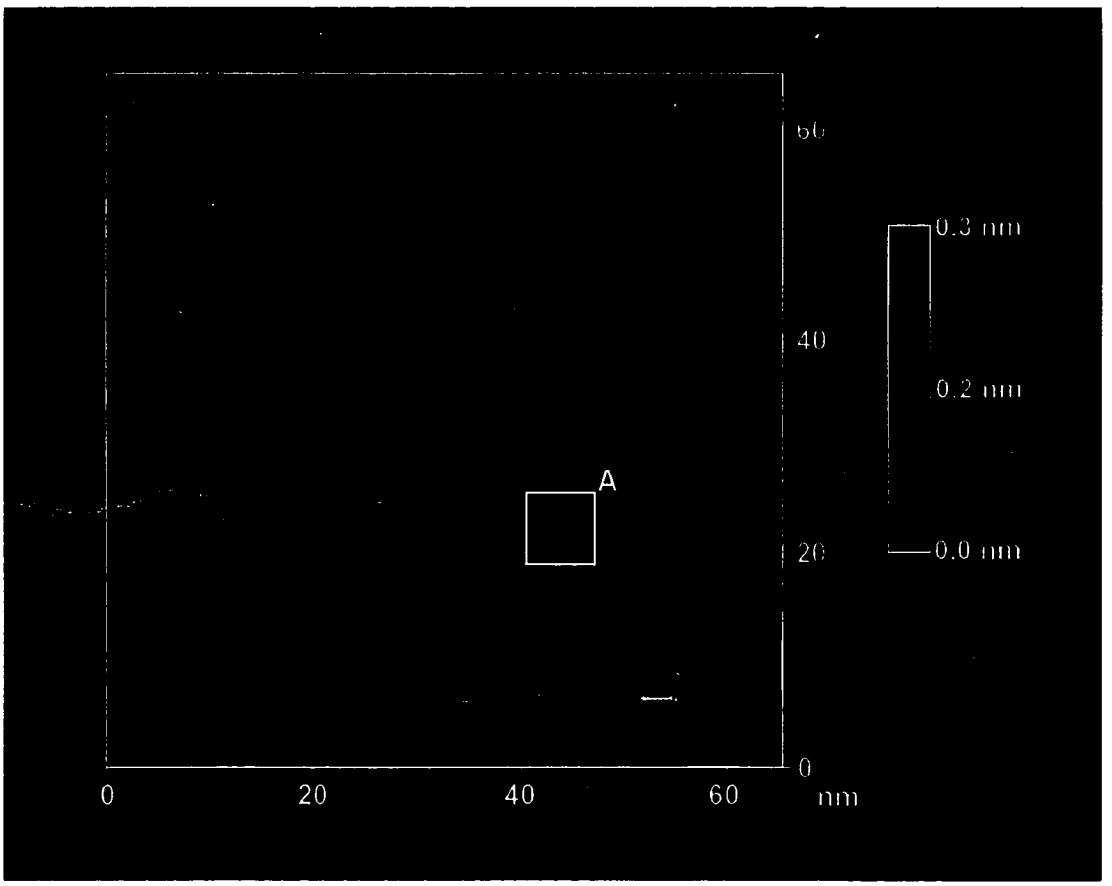

Figure 2.9. Scanning tunneling microscope image of a monolayer formed from $(C_7S)_2$. tunneling current: 400 pA, Bias voltage: -200 mV.

Atomic Force Microscopy. The images obtained using AFM also reflect the similarities and differences between thiol and disulfide monolayers on a microscale. AFM of alkanethiols adsorbed at Au(111) has been previously described [41]. Disulfide images, such as that shown in Figure 2.10, also display the hexagonal packing pattern characteristic of thiol monolayers. However, the size of the ordered regions were generally smaller than the ordered domains seen with thiol monolayers. For the disulfide images, ordered domain sizes of 30 nm^2 or less were observed. In contrast, the ordered domains in the thiol images are typically in the 20-40 nm^2 range a few regions more than 70 nm^2 in size [42].

The results in Figure 2.11 summarize the differences found for the two types of systems. The data were developed by determinations of domain sizes in AFM images for the layers formed from decanethiol and di-*n*-decyl disulfide. As is evident, the thiol layer exhibits a larger domain size in comparison to the disulfide layers. Importantly, this finding is consistent with the results from the above macro- and microscopic characterizations. Both the STM and AFM data also provide insights into the origin of the disorder found in the macroscopic characterizations. The difference in the sizes of the ordered regions determined from AFM relative to those determined with STM is attributed to the differing imaging mechanisms of the two techniques. We believe that imaging takes place near the sulfur head group with STM and close to the chain ends with AFM [41]. Thus, it becomes apparent that both the thiol and disulfide monolayers exhibit more disorder near the outermost portion of the monolayer structure.

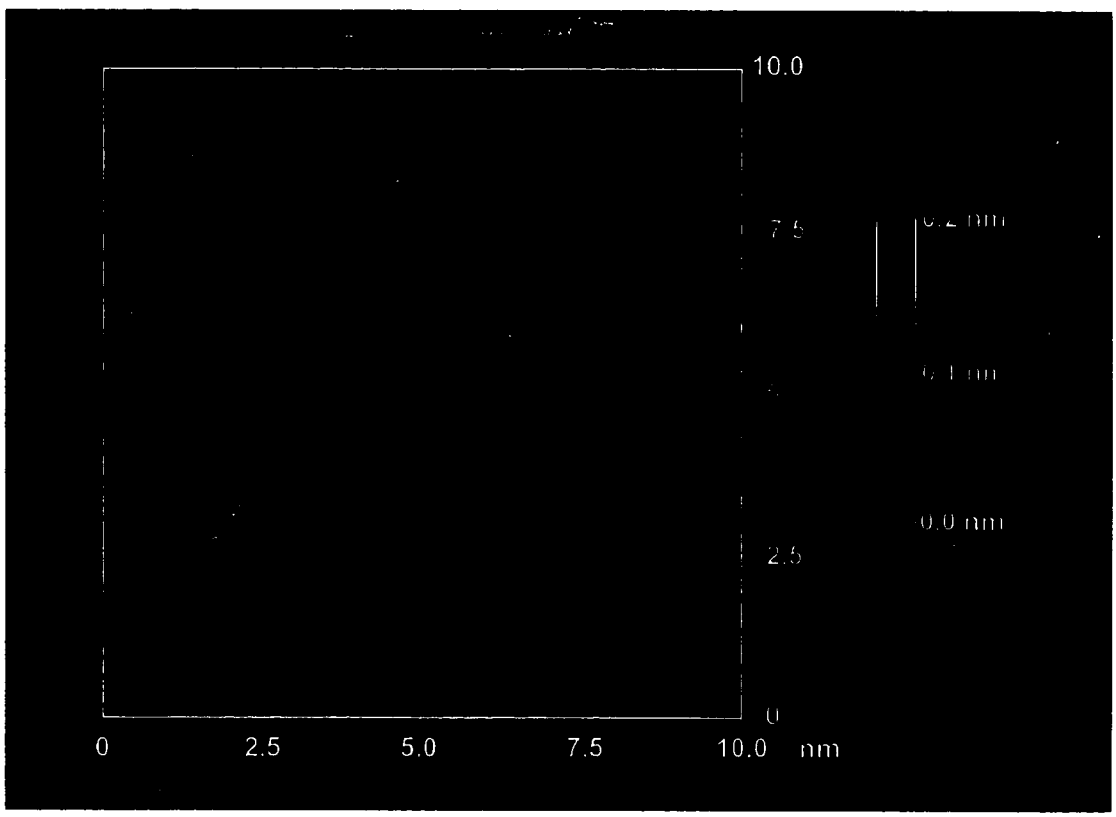

Figure 2.10. Atomic force microscope image of a monolayer formed from $(C_{10}S)_2$. Image was low pass filtered.

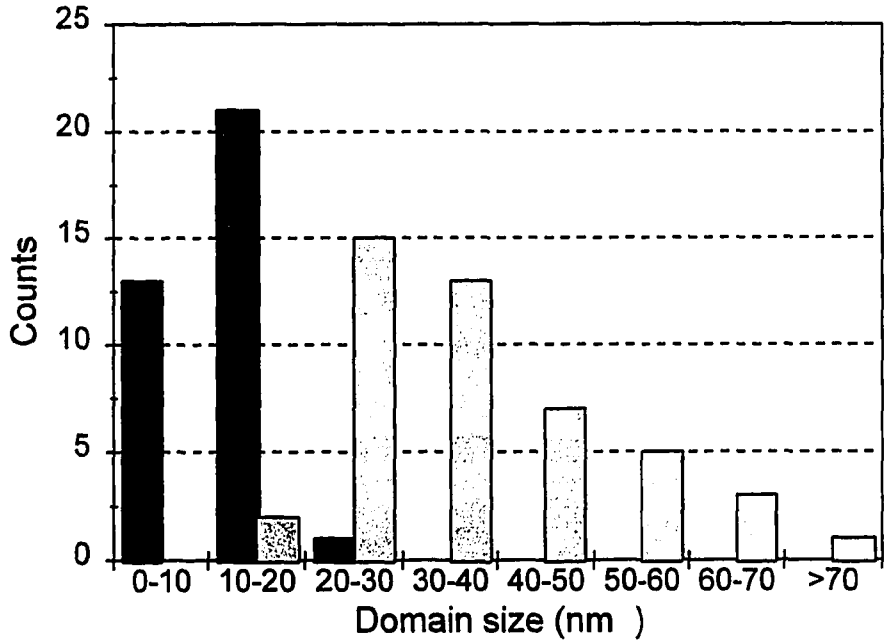

Figure 2.11. Comparison of the average size of ordered domains observed in AFM for monolayers formed from dialkyl disulfides and alkanethiols.

Defect Refilling Experiments. In order to probe the characteristics of monolayer defects which result from assembly from disulfide solutions, a series of "refilling" experiments were conducted. The rationale behind this study was to determine if the defects resulting from assembly from disulfides were of larger size than those resulting from thiol assembly.

First, monolayers were assembled from octadecane thiol and octadecyl disulfide solutions under typical conditions and examined using IRRAS and reductive desorption. Fresh samples of these films were immersed for varying times in 0.5 mM 16-mercaptohexadecanoic acid (MHA) solution, emmersed, rinsed and examined as the octadecyl samples. MHA was chosen to provide a spectroscopic tag for any refilling which may occur.

For brief (1 min) immersion in MHA solution, essentially no changes were observed in either the IR spectra or desorption voltammetry for both the thiol- and disulfide-derived monolayers. With prolonged immersion (1 hr), the disulfide monolayers showed a small (~10 %) increase in Q_{rd}, approaching the value for thiol monolayers. Spectra for these samples, however, did not show the presence of the ν(C=O) for MHA, although this may be due to orientation or limit of detection. Prolonged immersion of octadecanethiol-derived monolayers in the MHA solution showed no evidence for increased Q_{rd}. These results may indicate that the size distribution of the defects in disulfide-derived monolayers may be skewed toward larger diameters which are large enough to accommodate additional thiol adsorbates, but too small to accommodate the added bulk of a disulfide.

Conclusions

Evidence relating structure and coverage of disulfide monolayers adsorbed at Au(111) to thiol monolayers at the same surface has been presented. Generally, thiols and disulfides form the same surface adsorbed thiolate, however subtle differences in the surface structure

exist. The results indicate that disulfide layers have a lower surface coverage, resulting in a higher propensity of defects.

Because of their less well packed structures, disulfide films exhibit poorer barrier properties than their thiol counterparts. The added kinetic limitations imposed by the addition of the second thioalkyl moiety preclude the formation of a well packed monolayer assembly. The apparent absence of an annealing process which would lead to a well packed structure points to the formation of a stable, relatively immobile gold-sulfur linkage.

References

1 .Ulman, A. *An Introduction to Ultrathin Organic Films: from Langmuir-Blodgett to Self Assembly*; Academic Press: San Diego, CA, 1991.

2 . Dubois, L. H.; Nuzzo, R. G. *Annu. Rev. Phys. Chem.* **1992**, *43*, 437-463.

3 . Porter, M. D.; Bright, T. B.; Allara, D. L.; Chidsey, C. E. D. *J. Am. Chem. Soc.* **1987**, *109*, 3559-3568.

4 . Resent STM studies have revealed the presence of non-($\sqrt{3} \times \sqrt{3}$) submonolayer phases in these samples, as well as the presence of a ($\sqrt{3} \times \sqrt{3}$)-based c(4 × 2) superlattice. See references 39-40 for examples.

5 . Bain, C. D.; Biebuyck, H. A.; Whitesides, G. M. *Langmuir* **1989**, *5*, 723-727.

6 . Nuzzo, R. G.; Zegarski, B. R.; Dubois, L. H. *J. Am. Chem. Soc.* **1987**, *109*, 733-740.

7 . Nuzzo, R. G.; Allara, D. L. *J. Am. Chem. Soc.* **1983**, *105*, 4481-4483.

8 . Nuzzo, R. G.; Fusco, F. A.; Allara, D. L. *J. Am. Chem. Soc.* **1987**, *109*, 2358-2368.

9 . Whitesides, G. M.; Laibinis, P. E. *Langmuir*, **1990**, *6*, 87-96.

10 . Biebuyck, H. A.; Bain, C. D.; Whitesides, G. M. *Langmuir* **1994**, *10*, 1825-1831.

11 . Hagenhoff, B.; Benninghoven, A.; Spinke, J; Leley, M.; Knoll, W. *Langmuir* **1993**, *9*, 1622-1624.

12 . Taniguchi, I.; Iseki, M.; Yamaguchi, H.; Yasukouchi *J. Electroanal. Chem.* **1985**, *186*, 299-307.

13 . Taniguchi, I.; Iseki, M.; Yamaguchi, H.; Yasukouchi J. *Electroanal. Chem.* **1984**, *175*, 341-348.

14 . Garrell, R. L.; Szafranski, C.; Tanner, W. *SPIE Raman an Luminescence Spectroscopies in Technology II* **1990**, *1336*, 264-271.

15 . Szafranski, C. A.; Tanner, W.; Laibinis, P.; Garrell, R. L. *Langmuir* (submitted) **1994**.

16 . Strong, L.; Whitesides, G. M. *Langmuir*, **1988**, *4*, 546-588.

17 . Porter, M. D.; Bright, T. B.; Allara, D. L.; Chidsey, C. E. D., unpublished results.

18 . Widrig, C. A.; Alves, C. A.; Porter, M. D. *J. Amer. Chem. Soc.* **1991**, *113*, 2805-2810.

19 . Walczak, M. M.; Alves, C. A.; Lamp, B. D.; Porter, M. D. *J. Electroanal. Chem.* **1995**, *396*, 103-114.

20 . Stole, S. M.; Porter, M. D. *Appl. Spec.* **1990**, *49*, 1418-1420.

21 . Walczak, M. M.; Chung, C.; Stole, S. M.; Widrig, C. A.; Porter, M. D. *J. Am. Chem. Soc.* **1991**, *113*, 2370-2378.

22 . Lindberg, B. J.; Hamrin, K.; Johansson, G.; Gelius, U.; Fahlman, A.; Nordling, C.; Siegbahn, K. *Physica Scripta* **1970**, *1*, 286-298.

23 . Widrig, C. A.; Chung, C.; Porter, M. D. *J. Electroanal. Chem.* **1991**, *310*, 335-359.

24 . Walczak, M. M.; Popenoe, D. D.; Deinhammer, R. S.; Lamp, B. D.; Chung, C.; Porter, M. D. *Langmuir* **1991**, *7*, 2687-2693.

25 . Weisshaar, D. E.; Lamp, B. D.; Porter, M. D. *J. Am. Chem. Soc.* **1992**, 114, 5860-5862.

26 . Weisshaar, D. E.; Walczak, M. M., Porter, M. D. *Langmuir* **1993**, *9*, 323-329.

27 . Zhong, C. J.; Porter, M. D. *J. Am. Chem. Soc.* **1994**, *116*, 11616-11617.

28 . Desorption at rougher gold surfaces exhibits miltiple waves, which we attribute to adsorption at the larger number of atomic steps present at these surfaces [19].

29 . During the desorption process, at most 18 mC/cm^2 is required to charge the electrical double layer (Zak, J.; Simmons, N. J.; Porter, M. D., in preparation). This, as well as the ±10% sample to sample variability must be considered in discussiond relating Q_{rd} to monolayer coverage. Our recent desorption modelling studies (Zhong, C. J.; Porter, M. D., in preparation) support the validity of our coverage analysis.

30 . Hill, I. R.; Levin, I. W. *J. Chem. Phys.* **1979**, *70*, 842-851.

31 . Durig, J. R.; Thompson, J. W.; Thyagesan, V. W.; Witt, J. D. *Journal of Molecular Structure* **1975**, *24*, 41-58.

32 . Nuzzo, R. G.; Dubois, L. H.; Allara, D. L. *J. Am. Chem. Soc.* **1990**, *112*, 558-569.

33 . Walczak, M. M.; Chung, C.; Stole, S. M.; Widrig, C. A.; Porter, M. D. *J. Am. Chem. Soc.* **1991**, *113*, 2370-2378.

34 . Cassie, A. B. D. *Disc. Farad. Soc.* **1948**, *3*, 11-16.

35 . Johnson, R. E.; Dettre, R. H. *J. Phys. Chem.* **1964**, *68*, 1744-1750.

36 . Johnson, R. E.; Dettre, R. H. *J. Phys. Chem.* **1965**, *69*, 1507-1515.

37 . Whitesides, G. M.; Laibinis, P. E. *Langmuir* **1990**, *6*, 87-96.

38 . McDermott, C. A.; McDermott, M. T.; Green, J.-B., Porter, M. D. *J. Phys. Chem.* **1995**, *99*, 13257-13266, and references therein.

39 . Poirier, G. E.; Tarlov, M. J. *Langmuir* **1994**, *10*, 2853-2856.

40 . Poirier, G. E.; Tarlov, M. J.; Rushmeier, H. E. *Langmuir* **1994**, *10*, 3383-3386.

41 . Alves, C. A., Smith, E. L.; Porter, M. D. *J. Am. Chem. Soc.* **1992**, *114*, 1222-1227.

42 . It is worth noting that the thiol data may be skewed toward large domain size simply due to the conventions used in data acquisition, that is, generally images with the largest attainable ordered domains are preserved. So, sampling at lower domain sizes may be inadequate.

3. AN IN SITU INFRARED SPECTROSCOPIC EXAMINATION OF STRUCTURAL CHANGES AT ALKANETHIOLATE-MODIFIED GOLD ELECTRODES AT DESORPTION POTENTIALS

Introduction

In recent years, a host of information has been obtained regarding the structure and applications of thiolate based monolayer films on metal surfaces [1, 2]. Studies indicate that these materials form comparatively well ordered, covalently bound , stable monolayer structures at the electrode surface. Such properties should lend to their utility as model structures for the study of interfacial systems. While a large base of information exists concerning the molecular structure in these systems, the bulk of the data pertains to ex situ characterizations. To asses fully the utility of thiolate based monolayers, corresponding studies which characterize the in situ behavior of these systems need to be undertaken. To date, however, only a small number of these studies have been done [3-8], primarily due to the difficulties developing methods for molecular characterizations under typical electrochemical conditions.

The bulk of the in situ characterization studies of monomolecular films have involved the utilization of optical techniques such as infrared reflectance absorbance spectroscopy (IRRAS), surface enhanced Raman spectroscopy (SERS), and second harmonic generation (SHG). These techniques previously have been able to provide a large amount of information involving the structure of chemically modified electrodes and of the electrode/electrolyte interface in general [9-12]. Each of these measurements have their own set of complications which limit the scope of their utility. While SERS [13] and SHG [14],

are well suited for most aqueous environments, the relationship between signal and orientation in the monolayer film are not entirely straightforward. In the case of infrared spectroscopy, while the relation between molecular orientation and infrared signal are well characterized, the large absorbance of most typical electrochemical solvents presents a formidable problem [9]. Several adaptations of the IRRAS technique have been utilized to minimize this situation, the majority of which utilize a modulation in the applied potential at the electrode to compensate for solution absorbance [7, 15-21,]. Polarization modulation infrared spectroscopy (PMIRS) has also been utilized to study structure at the electrode/electrolyte interface. The PMIRS technique takes advantage of the preferential excitation of surface species by p-polarized light to cancel contributions of solution species [5, 8].

We have previously described a method by which absolute spectra of species adsorbed at electrode surfaces can be studied by in situ IRRAS without modulation techniques [3, 4]. This method allows the collection of spectra with respect to an independent reference substrate, analogous to an ex situ measurement. The intensity of solvent bands is reduced in this technique by "matching" the solution layer thickness of the reference and sample spectra. This particular method is ideally suited to the study of aliphatic C-H bands in alkanethiolate monolayers since these bands fall outside the regions obscured by typical electrochemical solvents.

We have been interested in the characterization of potential-dependent structural changes of sulfur-derivatized compounds adsorbed at gold electrodes. A technique which has

been utilized quite readily in our group has been electrochemical reductive desorption which involves the application of a cathodic voltage sweep (or step) which induces gold-sulfur bond reduction and desorption of the monolayer film.

Of particular interest is the observation of any structural changes in the film that result from application of these potentials. Previous experiments at less severe potentials have shown little evidence for structural change [8]. However, at potentials nearing desorption, larger changes might be expected due to compensation for ion penetration into the film.

The application of large cathodic potentials has been recently shown to result in cleavage of the gold-sulfur bond and desorption of the thiolate monolayer [22-24]. What remains to be investigated in this process are any structural changes which occur prior to and after the application of the desorption potential. Such information could provide useful insights into the method by which these relatively stable films break down to allow ion and solvent penetration.

This chapter describes a series of infrared spectroscopic measurements which monitor the structure of alkanethiolate films subject to desorption potentials. The experiments are conducted utilizing monolayers terminated with methyl and acid functionalities in basic deuterium oxide solutions to mimic closely conditions undertaken in electrochemical desorption experiments. Results of this study provide insight into the potential-dependent and double layer structure present in these experiments.

Experimental

Materials. Decanethiol (C_{10}), sodium deuteroxide, and deuterium oxide (99.9 atom% D) were purchased from Aldrich and used as received. Octadecanethiol (C_{18}) (Aldrich), was recrystallized twice from ethanol prior to use. Absolute ethanol (Quantum) was used for all monolayer formation solutions. 11-mercaptoundecanoic acid was synthesized from 11-bromoundecanoic acid by a previously described procedure [25].

Electrode preparation. Electrodes were prepared by the evaporation of gold onto glass or prepolished stainless steel plungers. Prior to evaporation, the stainless steel plungers were polished to a mirror finish with 0.5 μm diamond paste on a felt pad and rinsed repeatedly in hexane and water to remove polishing residue. Immediately prior to evaporation, both glass and stainless steel electrodes were cleaned in piranha solution (1:1 30% H_2O_2: concentrated H_2SO_4), **Caution!** *Piranha solution reacts violently with organic compounds and should be disposed of immediately after use.* After cleaning, the electrodes rinsed with water and methanol, and dried under argon.

All evaporations were conducted in a cryopumped Edwards (Wilmington, MA) model E306A coating system at a base pressure of 1×10^{-6} torr. Once base pressure was obtained, a 15 nm chromium adhesive layer was deposited on the substrates at a rate of 0.1 nm/s. Following chromium deposition, 300 nm of gold was deposited at a rate of 0.3-0.4 nm/s. After cooling, the system was backfilled with nitrogen and the samples removed.

Instrumentation and cell design. Infrared spectra were collected using an auxiliary bench which is attached to a Nicolet MAGNA 750 infrared spectrometer utilizing a narrow band liquid nitrogen cooled MCT detector. The auxiliary optics have been previously described [4] and allow for reproducible repositioning of the spectroelectrochemical cell during data collection. Data collection consists of 500 co-added scans at 4 cm^{-1} resolution with one level of zero filling.

The cell configuration used in this study has been previously described [4], and is shown in Figure 3.1. Basically, the cell consists of a Kel-F body which has been bored out to accept Kel-F sheathed glass or stainless steel plungers. The face of the plunger has been mechanically polished and coated with 300 nm of gold preceded by a 15 nm adhesive layer of chromium. The end opening of the cell is covered with a hemispherical window of calcium fluoride which is sealed to the cell body by a Viton O-ring. The gold coated plungers are pressed up to the back of the CaF_2 window, resulting in a solution layer thickness on the order of 1 μm, as evidenced by the observation of Newton's rings at the interface.

Electrochemical control was accomplished with a Bioanalytical Systems (West Lafayette, IN) CV-27 potentiostat, accompanied by an x-y recorder (The Recorder Company). A Ag/AgCl (saturated KCl) reference electrode was used in all experiments. All potentials herein are quoted with respect to this reference.

Experimental Protocol. Initially, the $C_{18}D_{37}S$/Au reference plunger was inserted into the cell, the cell filled with electrolyte solution, and the plunger pressed up against the

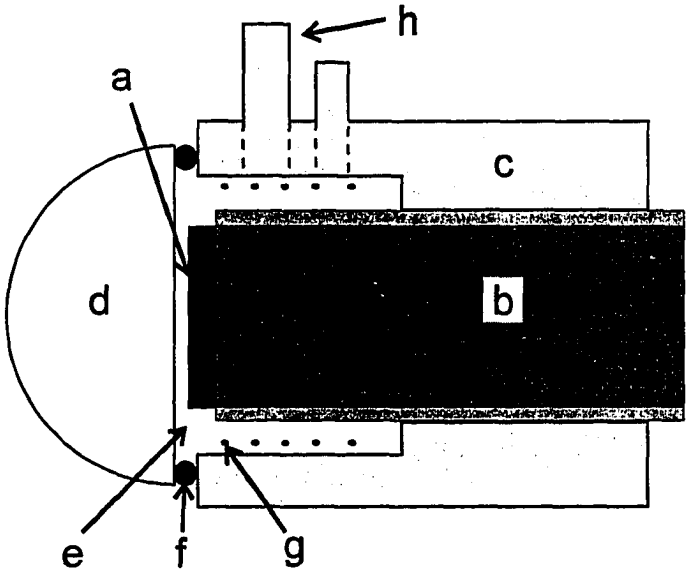

Figure 3.1. In situ cell design. a. electrode surface evaporated onto either glass or stainless steel plungers, b. Kel-F sheath, c. Kel-F cell body, d. IR transparent hemispherical window (CaF_2, ZnSe), e. solution reservoir, f. O-ring seal, g. platinum counter electrode, h. ports for reference electrode and solution introduction. Working electrode contact is made through the rear of the stainless steel plunger.

back of the CaF_2 hemisphere until the presence of Newton's rings was observed. Upon assembly, the cell was placed in the auxiliary bench of the spectrometer and aligned to yield maximum reflected signal. After purging, a set of reference spectra were collected, and the reference plunger removed.

Sample spectra were obtained by inserting the sample plunger into the cell assembly, pressing the plunger lightly against the hemispherical window, and inserting the assembly into the external bench. Once in the optical path, the position of the plunger in the assembly was adjusted to maximize sample intensity in preliminary scans, while minimizing the presence of solvent absorbance. A set of sample spectra were then collected and ratioed to the reference spectra to generate the resulting absolute in situ data.

For potential-dependent spectra, the electrode potential was swept at 10 mV/s to the potential of interest and held constant during data while collecting the spectra. The electrochemical current was given sufficient time (~5 min) to equilibrate prior to data collection. Data collection time was on the order of five minutes per spectrum.

Results and Discussion.

Figure 3.2 presents a series of absolute in situ spectra for a C_{18} monolayer under potential control. Mode assignments and peak positions for the spectra at the potential extremes, as well as for open circuit in situ and ex situ spectra are presented in Table 3.1. As evident in the spectra, essentially no structural changes are observed until E_{app} is -1.30 V. At this potential, the onset of solvent reduction convolutes the spectral information with changes

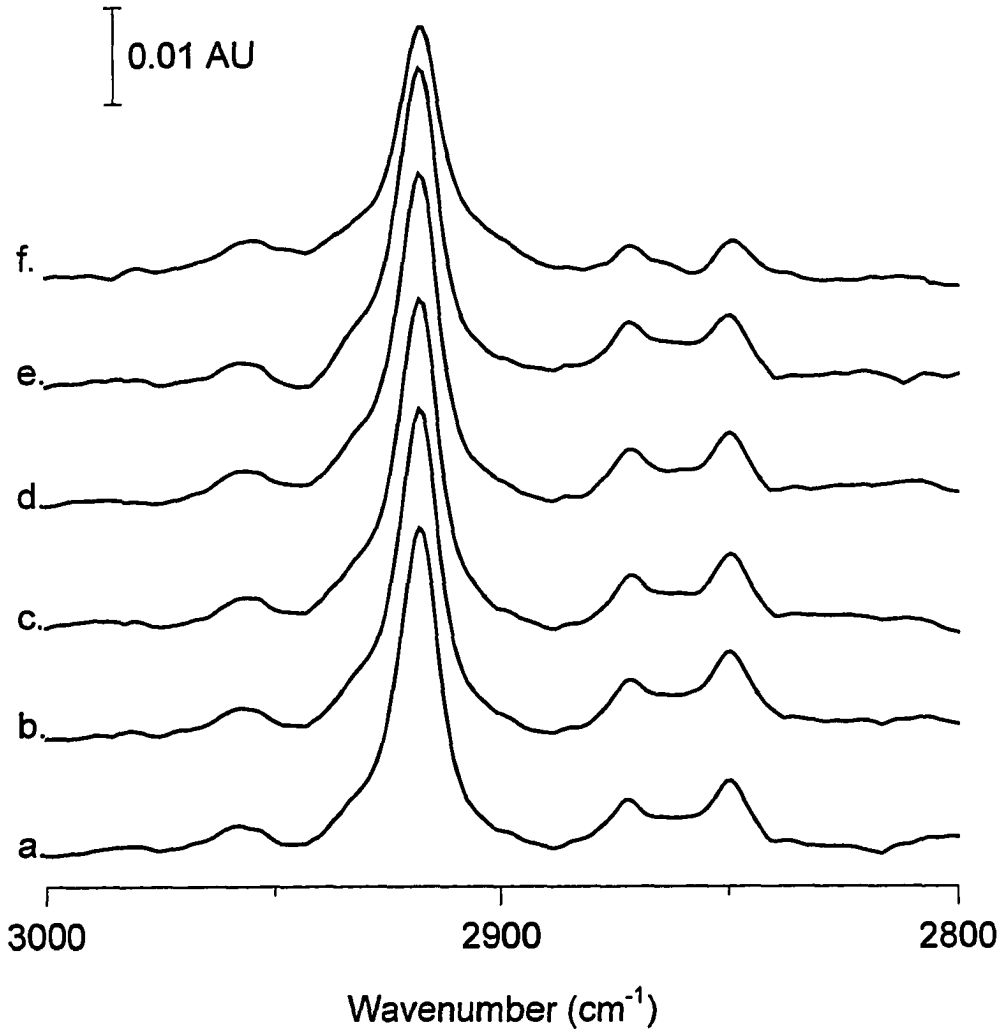

Figure 3.2. Potential dependent in situ reflectance spectra of C_{18}/Au under 0.4 M NaOD in D_2O. Applied potentials: a. -0.40 V, b. -0.80 V, c. -1.00 V, d. -1.10 V, e. -1.20 V, f. -1.30 V.

Table 3.1. Peak position as a function of applied potential (E_{app}) for monolayers of $CH_3(CH_2)_{17}SH$, $CH_3(CH_2)_9SH$, and $HOOC(CH_2)_{11}SH$ assembled at gold.

		Peak Position (cm^{-1})				
Monolayer	E_{app} (V)	$\nu_a(CH_3)$	$\nu_s(CH_3)_{FR1}$	$\nu_a(CH_2)$	$\nu_s(CH_3)_{FR2}$	$\nu_s(CH_2)$
$CH_3(CH_2)_{17}S/Au$	ex situ	2963	a	2918	2877	2850
	OC	2958	a	2918	2872	2850
	-0.40	2958	a	2918	2872	2850
	-1.20	2957	a	2918	2871	2850
$CH_3(CH_2)_9S/Au$	ex situ	2964	2935	2921	2878	2850
	OC	2958	a	2925	2872	2856
	-0.40	2958	a	2925	2872	2856
	-1.15	2956	a	2926	2871	2856
$HOOC(CH_2)_{11}S/Au$	OC	b	b	2922	b	2854
	-0.40	b	b	2921	b	2854
	-1.15	b	b	2927	b	2857

[a]Band not observed due to overlap of the $\nu_a(CH_2)$ mode.
[b]Modes not present in the adsorbate molecule.

in the solution layer. However, it is apparent that the overall intensity of each of the methylene modes remains essentially constant up to this potential, indicating, as previously reported for smaller potential excursions [8], that the structure of C_{18} monolayer films is stable throughout this potential range.

The above assertion is supported by the positions of the C-H stretching modes listed in Table 3.1. In particular, the positions of the methylene modes correspond to polymethylene chains in an densely packed environment [26, 27]. This is not unexpected, given the hydrophobicity of the monolayer surface in the presence of a strongly hydrophilic solution. The relatively small changes in the positions of the methyl groups also provide evidence for the stability of the C_{18} film at a variety of potentials.

Examination of the potential dependent in situ spectra of a shorter chain methyl-terminated alkanethiolate monolayer, C_{10}, yields similar results, as shown in Figure 3.3 and Table 3.1. Even at open circuit potential, the positions of the methylene modes are at considerably higher energy than in the ex situ spectrum, indicating an inherent decrease in the crystallinity of the film. This is not unexpected due to the increased permeability which has been demonstrated for shorter chain monolayer films [28].

The methyl modes, however, are slightly more influenced by potential than in the C_{18} case. Both observed bands tend to move to lower energy and diminish slightly in magnitude as the potential shifts increasingly negative, with the most pronounced change in the $\nu_a(CH_3)$ mode [29]. The shift to lower energy may indicate a change in average orientation of the methyl group in which the out-of-plane component of the methyl mode is oriented closer to the surface normal. Such changes have been previously observed for C_{18} films under nonaqueous solvents and electrolytes [3, 8].

Most notable is the lack of dramatic changes in the infrared spectra with prolonged application of potential which should drive desorption. This lack of change may still be due to the dramatic difference in the hydrophobicity of the alkyl chains in the monolayer and the hydrophilic solvent/electrolyte system. There may also be a contribution from solubility considerations which result from the cell design. Assuming complete desorption into the thin solution layer, a thiolate concentration on the order of 10 μM is generated. Any desorbed thiolate must diffuse along this thin layer to reach bulk solution and to leave the

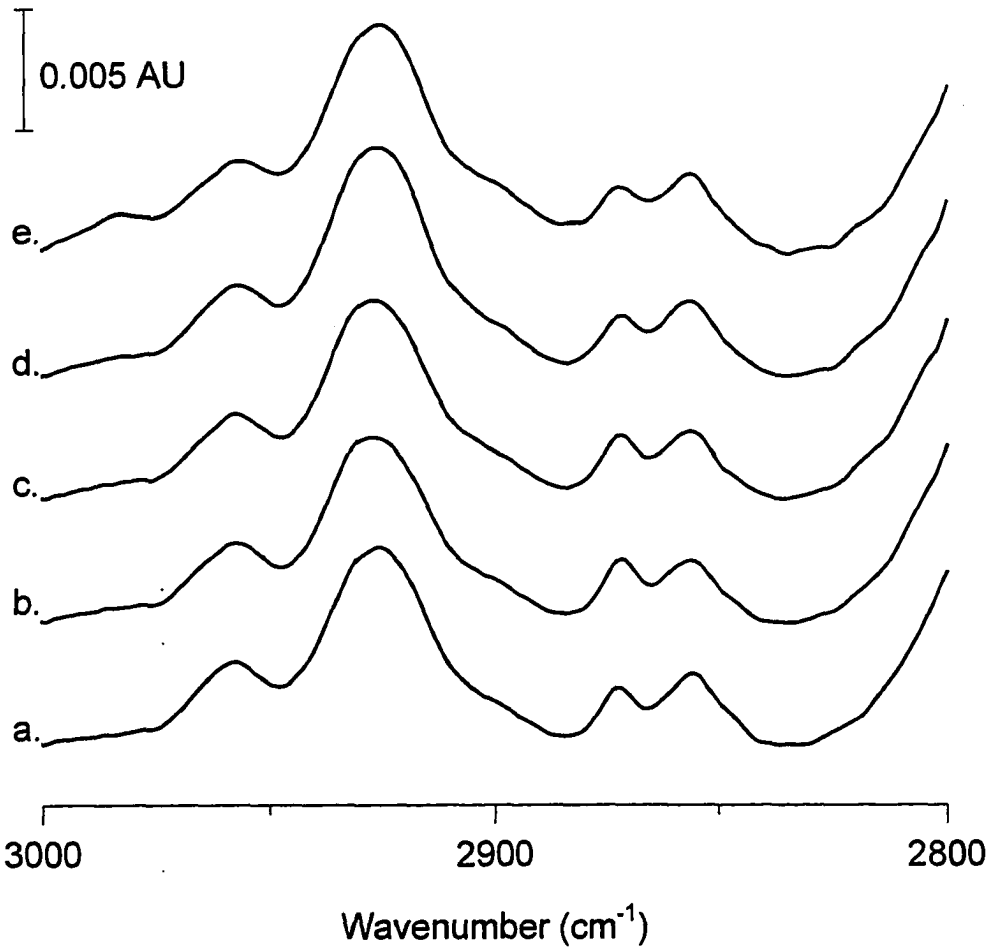

Figure 3.3. Potential dependent in situ reflectance spectra of C_{10}/Au under 0.4 M NaOD in D_2O. Applied potentials: a. -0.40 V, b. -0.80 V, c. -1.00 V, d. -1.10 V, e. -1.15 V. The rise at the low energy side of the spectra is due to presence of the O-D stretch of the solvent.

optical path. The relative immiscibilty of the thiolate in this highly polar electrolyte system evidently precludes such a diffusional process.

To better assess the diffusional characteristics of the desorption mechanism, a monolayer system consisting of a carboxylic acid terminated alkanthiolate was studied. At the pD of these studies, this acid functionalized species should be appreciably more soluble in the electrolyte solution, resulting in better evaluation of the diffusional characteristics of desorbed thiolate films.

Figure 3.4 presents the potential dependent infrared spectra for a monolayer of 11-mercaptoundecanoic acid (MUA) adsorbed at gold, at the potentials corresponding to those shown in Figure 3.2 and Figure 3.3 for methyl terminated films. As is readily apparent, the acid functionalized monolayer undergoes a much more noticeable potential-dependent structural change. Unfortunately, the corresponding spectra in the lower energy region is obscured by O-D vibrational modes, making the observation of carbonyl and carboxylate modes unattainable.

Most noticeable in the C-H region is the gradual broadening of both of the methylene stretching vibrations, accompanied by a shift in peak position to higher energy (see Table 3.1). This shift to higher energy results from an increase in disorder of the polymethyene chains in the monolayer structure. The broadening of the bands indicates a larger distribution of environments for the polymethylene chains. Even at E_{app} of -1.15 V, there is a strong contribution of the chains in their most crystalline orientation. This may be related to the "leakiness", or preferential desorption of thiolates from domain boundaries and

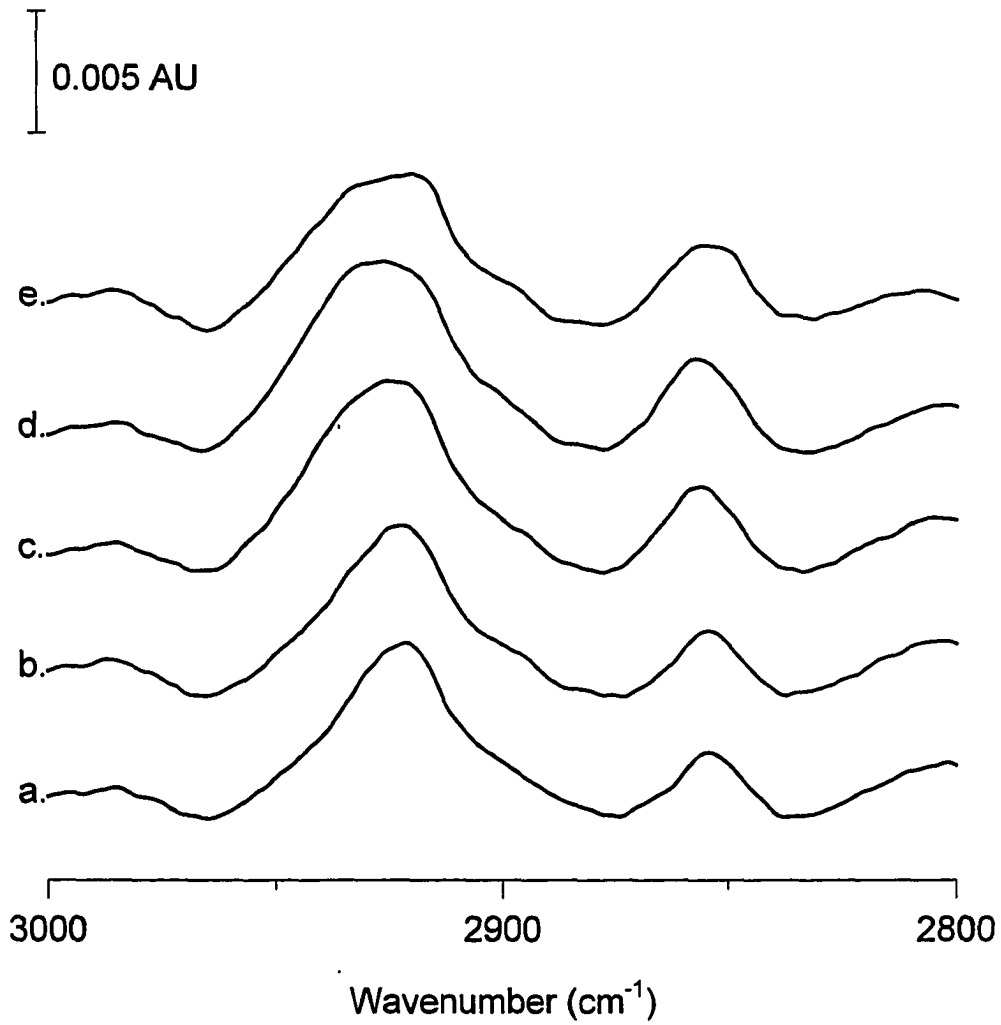

Figure 3.4. Potential dependent in situ reflectance spectra of MUA/Au under 0.4 M NaOD in D_2O. Applied potentials: a. -0.40 V, b. -0.80 V, c. -1.00 V, d. -1.10 V, e. -1.15 V.

the presence of relatively intact, ordered thiolate domains, even at extreme potentials.

Figure 3.5 presents an examination of the reversibility of the potential-dependent MUA spectra at intermediate applied potentials. These spectra were acquired by repeatedly sweeping the applied potential between -0.40 V and -1.15 V and collecting spectra at either potential extreme. The spectra in Figure 3.5a and b correspond to the spectra in Figure 3.4a and e, with the remaining spectra in Figure 3.5 collected after spectrum b.

Examination of the spectra in Figure 3.5 provides some insights into the stability of the monolayer structure with repetitive application of extreme potential. The highly reversible character of the spectra indicates that the monolayer structure is not severely disrupted by the inclusion of electrolyte and solvent molecules which result in the broadening observed in Figure 3.5b and d. This implies that the bulk of the disruption of the crystalline structure of the alkyl chains occurs either at the outer portion of the film, or in defect sites where there is sufficient free volume to accommodate the volume of counterion and solvent incorporated into the film, without severely distorting the head group binding geometry.

Prolonged application of potentials negative of -1.15 V results in irreversible decrease in intensity of both methylene modes, as shown in Figure 3.6. This prolonged application also results in increased broadening to higher energy for both modes, indicating further perturbation of the crystalline structure of the polymethylene chains.

The irreversibility of the decrease in signal intensity in the spectra suggests an overall loss of MUA adsorbate. This results from increased solubility of the acid functionalized

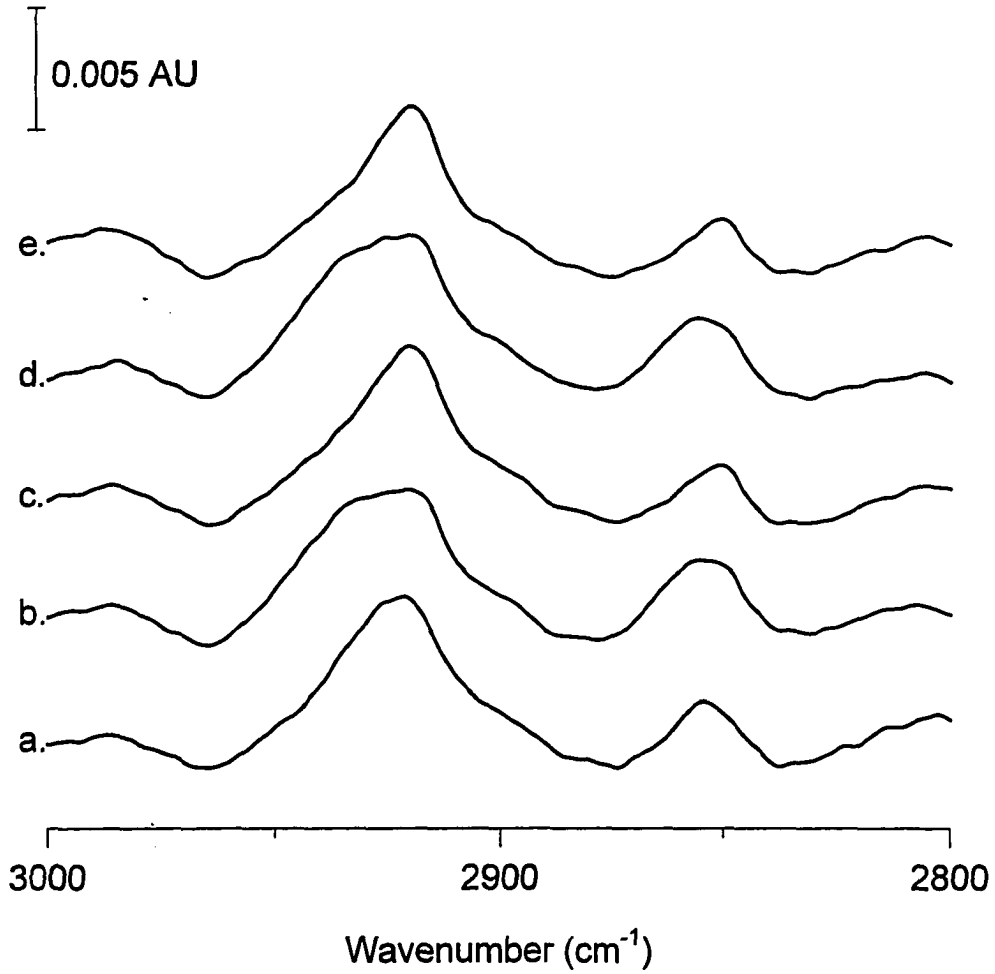

Figure 3.5. Reversibility of the potential dependent in situ reflectance spectra of MUA/Au under 0.4 M NaOD in D_2O. Applied potentials: a. -0.40 V, b. -1.15 V, c. -0.40 V, d. -1.15 V, e. -0.40 V.

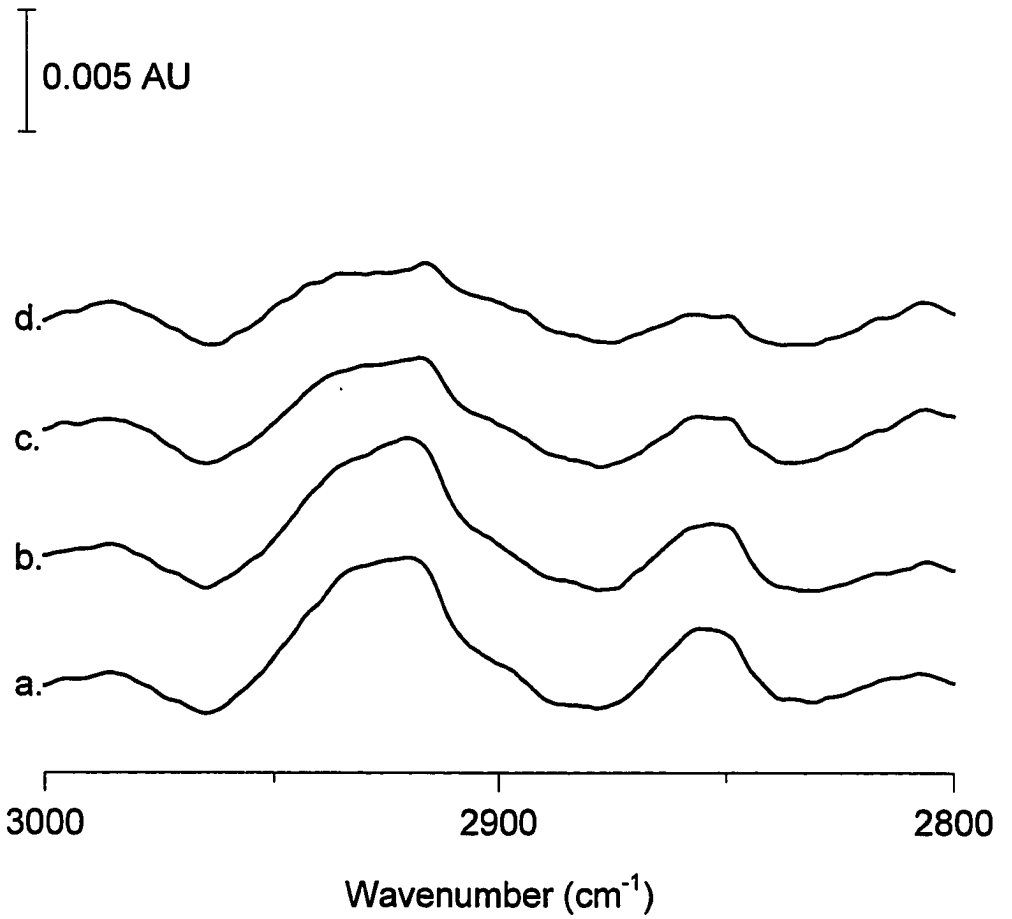

Figure 3.6. Effect of prolonged exposure to desorption potentials on the potential dependent in situ reflectance spectra of MUA/Au under 0.4 M NaOD in D_2O. Applied potentials: a. -1.15 V, b. -1.20 V, c. -1.28 V, d. -1.28 V (held for 30 min), e. -0.20 V.

thiolate versus the methyl terminated structure. The introduction of the highly polar carboxylate should serve to have a dramatic effect on the solubility of the desorbed thiolate. Concentration driven diffusion then results in a general loss of MUA from the area near the electrode surface and the optical path.

Conclusions

This study has presented results from a series of in situ structural investigations of alkanethiolate monolayer films adsorbed at gold as a function of potential. Methyl terminated films derived from the adsorption of C_{10} or C_{18} at gold present little structural dependence on applied potential, even at extreme cathodic potentials which drive desorption. The absence of structural changes may result form the differences in hyrophobicity of the strongly hydrophobic methyl terminated structures and the hydrophilic electrolyte system.

When the methyl-terminated thiolate film is replaced by a monolayer terminated by an acid functionality, the potential-dependence of the monolayer structure is dramatically increased. With increasingly cathodic potential, the monolayer film becomes increasingly disordered, until, after prolonged application of desorption potentials, the desorbed thiolate diffuses out of the optical path and into bulk solution.

Aside from the characterization data, these studies provide further evidence for the utility of in situ IRRAS in the characterization of modified electrodes in the presence of solution phases. These types of studies will prove critical in the application of such materials in areas such as chemical sensors, molecular electronics, and microfabrication.

References

1 . Ulman, A. *An Introduction to Ultrathin Organic Films: From Langmuir-Blodgett to Self-Assembly*, Academic: Boston, 1991.

2 . Dubois, L. H.; Nuzzo, R. G. *Annu. Rev. Phys. Chem.* **1992**, *43*, 437-463.

3 . Stole, S. M.; Porter, M. D. *Langmuir* **1990**, *6*, 1199-1202.

4 . Popenoe, D. D.; Stole, S. M.; Porter, M. D. *Appl. Spec.* **1992**, *46*, 79-87.

5 . Popenoe, D. D.; Deinhammer, R. S.; Porter, M. D. *Langmuir*, **1992**, *8*, 2521-2530.

6 . Duevel, R. V.; Corn, R. M. *Anal. Chem.* **1992**, *64*, 337-342.

7 . Shimazu, K.; Ye, S.; Sato, Y.; Uosaki, K. *J. Electroanal. Chem.* **1994**, *375*, 409-413.

8 . Anderson, M. R.; Gatin, M. *Langmuir* **1994**, *10*, 1638-1641.

9 . Stole, S. M.; Popenoe, D. D.; Porter, M. D. In *Electrochemical Interfaces: Modern Techniques for In-Situ Interface Characterization*; Abruña, H. D., Ed.; VCH: New York, 1991, 339-410.

10 . Foley, J. K.; Pons, S. *Anal. Chem.* **1985**, *57*, 954A-956A.

11 . Chang, S.-C.; Weaver, M. J. *J. Phys. Chem.* **1991**, *95*, 5391-5400.

12 . Seki, H. *IBM J. Res. Develop.* **1993**, *37*, 227-241.

13 . Gao, X.; Davies, J. P.; Weaver, M. J. *J. Phys. Chem.* **1990**, *94*, 6858-6864.

14 . Corn, R. M. *Anal. Chem.* **1991**, *63*, 285A-295A.

15 . Pons, S.; Bewick, A. *Langmuir* **1985**, *1*, 141-145.

16 . Habib, M. A.; Bockris, J. O. *Langmuir* **1986**, *2*, 388-392.

17 . Corrigan, D. S.; Leung, L.-W. H.; Weaver, M. J. *Anal. Chem.* **1987**, *89*, 2252-2256.

18 . Sasaki, T.; Bae, I. T.; Scherson, D. A.; Bravo, B. G.; Soriaga, M. P. *Langmuir* **1990**, *6*, 1234-1237.

19 . Chang, S.-C.; Weaver, M. J. *J. Phys. Chem.* **1990**, *94*, 5095-5102.

20 . Bae, I. T.; Huang, H.; Yeager, E. B.; Scherson, D. A. *Langmuir* **1991**, *7*, 1558-1562.

21 . Kim, C. S.; Korzeniewski, C. *J. Phys. Chem.* **1993**, *97*, 9784-9787.

22 . Widrig, C. A.; Chung, C.; Porter, M.D. *J. Electroanal. Chem.* **1991**, *310*, 335-359.

23 . Walczak, M. M; Popenoe, D. D.; Deinhammer, R. S.; Chung, C.; Porter, M. D. *Langmuir*, **1991**, *7*, 2687-2693.

24 . Weisshaar, D. E.; Lamp, B. D.; Porter, M. D. *J. Am. Chem. Soc.* **1992**, *114*, 5860-5862.

25 . Bain, C. D.; Troughton, E. B.; Tao, Y. T.; Evall, J.; Whitesides, G. M.; Nuzzo, R. G. *J. Am. Chem. Soc.* **1989**, *111*, 321-335.

26 . Snyder, R. G.; Strauss, H. L.; Elliger, C. A. *J. Phys. Chem.* **1982**, *86*, 5145-5150.

27 . MacPhail, R. A.; Strauss, H. L.; Snyder, R. G.; Elliger, C. A. *J. Phys. Chem.* **1984**, *88*, 334-341.

28 . Porter, M. D.; Bright, T. B.; Allara, D. L.; Chidsey, C. E. D. *J. Am. Chem. Soc.* **1987**, *109*, 3559-3568.

29 . The shift in peak position, while at the resolution limit of the measurement, was consistently observed for all samples examined.

4. ELECTROCHEMICAL INVESTIGATIONS OF ADSORPTION AND DESORPTION OF ALKANETHIOLATES AT STEP AND TERRACE SITES ON Au(111)

A paper to be submitted to *Langmuir*

Brian D. Lamp, Duane E. Weisshaar [1], Marc D. Porter.

Introduction

Given the widespread interest in the utilization of alkanethiolate monolayers adsorbed at gold electrodes as model systems for the study of interfacial reactivity as well as the potential application of these materials in a wide variety of settings [2-4], a fundamental understanding of the processes involved in monolayer formation is crucial. While the issues related to the chain structure have been extensively studied, little has been done to elucidate the interactions relevant to sulfur-gold bonding. Insights into the binding chemistry of the sulfur component of the alkanethiolate, as well as its influence in the structure and packing of the monolayer film, would be valuable in the design of stable, robust monolayer systems.

Recent investigations have exposed some intriguing dependencies of monolayer characteristics on the microscopic roughness of the underlying gold substrate [5, 6]. For example, the barrier properties (*i.e.* ability to block heterogeneous electron transfer) improve as the gold surface becomes microscopically rougher. This observation suggests that there is a fundamental difference in the structure of the monolayers assembled on atomically smooth substrates in comparison to a rougher, more stepped surface. That is, a monolayer formed at the smoother surface appears to be more defective than that at a rougher surface. What is

unclear is whether this difference in the external properties of the film arises from a difference in the nature of the Au-S interaction or from a difference in chain structure about the step.

In a recent report, we described the electrochemical desorption of alkanethiolate monolayers from gold films evaporated at chromium-primed glass and silicon substrates and compared the results to experiments conducted on smoother gold on mica substrates [7]. Mica substrates give surfaces which are strongly (111) terraced structures with large, flat crystallites separated by atomic steps and deeper grain boundaries. Gold films deposited on glass substrates, however, while still being heavily (111) textured, have a "rolling hill" structure which is characterized by the presence of small (111) terraces and a large number of atomic steps. Experiments at these electrodes indicate that while electrochemical desorption at mica results in essentially a single cathodic wave, desorption at the rougher glass and silicon substrates results in multiple waves. This difference was attributed to the greater heterogeneity of binding sites at the rougher surface, with the predominant waves in the desorption at glass were ascribed to (111) terrace sites for the most positive wave and to that from (100) and (110) step sites for the more negative components of the wave.

We have also presented results in which an adaptation of the electrochemical desorption experiment is conducted with the alkanethiolate precursor present in the electrolyte solution, providing insights into not only the desorption process but into the deposition process as well [8]. Surface characterizations indicate that these "electrodeposited" films show similar characteristics in the alkyl chain portion of the

monolayer, indicating that the film structure is strongly similar to those prepared by the more conventional spontaneous adsorption process.

This chapter describes an investigation in which electrochemical desorption is utilized to probe the kinetics/thermodynamics of monolayer adsorption/desorption at the different adsorption sites present at the rougher gold surfaces. The concentration and chain length dependence of the electrochemically controlled adsorption and desorption of alkanethiolates at gold will be used to assess the relative tendency for adsorption at step versus terrace sites. These findings are then examined to provide insights into the factors that influence details of the structure at rougher electrode surfaces.

Experimental

Materials. Semiconductor grade (99.9%) potassium hydroxide, propanethiol (C_3), hexanethiol (C_6), octanethiol (C_8), and decanethiol (C_{10}) were obtained from Aldrich. Tetradecanethiol (C_{14}) was obtained from Pfaltz and Bauer. All materials were used as received. Electrolyte solutions were 0.4 M KOH in an 80%:20% absolute ethanol (Quantum, punctilious grade): deionized water solvent. Such a system affords appreciable solubility of both electrolyte and the alkanethiolates, while providing an adequate solution resistance (~100 Ω/cm) for the electrochemical measurements.

Electrode Preparation. Electrodes were prepared by the resistive evaporation of gold onto either freshly cleaved mica or chromium-primed glass substrates using the subsequent procedure.

Mica substrates (The Mica Company) were cleaved with a razor blade and passed under a stream of high purity argon immediately prior to placement in the deposition chamber. Glass microscope slides (Fisher) were cleaned in piranha solution(1:1 30% H_2O_2 : conc. H_2SO_4) for ~1 hr. ***Caution:*** *The H_2O_2/H_2SO_4 solution reacts violently with organic compounds and should be handled with extreme care and disposed of immediately after use.* Samples were rinsed with deionized water and methanol (Fisher, HPLC grade), and dried under argon prior to placement in the deposition chamber.

Depositions were performed using an Edwards model E306A coating system operating at a base pressure of 10^{-6} torr. After base pressure was obtained, the glass substrates were primed with a 15 nm layer of chromium deposited at a rate of 0.1 nm s^{-1} followed by 300 nm of gold deposited at 0.4 nm s^{-1}. For the mica substrates, gold was deposited without the chromium adhesive layer.

Substrates were removed from the deposition chamber after cooling to ambient temperature. Upon removal, Au/Cr/glass electrodes were immediately stored in a dessicator until use. Au/mica electrodes were annealed for 4 hr at 300° C in a muffle furnace under ambient atmosphere and allowed to cool to room temperature before storage in a dessicator until use. With careful handling (*i.e.* storage in a dessicator and avoiding thiolate contamination), samples stored for as long as 3 weeks provided results which were indistinguishable from those obtained with samples used immediately after preparation.

Electrochemical Measurements. All electrochemical measurements were carried out in a conventional three electrode electrochemical cell with the 0.62 cm^2 geometric area of the working electrode defined by the opening in an inert elastomer O-ring. A platinum coil served as the counter electrode in all measurements. The reference electrode in all cases was a silver-silver chloride (saturated KCl) electrode; all potentials are given herein with respect to this reference.

Electrochemical data was collected using a BAS (Bioanalytical Systems, West Lafayette, IN) model CV-27 potentiostat coupled with either an X-Y recorder (the Recorder Company) or a computer controlled data acquisition system (Labtech Notebook, Laboratory Technologies). Solutions were purged with high purity argon immediately prior to use (see below).

After assembling the cell, a small (< 2 mL) volume of the thiolate containing electrolyte solution was introduced and allowed to purge for ~ 2 min. Voltammetric data were collected as according to two basic protocols. For experiments where a direct comparison to spontaneously adsorbed films was desired, the working electrode was maintained at open circuit to allow the thiolate layer to spontaneously adsorb during the purge. A potential of -0.60 V was applied. After allowing a few seconds for capacitive current to decay, the potential was swept between -0.60 V and -1.30 V until a steady state voltammogram was achieved, generally no more than two cycles.

In instances where such a comparison was not necessary, the working electrode potential was held at -1.30 V while the solution was being purged to prevent adsorption of

the thiolate film. After purge, the potential was subsequently swept between -1.30 V and -0.60 V until a steady state voltammogram was achieved, again typically no more than two cycles.

To avoid cross-contamination, each electrode was only exposed to a single thiolate chain length or concentration. For the sweep rate studies, each electrode was cycled at every sweep rate, to avoid convolution of sample to sample variability (~10% in current (i) and charge (Q) and ~10 mV in potential (E)) with the sweep rate trends.

Results and Discussion

General Observations. Figure 4.1 presents a comparison of the cyclic voltammetric current potential (CV i-E) curves that result from cycling the potential applied to the as-deposited and annealed gold electrodes between -0.60 V and -1.30 V at 100 mV/s in a 1 mM solution of octanethiol in 0.4 M KOH (80% ethanol: 20% water). The i-E curve at mica (dashed line) consists of a singe redox couple centered at -0.830 V which corresponds to the faradaic adsorption/desorption of octanethiolate at the predominately (111) terrace sites at Au/mica [8]. At Au/glass, however, two sets of waves are evident, one at -0.830 V, and the other at -1.140 V. We have attributed the presence of the additional, more negative waves at glass to the desorption of thiolate from terrace (-0.830 V) and step (-1.140 V) sites at the rougher Au/glass surface. Differences in the peak potentials of the two waves correlate well with the differences in the potential of zero charge (pzc) of Au(111) terrace sites and (110) type step sites [7, 9].

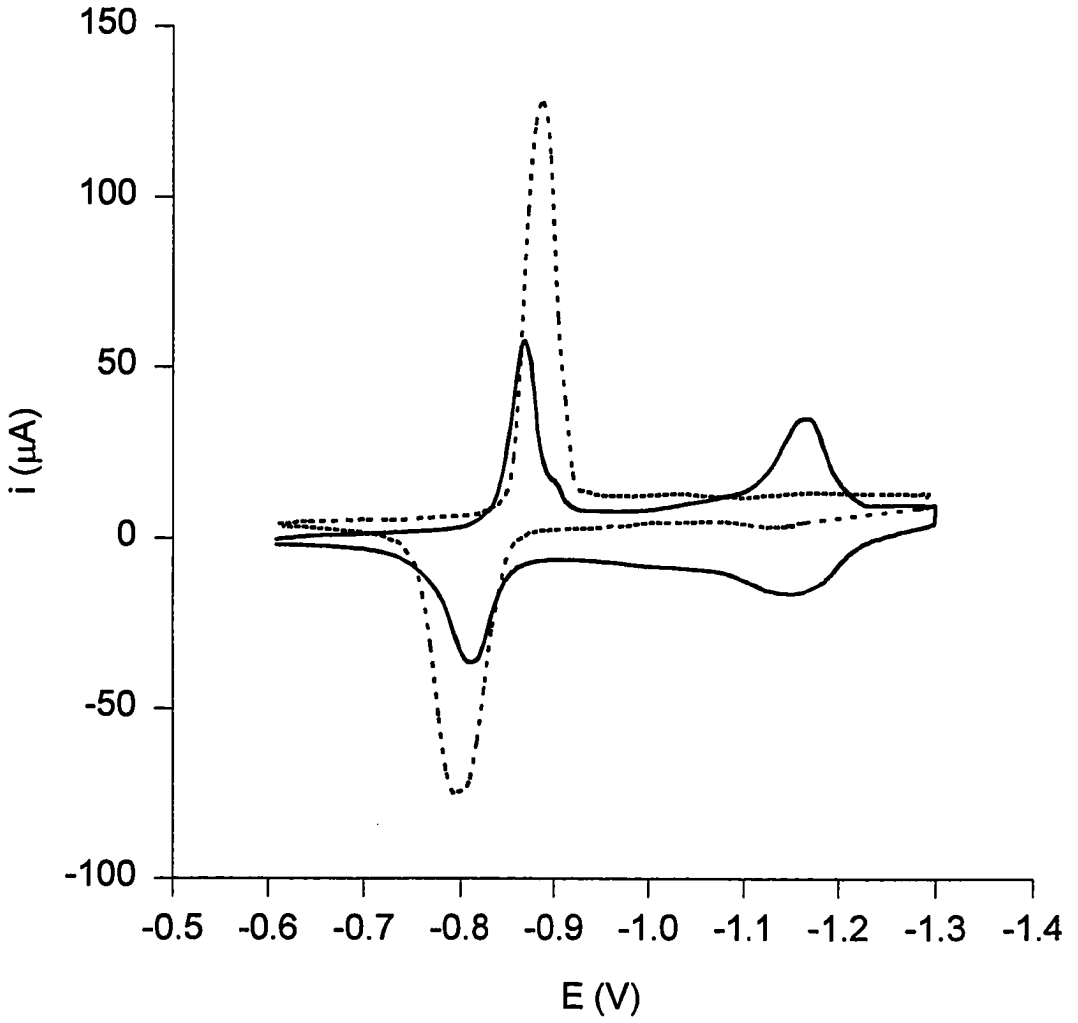

Figure 4.1. Electrochemical adsorption/desorption of C_8 at Au/mica (--------) and Au/glass (———). Experimental conditions: 1 mM C_8 in 0.4 M KOH in 80% ethanol. Sweep rate: 100 mV/s.

In an earlier study [8], the average structure of alkanethiolate monolayers generated at mica under potential control was compared with that for monolayers formed under standard spontaneous adsorption conditions. Characterizations of these films with infrared spectroscopy, wetting, and electrochemical desorption methods indicated that the two preparation schemes resulted in monolayers with chain structures that were essentially indistinguishable from each other.

Unlike those at Au/mica, voltammograms at Au/glass show a dependence on formation time. That is, at immersion times beyond that which is necessary for a complete monolayer to adsorb, voltammograms at Au/mica remain essentially unchanged while those at Au/glass exhibit waves of less defined character. While the i-E curves with the thiolate precursor in the solution consistently show two distinct waves, prolonged immersion in the thiolate solution and desorption in the absence of the precursor results in i-E curves which exhibit a larger quantity of charge passed at potentials intermediate of the two primary waves. This charge may be due to the presence of adsorption sites which may result from a gradual reconstruction of the underlying gold surface. Preliminary experiments monitoring the character of electrochemical desorption voltammetry as a function of immersion time in the assembly solution indicate an evolution of the voltammetry, in which the size of the "terrace" wave increases at the cost of the "step" wave. This evolution is attributed to the gradual reconstruction *via* surface diffusion of the step atoms into larger terraces [10].

Integration of the charge consumed under the two predominate waves provides insight into the coverage at Au/glass versus Au/mica electrodes. After accounting for surface

roughness [11], the total charge consumed in this process is 58 ± 10 $\mu C/cm^2$ and 51 ± 10 $\mu C/cm^2$ for the desorption and adsorption processes, respectively. This charge is somewhat smaller than that previously reported for electrochemical desorption of alkanethiolates from Au/mica [7]. A portion of the decreased charge can be ascribed to the typically slightly lower coverage observed for electrochemically formed films, which may be a result of slow deposition kinetics [8, 12]. This decreased total charge may also be a result on an omission of the charge consumed at potentials intermediate of the desorption peaks [13].

Chain Length Dependence. Figure 4.2 presents a series of i-E curves for the electrodeposition of several n-alkanethiolates (n = 3,6,8,10,14) at Au/glass. As previously shown for thiolates at Au/mica, the peak potential for cathodic desorption from terrace sites moves progressively negative as the chain length increases [14]. Similarly, the peak potential for adsorption at terrace sites moves progressively positive [8]. As shown in Figure 4.3, the trends in both cases are linear in n with slopes of -17 ± 2 and -9 ± 1 mV/CH_2 for desorption and adsorption respectively. These findings are independent of sweep rate (range tested: 10-1000 mV/s), consistent with earlier results obtained with Au/mica electrodes [8, 14, 15].

We believe that this difference in the slopes for adsorption and desorption processes reflects the increased influence of the alkane chain in the desorption process. For adsorption, the cohesive interactions in the alkane chain play only a minor role until a large portion of the film has been formed. At this point, formation of the remainder of the film becomes

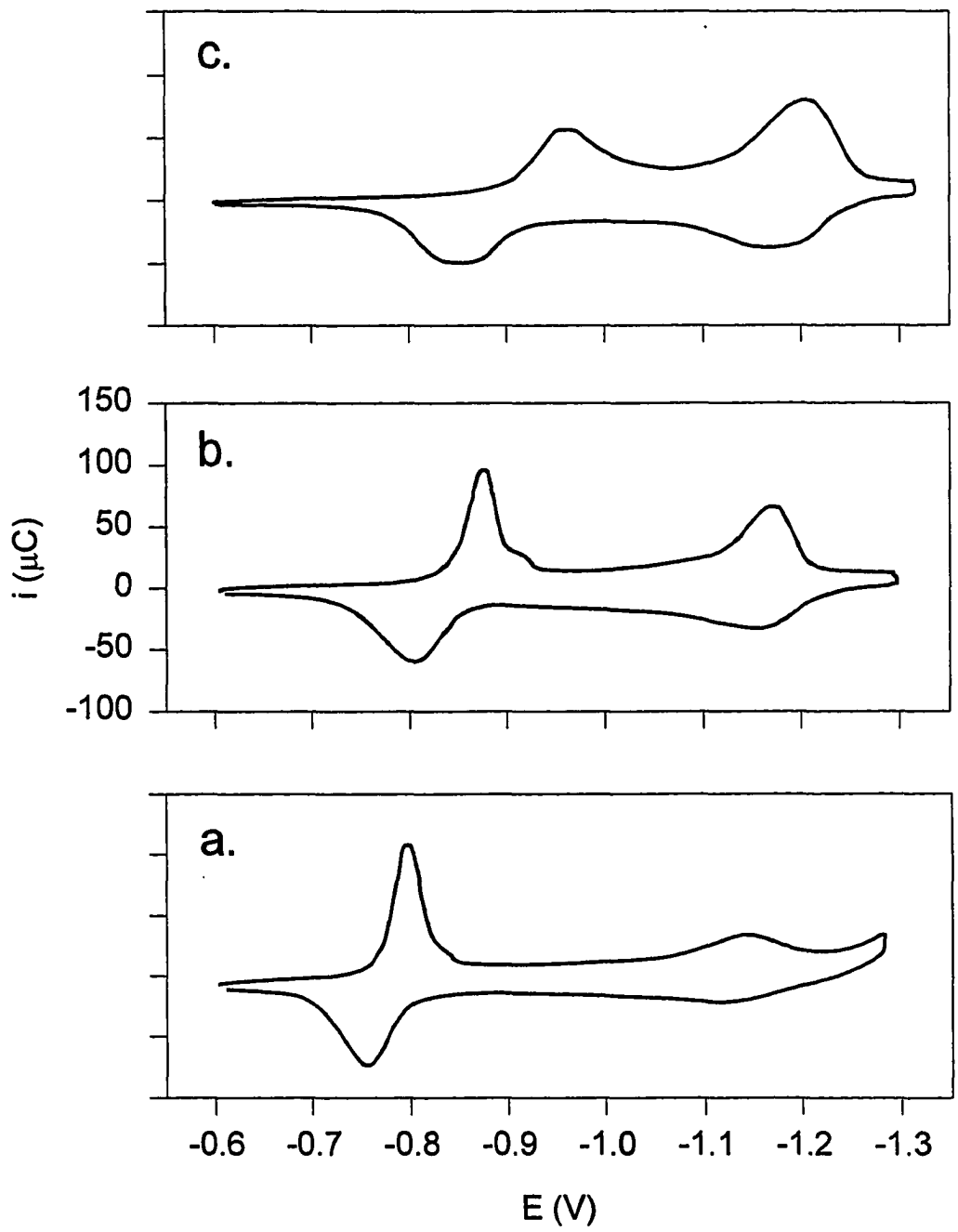

Figure 4.2. Effect of chain length on the electrochemical adsorption/desorption of C_n. a. n = 3, b. n = 8, c. n = 14. Sweep rate: 200 mV/s. All other conditions are as in Figure 4.1. Y-scale is identical for all plots.

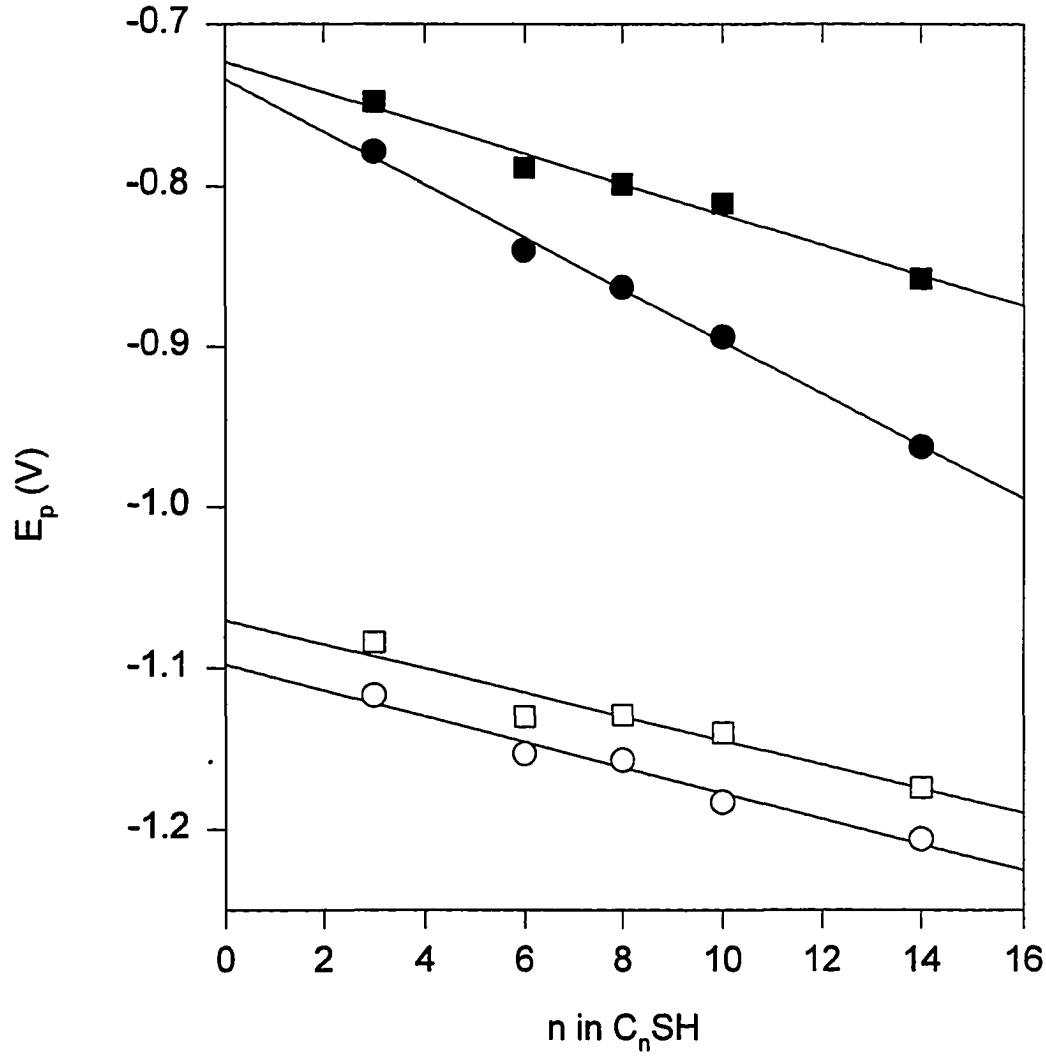

Figure 4.3. Peak potential (E_p), as a function of chain length for the data in Figure 4.2. Terrace adsorption (■), terrace desorption (●), step adsorption (□), step desorption (○). Lines represent least-squares fits to the data.

increasingly difficult. As the number of available adsorption sites diminishes, monolayer formation begins to be limited by the ability of the adsorbate as well as the monolayer film to adopt a conformation that allows penetration of the adsorbate through the film to the electrode surface. Such a rearrangement or reconstruction of the already formed film may not occur on the time scale of the voltammetric sweep. This effect will be most dramatic with longer chain lengths, given the larger degree of motion in the chain combined with larger cohesive interactions in the monolayer film [12].

For desorption, however, the capacitance of the film necessitates a larger overpotential to drive desorption as chain length increases [14], where this capacitance has its largest effect. As desorption is initiated, counter ion penetration into the structure decreases the net capacitance. We ascribe the sharp nature (full width at half maximum (FWHM) less than 60 mV for sweep rates less than 500 mV/s) of the desorption wave relative to the ideal FWHM for a surface bound electron transfer process to this effect [16].

At step sites, a similar trend is observed for both adsorption and desorption. That is, plots of peak potential (E_p) vs n are linear; however the slopes for the linear dependencies are -7.5 ± 0.6 and -7.1 ± 1.0 mV/CH_2 for desorption and adsorption respectively. The differences in the slopes for desorption at steps versus terraces reflects the decreased interchain interactions present at the stepped regions of the surface. This decrease stems from a combination of sources. At the cathodic potentials required for step desorption, the terrace portion of the film has already been desorbed, greatly reducing overall film capacitance while increasing the accessibility of the step adsorbates to electrolyte ions. Also, the smaller size of

the step and the decreased number of neighbors at the step site diminishes the interchain interactions which lead to the strong chain length dependence for terrace desorption. The similarity in the slope for adsorption with that for desorption also reflects this decreased effect of the alkyl chains which results in similar environments of the thiolate during desorption and adsorption.

Extrapolating the E_p versus n relation to n = 0 provides additional information on the relative magnitude of the gold-sulfur interaction. The intercept for terrace desorption is -0.73 ± 0.02 V compared to -0.73 ± 0.01 V for terrace adsorption, essentially independent of sweep rate. This suggests, at least in the limiting case of n = 0, electron transfer kinetics do not play a major role in the adsorption/desorption process. Intercepts for step desorption and adsorption are -1.10 ± 0.01 V and -1.08 ± 0.01 V. While we do not yet understand the cause for this difference in intercept for the step process, it may result from a change in local electronic structure at the step that occurs as a result of adsorption, leading to slightly different electronic environments for the sulfur during adsorption and desorption.

Sweep Rate Dependence Figure 4.4 presents a series of CV's for the electrochemical adsorption/desorption of C_8 at Au/Glass at sweep rates ranging from 10 mV/s to 1 V/s. Several trends are evident in the figure. First, peaks for both terrace and step processes broaden as sweep rate increases. This trend is essentially independent of chain length. The peak separation for terrace adsorption/desorption increases dramatically from 6 mV for C_3 at 10 mV/s to 168 mV for C_{14} at 1 V/s. The small peak separation for C_3 at

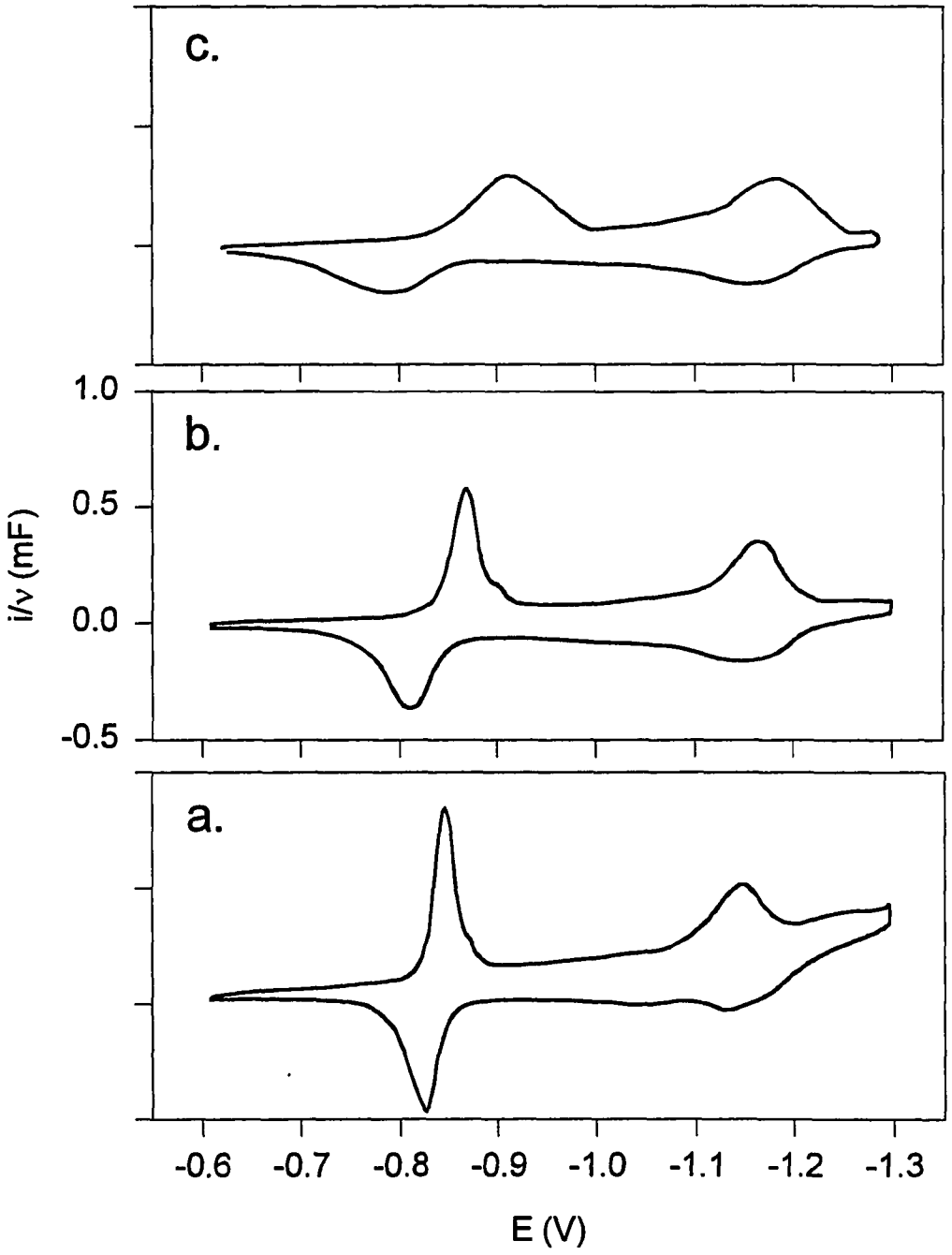

Figure 4.4. Effect of sweep rate on the electrochemical adsorption/desorption of C_8 at Au/glass. Sweep rates: a. 10 mV/s, b. 100 mV/s, c. 1000 mV/s. All other conditions are as in Figure 4.2. Y-scale is identical for all plots.

slow sweep rates reflects the dominance of the gold-sulfur interaction and the diminished importance of chain-chain interactions for short chain lengths. We have previously modeled these interfaces as two capacitors in series, one corresponding to the capacitance of the sulfur head group (C_{HG}), and the other to the capacitance of the hydrocarbon tail (C_{TG}) [14]. For short chain lengths, such as C_3, the contribution of C_{TG} is quite small, affording the small peak separation, especially at slow sweep rates. As the length of the alkyl chain increases, as in the case of C_{14}, interchain interactions cause C_{TG} to decrease and result in increase in the potential which is dropped across the tail group. This increase leads to the requirement for a larger overpotential to drive desorption, and increased peak separation. Even at sweep rates of 10 mV/s, peak separation for C_{14} is 62 mV. This effect appears to be essentially absent at the steps, as peak separation for step adsorption/desorption are consistently on the order of 31 ± 7 mV, regardless of sweep rate or chain length.

A compounding effect that contributes to increased peak separation relates to the inherent resistance of the film. This resistance runs in parallel to the film capacitance and acts as a potential source of iR drop during the voltammetric sweep, resulting in increased peak separation. This contribution will be largest at higher sweep rates where the magnitude of the current passed is largest and for longer chain lengths where the magnitude of the film resistance is greatest. Given their similar fundamental characteristics, separation of the resistive and capacitive components of the trends regarding peak separation is difficult.

Figure 4.5 presents a plot of peak current as a function of sweep rate for terrace and step adsorption/desorption of C_8. The data indicate that the step process exhibits linearity

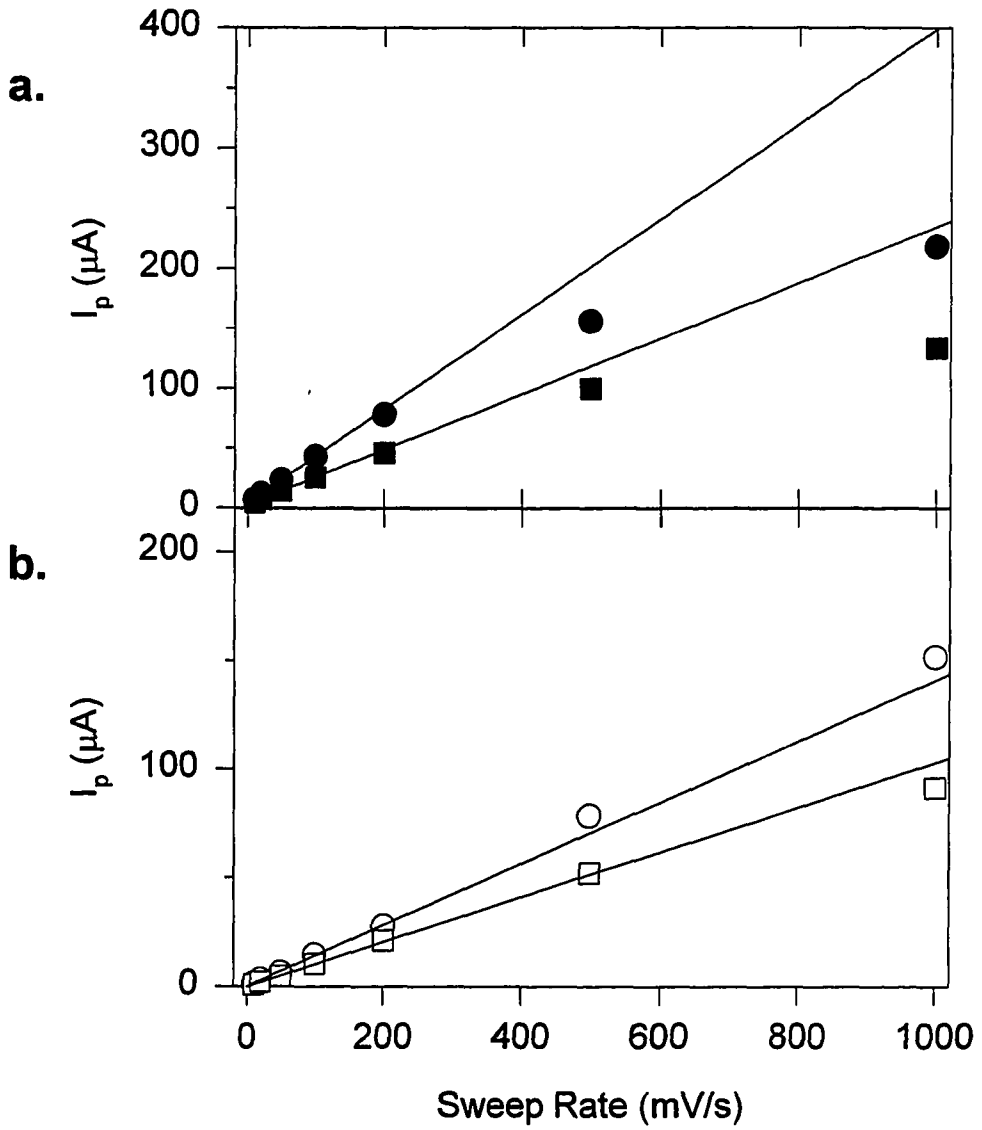

Figure 4.5. Voltammetric peak current (I_p), as a function of sweep rate for the data in Figure 4.4. a: terrace adsorption (■), terrace desorption (●); b: step adsorption (□), step desorption (○). Lines represent least-squares fits to the data at the four slowest sweep rates in each data set.

over a broader range of sweep rates than does the terrace process, suggesting, in part, that adsorption at steps has a smaller diffusional component as this concentration.
This observation, again, provides an indication into the influence of the alkane chain to the adsorption/desorption at the two types of surfaces. At the stepped regions of the surface, the necessity to accommodate the alkane chain is greatly diminished, due to the larger free volume and counter ion accessibility about the step. This allows the adsorption/desorption process to be driven primarily by the gold-sulfur interaction and less by chain-chain type interactions.

At the terraces, however, the large influence of neighbors on the adsorption (and desorption) of thiolate adsorbates results in a process which is limited by the approach of adsorbates to the electrode surface. That is, formation of a full monolayer is limited by the ability of an incoming adsorbate to penetrate the partially formed film sufficiently for the sulfur to approach the electrode close enough to allow electron-transfer to occur. For desorption, it is becomes necessary for chain structure of the thiolate to be disrupted such that enough electrolyte can penetrate into the film to accommodate the potential drop across the Au-S bond necessary to induce cleavage.

Concentration Studies. As a further probe of the interactions which influence adsorption/desorption at the various surface sites, electrochemical adsorption/desorption was studied at a range of thiolate concentrations, from 10 μM to 10 mM. At concentrations of 1 mM and 10 mM, the shapes and positions of the i-E curves are similar and behave as

described in the previous section. This provides evidence that, at these concentrations, depletion of the diffusion layer is not limiting the adsorption/desorption of the alkanethiolate on the timescale of the voltammetric sweep, even at sweep rates of 1 V/s [17].

At very low concentration, 10 μM, only adsorption/desorption at steps is observed at all sweep rates, as shown in Figure 4.6. The absence of a terrace component is a result of the increased thermodynamic stability of the adsorption at step sights which results from the increased accessibility of the bonding orbitals at the atomic step [18]. At sweep rates of 50 mV/s or below, the charge required for desorption (Q_d) is essentially constant, indicating that full coverage of the step sites is obtained in the time necessary to complete a single cycle. At faster scan rates, diffusion limits thiolate adsorption and Q_d steadily decreases. The consistently smaller magnitude of charge passed during adsorption at all sweep rates reflects the diffusional character of the voltammetry at this concentration. That is, adsorption is occurring at the step sites at all potentials positive of -1.20 V, with terrace adsorption occurring at potentials positive of -0.90 V. Diffusion of adsorbates to the electrode surface after the initial depletion of the diffusion layer results in increased charge for desorption relative to that for adsorption. Interestingly, while adsorption essentially saturates the step sites, especially at slow sweep rates, no evidence for terrace adsorption is observed. This may imply that, at the low thiolate concentrations in the diffusion layer, the terrace equilibrium is not strongly driven toward adsorption.

At intermediate concentration the presence of terrace and step adsorption is strongly sweep rate dependent, as presented for 100 μM at selected sweep rates in Figure 4.7 and

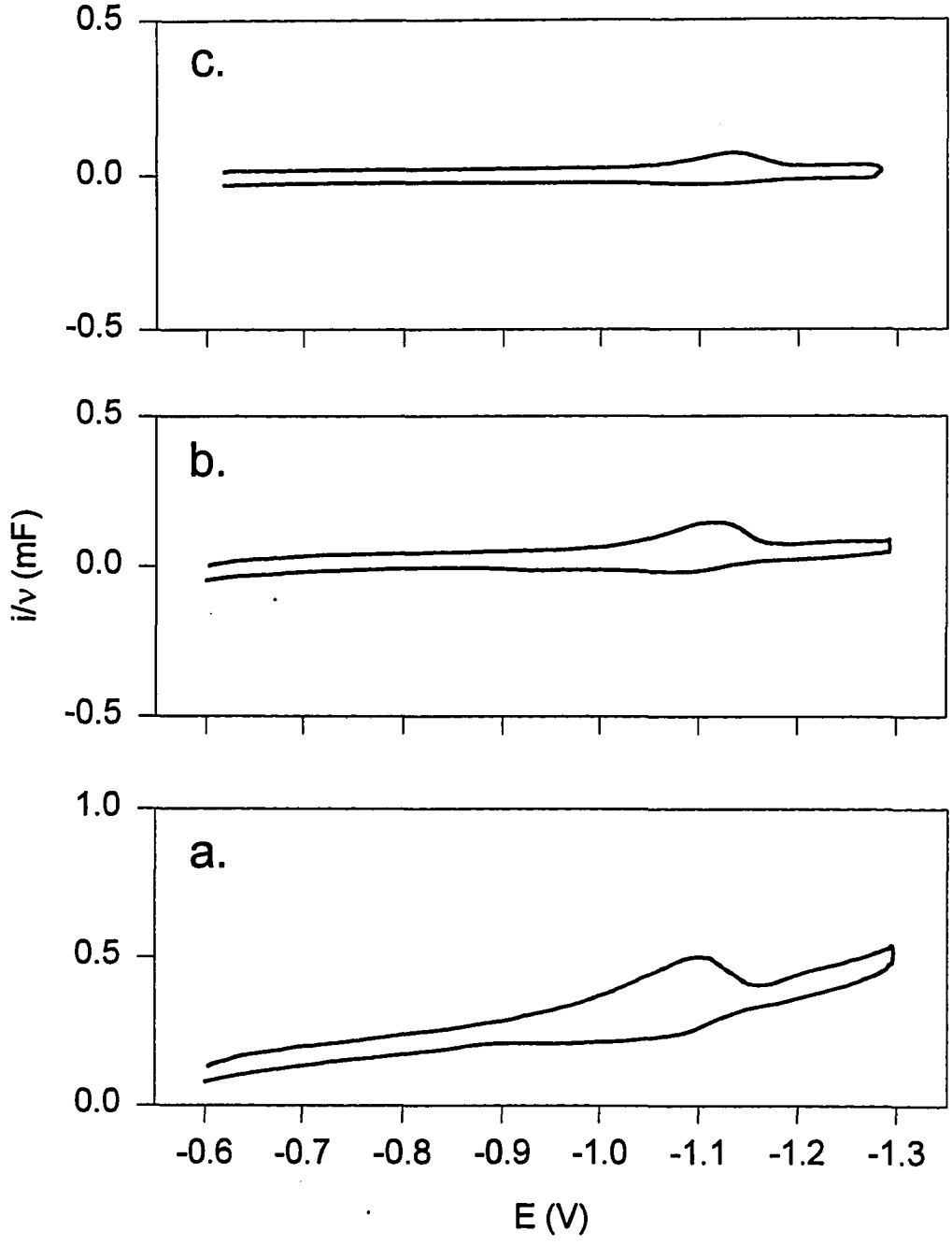

Figure 4.6. Dependence of sweep rate on the electrochemical adsorption/desorption at Au/glass in a 10 μM C_8 solution. Electrolyte: 0.4M KOH in 80% ethanol. a. 10 mV/s, b. 100 mV/s, c. 1000 mV/s.

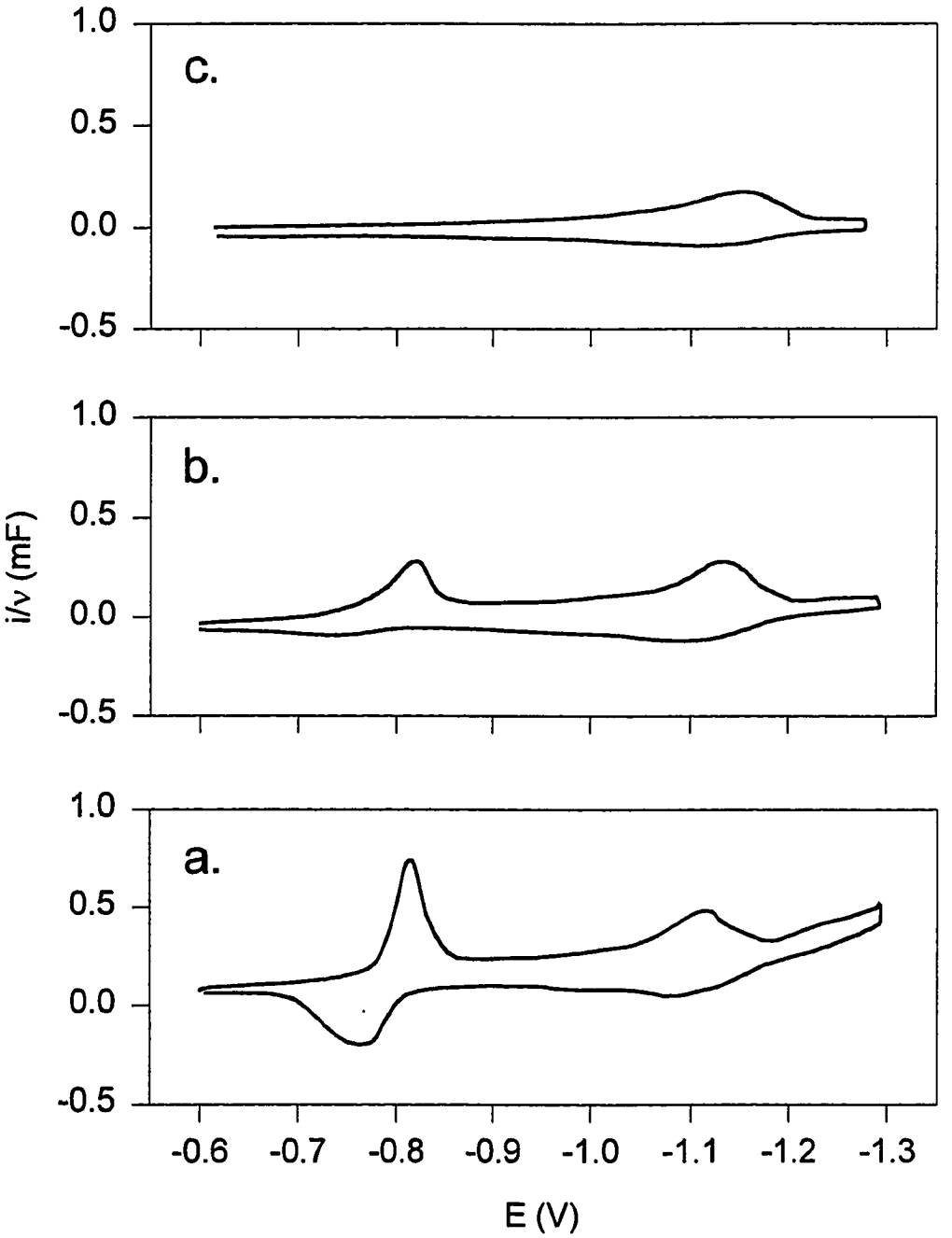

Figure 4.7. Dependence of sweep rate on the electrochemical adsorption/desorption at Au/glass in a 100 μM C_8 solution. Electrolyte: 0.4M KOH in 80% ethanol. a. 10 mV/s, b. 100 mV/s, c. 1000 mV/s.

summarized for all sweep rates in Figure 4.8. At 10 mV/s the CV strongly resembles that for thiolate concentration of 1 mM, with evidence of essentially complete monolayer coverage at both terrace and step sites. As sweep rate increases, the terrace adsorption exhibits a "diffusional" tail and diminishes as sweep rate increases, disappearing at 500 mV/s. At 1 V/s, no evidence for terrace adsorption is observed.

Terrace desorption follows a similar trend, with the decrease lagging that for adsorption, as in Figure 4.8a. In fact, even after the peak current for the adsorption wave begins to decrease, the peak current for desorption continues to rise. This, again is a result of the time lag between the application of a potential which allows adsorption and the application of a potential which drives desorption. Only at very slow sweep rates does the peak current (and charge) for terrace adsorption approach that observed for desorption.

As in the 10 μM case, step adsorption is observed for all sweep rates for thiolate concentrations of 100 μM. For sweep rates of 200 mV/s or less, the charge for desorption and adsorption are essentially constant and equal. For faster sweep rates, desorption charge remains essentially constant, but the charge for adsorption begins to diminish. This decrease reflects the increased diffusional character of the adsorption wave at fast sweep rates. This effect is displayed graphically in Figure 4.8b. The solid lines through both plots were generated by fitting the points at 200 mV/s and below as a linear function of sweep rate. The points at 200 mV/s and above were fit as linear functions of the square root of sweep rate. The high quality of the fit reflects the evolution of the data from a primarily surface

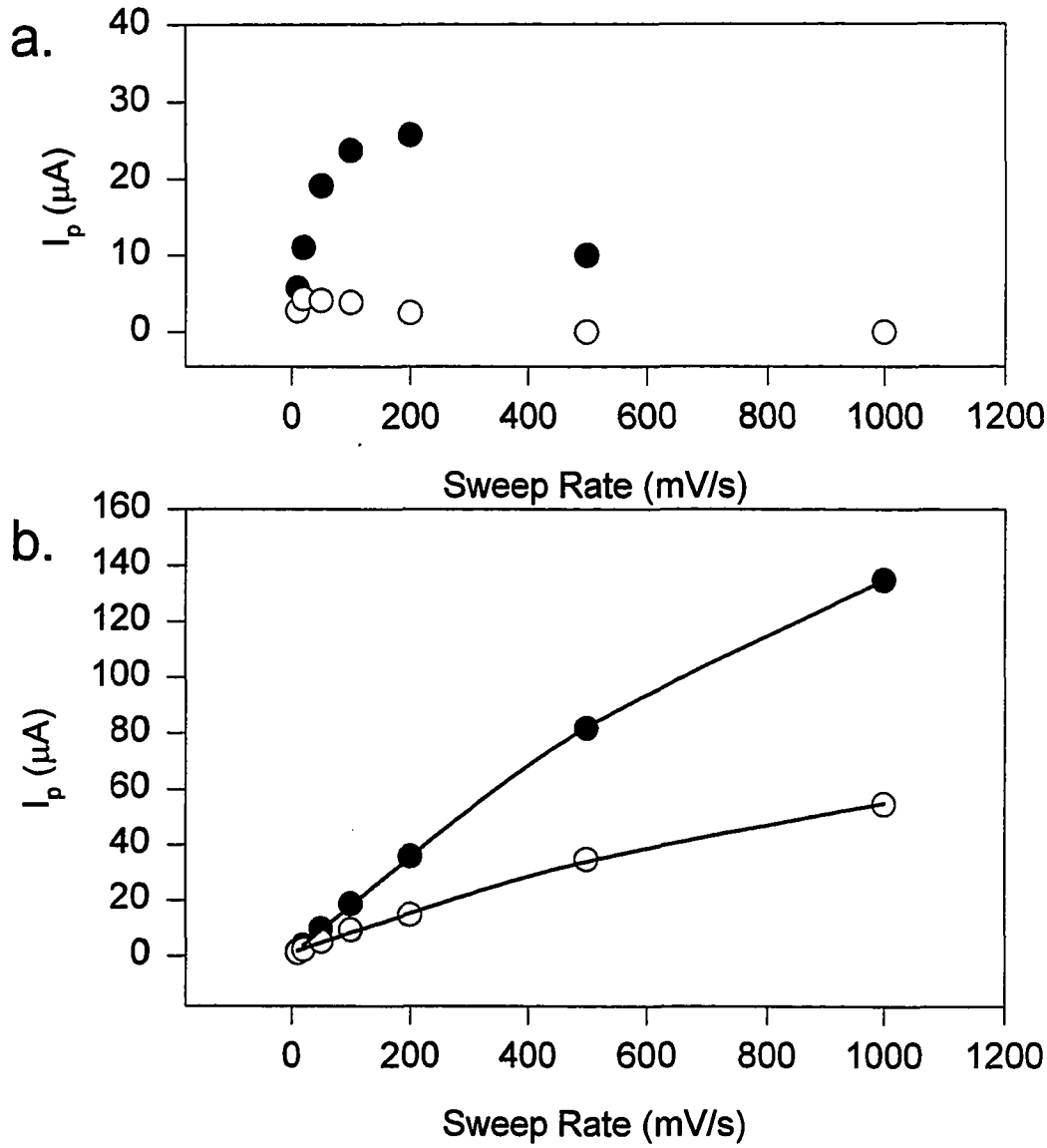

Figure 4.8 Dependence of the electrochemical adsorption/desorption at Au/glass in a 100 μM C_8 solution on sweep rate. a. terrace adsorption (O) and desorption (●). b. step adsorption (O) and desorption (●). Experimental conditions are as in Figure 4.7.

controlled process at slow sweep rate to a diffusion controlled process at fast sweep rates. The fact that the desorption wave also appears to have a large diffusional component at fast sweep rates again reflects the influence of the cohesive interactions of the alkyl chains.

Conclusions

This study has investigated the relationship between adsorption/desorption of alkanethiolates at gold steps versus terraces. At all concentrations of thiolate adsorbate, adsorption at steps occurs more readily and at potentials ~300 mV negative of that for the corresponding process at terraces. Where the length of the alkyl chain is significant, chain-chain interactions result in increased diffusional character in the adsorption/desorption voltammetry. The increased influence of the alkyl chains is most dramatic at the terrace sites where it results in extensive broadening of the voltammetric wave as well as an increase in peak separation for the adsorption/desorption couple. This reflects limitations imposed due to reorientation of the alkyl chains which is necessary to accommodate adsorption (and desorption) of the complete monolayer film.

At step sites, this effect is greatly diminished, as observed by essentially constant peak separation in the voltammetry. This decrease in chain length dependence at the steps results from the increased free volume about the step which affords more facile approach of counter ions to the electrode surface.

In dilute solutions, the increased accessibility as well as availability and density of dangling bonds adds thermodynamic stability to the step site, resulting in preferential

adsorption at the step. Only after saturation of the steps does terrace adsorption proceed to completion.

To reiterate, the trends observed in the data may result from a number of effects. These effects may involve reconstructions of the underlying gold surface, variations in electron transfer and overall adsorption kinetics at steps versus terraces, and strong effects from intermolecular interactions in both the adsorption and desorption processes. Absolute separation of these types of effects is extremely difficult as each effect has an impact on the other processes. At best, a general idea regarding the relationship of these effects can be obtained.

References

1 . Permanent address: Department of Chemistry, Augustana College, Sioux Falls, SD, 57197.

2 . Ulman, A. *An Introduction to Ultrathin Organic Films: From Langmuir-Blodgett to Self-Assembly*, Academic: Boston, 1991.

3 . Dubois, L. H.; Nuzzo, R. G. *Annu. Rev. Phys. Chem.* **1992**, *43*, 437-463.

4 . Zhong, C. J.; Porter, M. D. *Anal. Chem.* **1995**, in press, and references therein.

5 . Creager, S. E.; Hockett, L. A.; Rowe, G. K. *Langmuir* **1992**, *8*, 854-861.

6 . Guo, L.-H.; Facci, J. S.; McLendon, G.; Mosher, R. *Langmuir* **1994**, *10*, 4588-4593.

7 . Walczak, M. M.; Alves, C. A.; Lamp, B. D.; Porter, M. D. *J. Electroanal. Chem.* **1995**, *396*, 103-114

8 . Weisshaar, D. E.; Lamp, B. D.; Porter, M. D. *J. Am. Chem. Soc.* **1992**, *114*, 5860-5862.

9 . At present, we do not understand why only waves for the (111) and (110) sites are present, while a wave for the (100) sites is absent in these data. Whether this absence results from the presence of only a statistically small number of (100) sites or from other kinetic or thermodynamic factors is currently under investigation.

10 . Zhong, C. J.; Porter, M. D.; unpublished results

11 . Roughness factors for Au/glass and Au/mica produced in our lab have been determined to be 1.3 ± 0.3 and 1.1 ± 0.1 respectively [7].

12 . Investigations into the kinetics of monolayer formation indicate that thiolate monolayers form in a two step process in which the first 80% of the monolayer film forms quite repidly, followed by a slower annealing and formation of the remaining 20%. See Hähner, G.; Wöll, C.; Buck, M.; Grunze, M. *Langmuir* **1993**, *9*, 1955-1958, and Biebuyck, H. A.; Bain, C. D.; Whitesides, G. M. *Langmuir* **1994**, *10*, 1825-1831 for examples.

13 . This charge is determined by integration of the two distinct peaks in the CV and does not include faradaic charge which may be passed at potentials intermediate of these two peaks.

14 . Widrig, C. A.; Chung, C.; Porter, M. D. *J. Electroanal. Chem.* **1991**, *310*, 335-359.

15 . Weisshaar, D. E.; Lamp, B. D.; Simmons, N. J.; Zhong, C. J., Porter, M. D., manuscript in preparation.

16 . FWHM for thiolate desorption at Au/mica is typically on the order of 60 mV or less, significantly less than the 90 mV FWHM expected for surface bound electron transfer species. (see, for example, Bard, A.J.; Faulkner, L R. *Electrochemical Methods: Fundamentals and Applications*; Academic: Boston, 1980; Chapter 12.)

17 . Estimation of the time necessary for one monolayer of adsorbates to diffuse to the electrode surface agree with this assertion. Assuming a diffusion coeffecient of 10^{-5} cm^2/s and a concentration of 1 mM, the time required for one monolayer of adsorbates to diffuse to the electrode surface is on the order of 20 ms.

18 . Chang, S.-L.; Thiel, P. A. *Crit. Rev. Surf. Chem.* **1994**, *3*, 239-296, and references therein.

5. CORRELATION OF STRUCTURE AND PERFORMANCE OF PYRIDINETHIOLATE SURFACE MODIFIERS FOR THE FACILITATION OF CYTOCHROME c HETEROGENEOUS ELECTRON-TRANSFER

A paper to be submitted to *Langmuir*

Brian D. Lamp [1], Marc D. Porter [1], Therese M. Cotton [1], Daisuke Hobara [2], Shin-ichiro Iamabayashi [2], Katsumi Niki [2]

Introduction

Studies of the heterogeneous electron transfer reactions of a variety of redox proteins have been of high interest since the early 1980s [3]. Most electron transfer proteins undergo irreversible adsorption on bare metal surfaces and lose their intrinsic redox activities as a result. The interfacial character of the electrode is of large importance in determining the reversibility of the electrode reactions of the redox protein. It is believed that appropriate modification of the electrode surface prevents irreversible unfolding or denaturing of the protein at the surface, and allows facilitation of these electron transfer reactions [4]. One electrode system that has been used very effectively in this area has involved the modification of gold electrodes with a spontaneously adsorbed layer of pyridinethiolate (PyS/Au), resulting from immersion of the electrode in a solution of 4-mercaptopyridine (PySH) or 4,4'-dipyridyl disulfide (PySS) [3a, 4a, 5].

These compounds are believed to form similar structures on the gold surface by cleavage of either the S-H bond in the case of PySH, or the S-S bond in the case of PySS. It has been reported that cytochrome c undergoes rapid electron transfer at the PySH or PySS modified electrodes and that the native conformation of the protein is maintained on the surface [4a]. During the course of a study aimed at characterization of the modifier surfaces and investigation of the structure/function relationships in the cytochrome c/PyS/Au system, an instability in the monolayer film was discovered. This instability leads to decreased efficiency of the electron transfer in the protein and has some dramatic implications to the utility of these films as surface modifiers in the electrode reactions of redox proteins.

Experimental

Materials. 4-Mercaptopyridine (90%), 2-mercaptopyridine (99%), 4,4'-dipyridyl disulfide (98%), 2-mercaptopyrimidine (99%), and potassium hydroxide (99.99%) were purchased from Aldrich and used as received. Water was deionized using a Millipore (Waters) purification system. Purified horse heart cytochrome c (Sigma type IV) was used without further purification.

Substrate Preparation. Gold electrodes were prepared by resistive evaporation onto either freshly cleaved mica (The Mica Company) or glass microscope slides (Fisher Scientific) All depositions were carried out in a cryogenically pumped Edwards (UK) model E306A coating system at a base pressure of 10^{-6} torr. Mica substrates were loaded into the evaporator immediately after cleaving and 300 nm of gold was deposited at ambient

temperature at a rate of 0.4 nm/s. Upon removal from the evaporation system, the Au/mica electrodes were annealed for 4 hr at 300° C in an oven under ambient pressure. Glass substrates were primed with 15 nm of chromium to improve gold adhesion, and were used directly after removal from the evaporator.

Microscopic examination of these substrates indicates that both consist primarily (>98%) of Au(111) crystallites separated by grain boundaries. In the Au/mica case, crystallite sizes are on the order of several hundred nanometers, while glass substrates have much smaller crystallites and a larger number of atomic steps [6].

Electrochemical measurements. Electrochemical measurements utilized a standard three electrode electrochemical cell with the area of the working electrode defined by an inert elastomer O-ring. A Ag/AgCl (saturated KCl) reference electrode was used, all potentials listed herein are with respect to this reference. Experiments were conducted using a BAS CV-27 potentiostat (Bioanalytical Systems) and either an X-Y recorder (the Recorder Company) or a computer controlled data acquisition system (Labtech Notebook, Laboratory Technologies).

Infrared Spectroscopy. Infrared spectra were acquired using either a Nicolet Instruments (Madison, WI) model 740 or MAGNA 750 Fourier transform infrared spectrometer equipped with a liquid nitrogen-cooled narrow band Mercury Cadmium Telluride detector. Spectra were collected using p-polarized light incident at 80° with respect to the surface normal. All spectra are presented as $-\log(R/R_0)$, where R is the reflectance

spectrum of the sample of interest, and R_0 is the reflectance spectrum of a perdeuterooctadecanethiolate monolayer adsorbed at gold.

X-Ray Photoelectron Spectroscopy. XPS spectra were acquired using a Physical Electronics model 5500 multi-technique surface analysis system equipped with a hemispherical analyzer, torroidal monochrometer, and a multichannel detector. Excitation was with monochromatic Al K-α radiation at 300 W, with detection at 45°.

Scanning Probe Microscopy. A Digital Instruments (Santa Barbara, CA) Nanoscope III imaging system equipped with a 0.7 μm STM scan head was used to probe the microstructure of the monolayer modified electrodes. Images were collected under ambient conditions, after allowing ~20 minutes for thermal equilibration after sample loading. STM tips were made by etching 0.25 mm tungsten wire (Aldrich) in 1 M KOH at 30 V ac. After etching, the tips were rinsed with deionized water and used immediately. Images were scanned in constant height mode with typical tunneling current of 500 pA with bias potential of 200 mV. A tip was discarded if, after scanning several regions of a sample, no well defined images were obtained. Horizontal displacements of the tip were calibrated against a sample of highly ordered pyrolytic graphite.

Results and Discussion

Voltammetry of Cytochrome c at pyridinethiolate modified gold electrodes. A primary emphasis was to investigate the structure-facilitation relationship of various pyridine functionalized thiolate modified electrodes in terms of the voltammetric behavior of

cytochrome c. A representative voltammogram of the electron-transfer of cytochrome c at a PyS/Au electrode which had been prepared by immersion in 1 mM PySH solution for a period of 1 min is presented in Figure 5.1a. The voltammetry is characterized by a well-defined, single redox couple, corresponding to the redox reaction of cytochrome c. The $E^{o\prime}$ for this couple is +0.12 V, consistent with previous reports for the redox reaction of cytochrome c at PyS/Au [3a, 5], compared to +0.5 V or cytochrome c at a bare gold electrode [3d, e].

An interesting trend develops if the ability of the modified electrode to facilitate the cytochrome c electron transfer reaction is monitored as a function of immersion time in the modifier precursor solution, as shown in Figure 5.1b. Initially, the film behaves such that the electron transfer of cytochrome c is quite facile, with easily discernible peaks and nearly ideal peak separation. With increasing immersion time, however, the voltammetric peak current decreases and peak separation increases. The ability of the modified electrode to facilitate the electron transfer diminishes until, at 24 hr immersion, the electrodes essentially cease to facilitate the cytochrome c electrode reaction.

This decreased ability to facilitate the electron transfer reaction of cytochrome c at PyS/Au modified electrodes and its cause have not been previously reported in the literature. This decrease is likely caused by a structural change in the modifier film during prolonged immersion of the gold electrode in the precursor solution. The results of an investigation of this structural evolution comprise the balance of this manuscript.

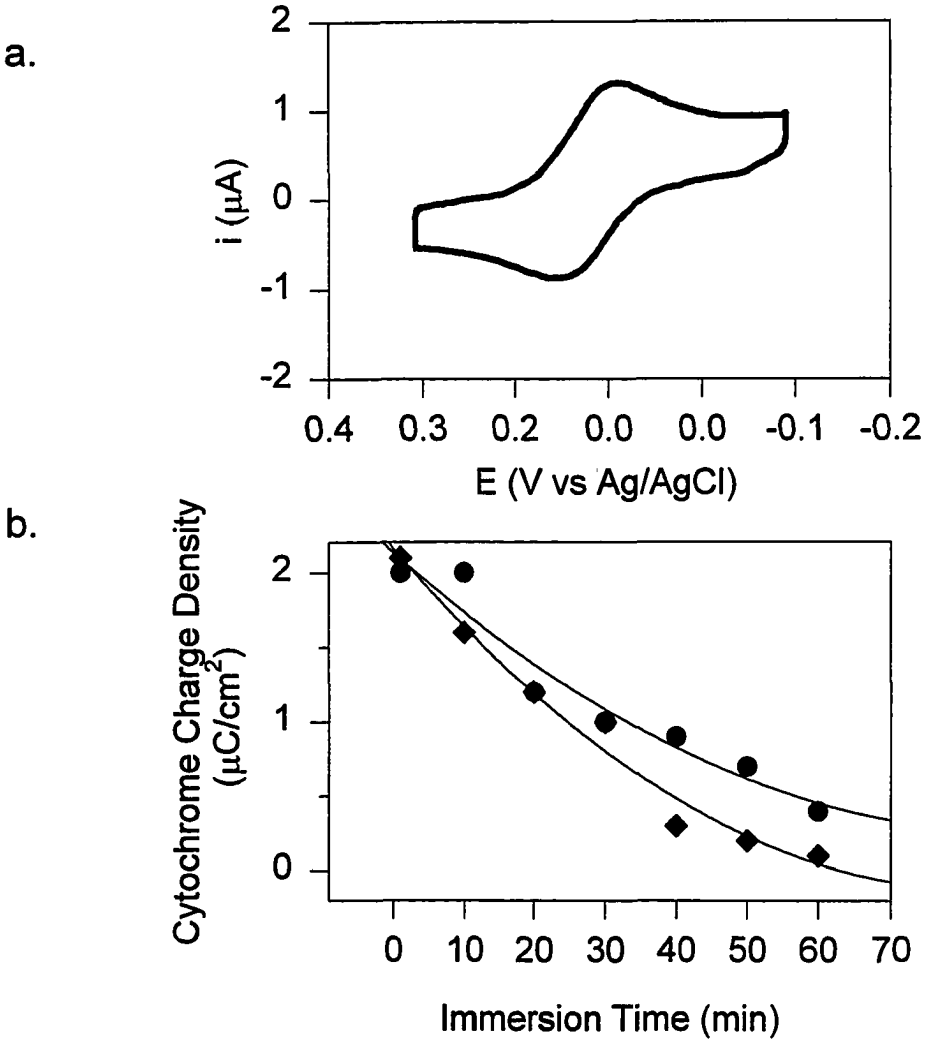

Figure 5.1. Electrolysis of cytochrome c at electrodes immersed for various time in 1 mM PySH (aq). Conditions: 100 μM cyt c in 30 mM pH 7 phosphate buffer, sweep rate 100 mV/s. a. Cyclic voltammetry of cytochrome c at PyS/Au immersed 1 min. b. Charge consumed for the redox of cytochrome c as a function of immersion time in the precursor solution (precursors: (•) PySH, (♦) PySS. Lines are guides to the eye.

Electrochemical desorption. We have previously described a method by which thiolate monolayers can be desorbed electrochemically *via* reaction 1.

$$RSAu + e^- \rightarrow RS^- + Au \quad (1)$$

Application of a cathodic voltage sweep in basic solution produces a single cathodic wave resulting from the desorption of the monolayer film. The peak potential, E_{rd}, for the desorption process is indicative of the thiolate species adsorbed at the electrode and is dependent not only on the strength of the gold-sulfur interaction, but also contains a component related to the strength of the intermolecular interactions between adjacent adsorbates [7, 8, 9, 10].

Integration of the charge consumed during the desorption process provides a measure of the surface coverage, Γ, of thiolates *via* equation 2,

$$Q = nFA\Gamma \quad (2)$$

where Q is the charge consumed, n is the number of electrons involved in the desorption process, F is the Faraday constant, and A is the electrode area. Typical values for charge consumed in the desorption of alkanethiolates is 75 μCcm^{-2} [11].

An experiment involving the desorption of a monolayer assembled for 1 min in 1 mM PySH solution is given in Figure 5.2. Linear sweep voltammograms (LSVs) for these samples are characterized by a single cathodic wave with E_{rd} = -0.55 V. The charge consumed by this process (~50 $\mu C\ cm^{-2}$) is considerably less than that observed for the desorption of monolayers formed from *n*-alkanethiols on similar surfaces. This lower charge

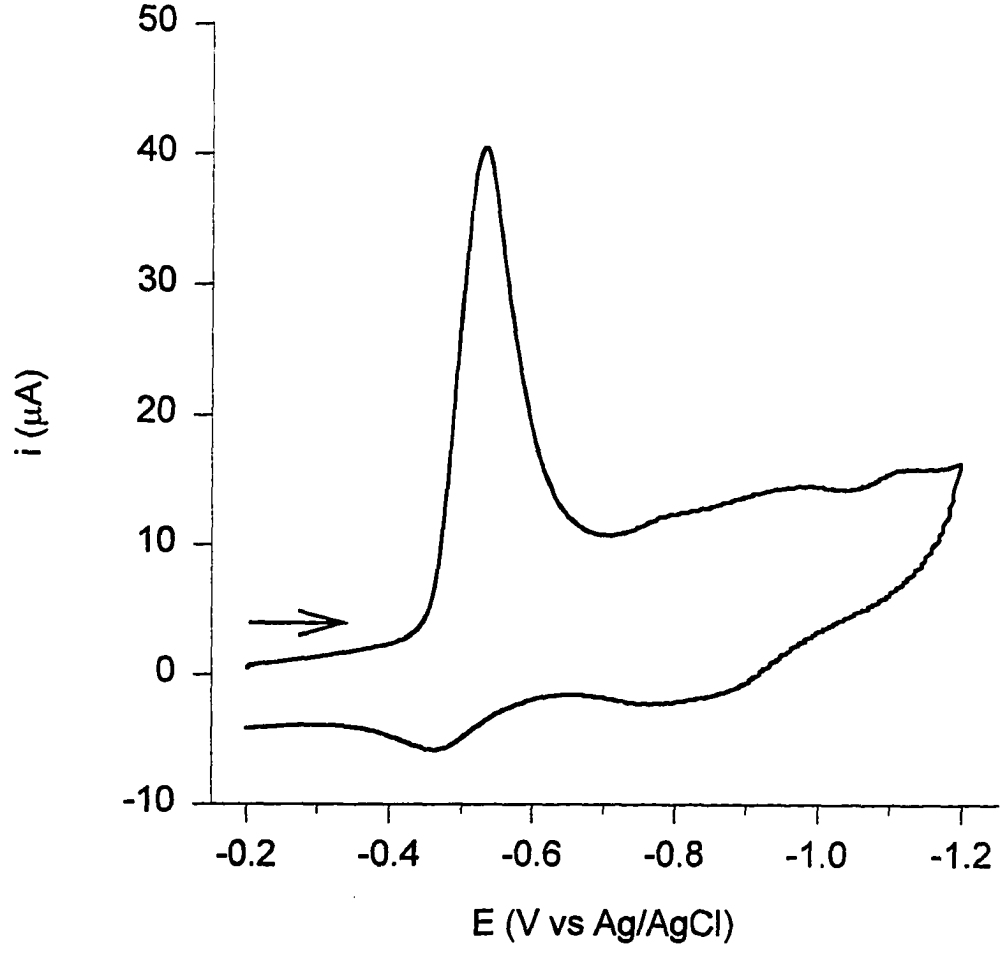

Figure 5.2. Electrochemical desorption of PyS/Au/mica. Immersion time: 1 min, sweep rate: 100 mV/s, electrode area: 0.62 cm^2.

can be attributed primarily to a lower surface coverage of PyS, which is not unexpected given the cross-sectional size of a pyridyl ring versus that of an alkyl chain. Maximum coverage for these systems is on the order of 70% of alkanethiol [12, 13]. Previous experiments utilizing thiophenol confirm these expectations [14].

Monitoring the desorption voltammetry as a function of immersion time in the pyridyl precursor solution gives rise to some interesting observations. Figure 5.3 shows LSVs for the desorption of PySH and PySS at immersion times ranging from 1 min to 24 hr. While short ($\leq$ 10 min) immersion samples give rise to voltammograms consisting primarily of one peak at -0.55 V, increasing immersion times result in the appearance of at least one additional wave located at -0.90 V. After about 5 hr immersion, the structure equilibrates to one giving a voltammogram consisting of a single, large wave at -0.90 V. The charge consumed by this process (~180 $\mu C\ cm^{-2}$) is much greater than that consumed by the process at -0.55 V as well as that observed for *n*-alkanethiols [15, 16].

Previous experiments in our laboratory monitoring the desorption of monolayers assembled from mercaptoethanol and mercaptoacetic acid have also shown similar trends in the desorption voltammetry [17]. In these cases, the cause for the transformation was ascribed to the oxidative cleavage of the C-S bond and the resulting formation of a monolayer that behaves much like a film of adsorbed atomic and oligomeric sulfur. A similar event may be operative in this case; however, given the differences in the adsorbate structure, the mechanism for such a reaction is likely different, perhaps resulting in different sulfur-containing products.

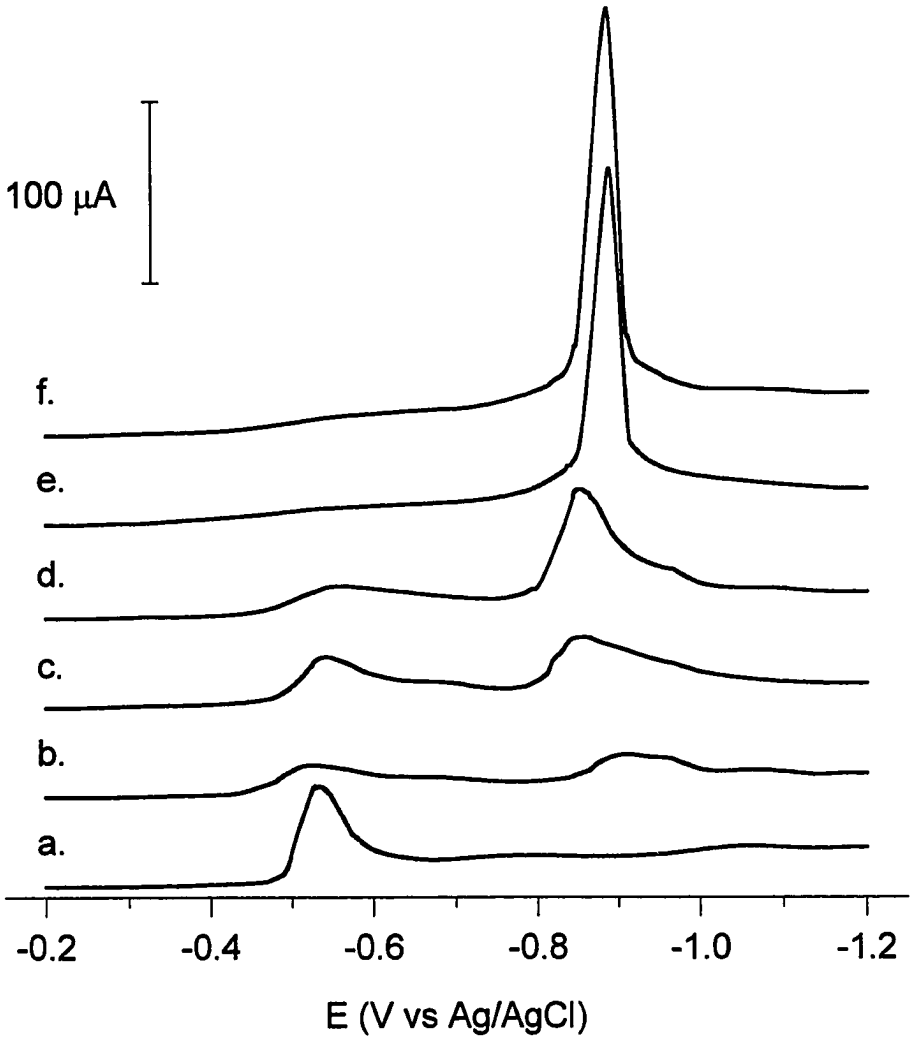

Figure 5.3. PyS/Au desorption as a function of immersion time in 1 mM PySH solution. Immersion times: a. 1 min, b. 15 min, c. 30 min, d. 60 min, e. 300 min, f. 1440 min. All other conditions are as in Figure 5.2.

To confirm that the transformation seen as a function of assembly time is not related to a change in the binding of the aromatic thiolate, and that the charge determined is representative of adsorbed aromatic thiolates, analogous experiments were conducted usingthiophenol (TP) as the adsorbate. Electrochemical desorption data for monolayers assembled from TP solution for 1 min and 24 hr are presented in Figure 5.4. At short immersion time, the voltammetry is dominated by a single wave at -0.70 V, again indicative of desorption of the thiolate adlayer. The charge consumed for the desorption of TP is 55 $\mu C/cm^2$ corresponding to the expected lower surface coverage of aromatic adsorbates versus that for alkane-based precursors, and consistent with the charge determined for short immersion PyS samples. Comparison of LSVs for short and long immersion time samples indicates no dramatic change in the desorption volatmmetry, such as seen for PyS/Au. The similarity in the voltammetry for samples immersed 1 min and 24 hr indicates that thiophenol monolayers do not undergo the similar structural conversion as seen in the PyS/Au electrode system.

Infrared characterization. Figure 5.5 provides a comparison of the infrared spectra of bulk PySH with a monolayer formed from PySH solution. Peak positions and mode assignments are given in Table 5.1. The bulk spectrum, which is dominated by four features, can essentially be divided into three sections related to different motions within the system.

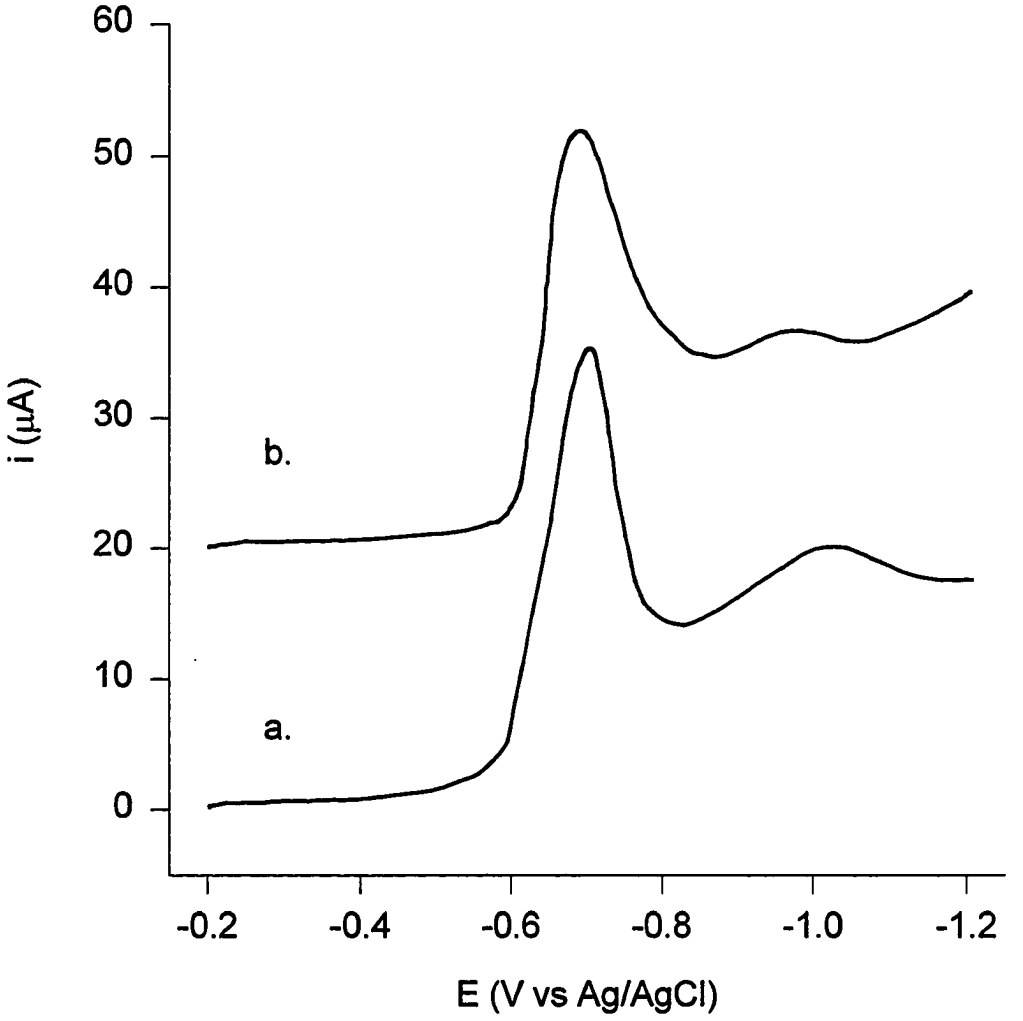

Figure 5.4. Electrochemical desorption of electrodes immersed in 1 mM TP for a. 1 min and b. 24 hr. All other conditions are as in Figure 5.2.

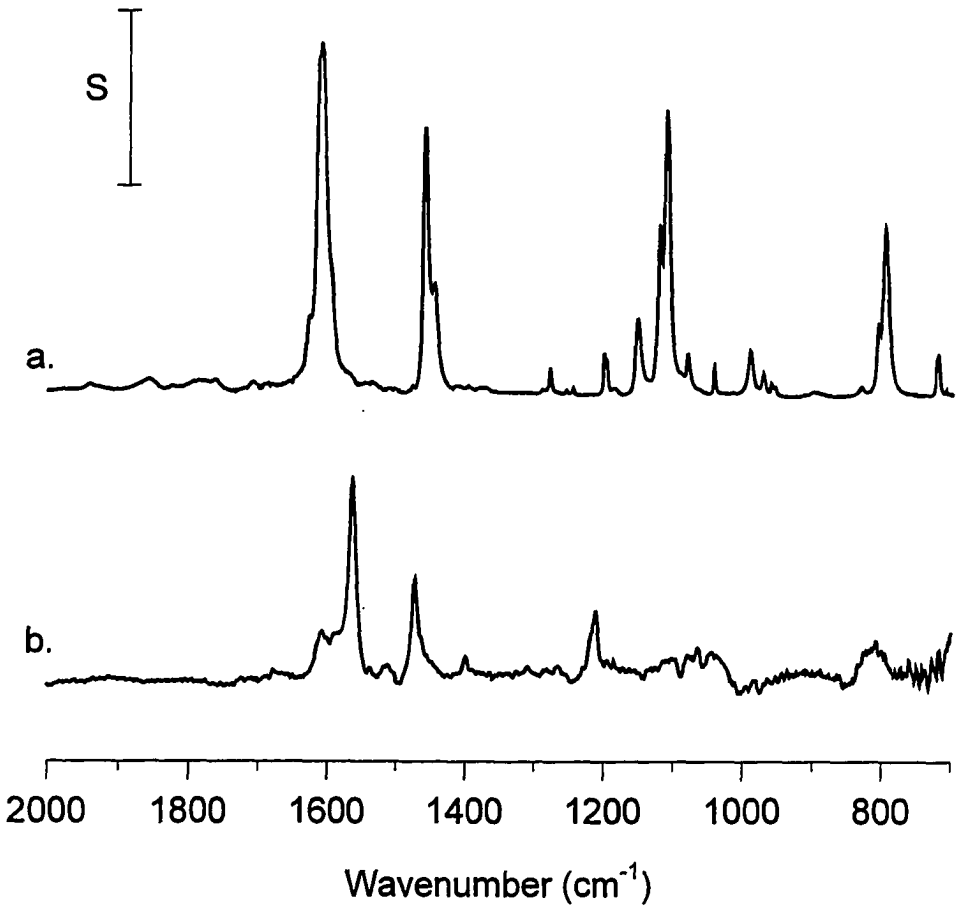

Figure 5.5. a. FTIR spectrum of PySH dispersed in KBr. b. IRRAS spectrum of a monolayer formed by 1 min immersion in 1 mM PySH. S = 1.0 AU and 0.001 AU for a and b, respectively.

Table 5.1. Peak positions and mode assignments for bulk and monolayer spectra of PyS[a]

Position (cm^{-1})	Assignment [18-20]	KBr	1 min Immersion	24 hr Immersion
1723	ν(C=C, C=N)	w	b	b
1613	ν(C=C, C=N)	s	b	w
1564	ν(C=C, C=N)	w	s	w
1473	ν(C=C, C=N)	s	m	w
1210	$\delta(CH)_{ip}$	w	m	vw
1111	$\delta(CH)_{ip}$	s	b	w
1070	$\delta(CH)_{ip}$	w	vw	[a]
805	$\delta(CH)_{op}$	m	w	m

[a]s = strong, m = moderate, w = weak, vw = very weak
[b]Peak not observed in this spectrum

Between 1700 cm^{-1} and 1400 cm^{-1} occur modes corresponding to the C=C and C=N stretching modes of the pyridyl ring. In the KBr spectrum, two bands dominate this region, at 1612 cm^{-1} and 1460 cm^{-1}. These bands have been assigned to in-plane components of C=C and C=N ring stretches. Single bands dominate the in-plane (1350 cm^{-1} -1000 cm^{-1}) and out of plane (1000 cm^{-1}-700 cm^{-1}) C-H bending regions at 1111 cm^{-1} and 797 cm^{-1} respectively [18-21,].

In the monolayer spectrum, fewer modes give rise to strong absorbance. The strongest band corresponds to the $\nu_{C=C,\,C=N}$ mode at 1564 cm^{-1}. There is also a strong contribution of $\nu_{C=C,\,C=N}$ modes at 1613 cm^{-1} and 1474 cm^{-1} and the δ_{C-H} band at 1210 cm^{-1} all of which lie in the plane of the pyridyl ring. The only out of plane mode which gives rise to any appreciable absorbance is the out of plane δ_{C-H} band at 800 cm^{-1}.

The relative intensities of the observed bands can be used to provide insights into the orientation of the pyridyl ring at the interface. The preferential appearance of several strong bands which correspond to the in-plane modes of the pyridyl ring suggest that the ring stands fairly upright on the electrode surface. The presence of an observable out of plane mode indicates some cant of the ring with respect to the surface normal [22]. Previous SERS studies of thiophenol adsorbed at gold indicate an orientation of the ring which is primarily in the plane of the electrode, lying nearly flat at the electrode surface [23, 24].

Prolonged immersion in the assembly solution also results in a gradual evolution of the infrared spectra. An illustration of this evolution is provided in Figure 5.6, which presents the infrared spectra for monolayers formed by increased immersion time in PySH solution. With increasing immersion time, spectral quality in general begins to decay. Within 5 hours the in-plane peaks at 1600, 1470, 1210 cm^{-1} have diminished considerably in intensity with the out of plane mode increasing slightly. The change in intensities could be ascribed to the following effects.

First, a gradual decrease in the amount of adsorbed PyS at constant orientation would result in an overall decrease in intensity for all modes. Second, a change in orientation by which the in-plane modes become oriented more parallel to the surface, would result in an overall decrease in intensity for the in-plane modes with an accompanying increase in the intensity for the out of plane modes. This orientation change may be due to increased cant of intact pyridinethiolates or physisorbed pyridine moieties which remain at the electrode

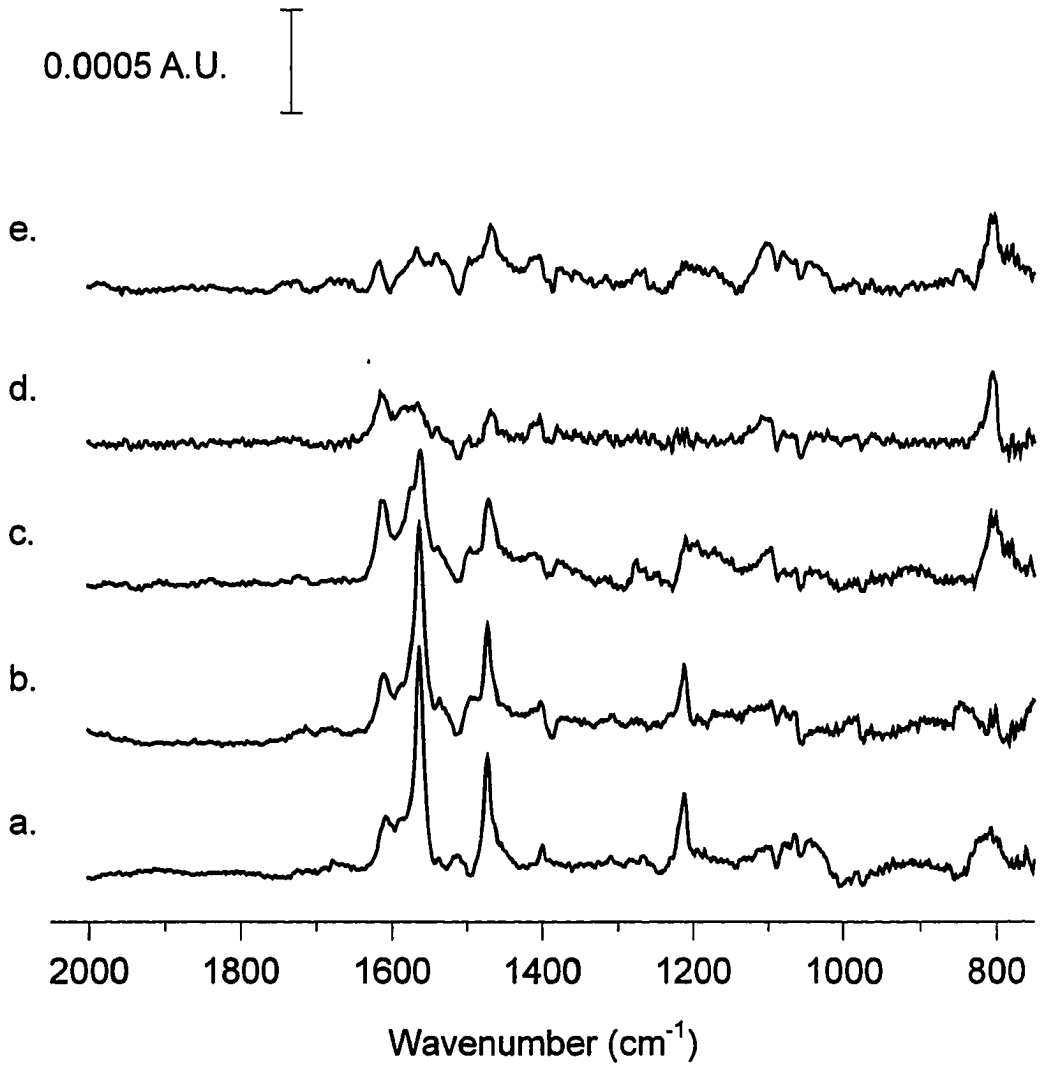

Figure 5.6. Dependence of immersion time in PySH precursor solution of IRRAS spectra. Immersion time a. 1 min, b. 15 min, c. 1 hr, d. 5 hr, e. 24 hr.

surface after cleavage of the C-S bond The small increase in $\delta(C\text{-}H)_{op}$ relative to the large decrease in the in-plane modes suggests that both may be operational.

X-Ray Photoelectron Spectroscopy. Monolayer samples were also studied using X-Ray photoelectron spectroscopy (XPS), to provide a measure of the oxidation state of the adsorbed sulfur. Figure 5.7 provides a comparison of the sulfur 2p and nitrogen 1s region of the XPS spectrum for short and long immersion time PyS monolayers. For the short immersion time sample (Figure 5.7a) the nitrogen 1s spectrum indicates a single peak at 399.0 eV which is consistent with nitrogen in a pyridine ring [25]. The spectrum in the sulfur 2p region is representative of sulfur as an adsorbed thiolate with the $2p_{1/2}$ and $2p_{3/2}$ bands at 161.2 eV and 162.4 eV, respectively. Previous studies of alkanethiolate monolayers have shown XPS spectra with the $2p_{1/2}$ and $2p_{3/2}$ binding energies at ~161.1 eV and ~162.3 eV respectively [10, 26-29]. A comparison of the calculated atomic coverage of sulfur versus nitrogen indicates a sulfur to nitrogen ratio of 1:1 for samples at short immersion time, consistent with the expected relation.

Long immersion time samples (Figure 5.7b) give rise to a different XPS signature, dominated by a broadening of the both the nitrogen and sulfur peaks. The broadening of the sulfur band to higher binding energy is very reproducible and results in a loss of definition of the $2p_{1/2}$ and $2p_{3/2}$ bands. The integrated intensity of the sulfur peak also increases by a factor of about two. This broadening to higher binding energy is indicative of an increase in the oxidation state, or partial charge on the sulfur species. The nitrogen spectrum also shows a broadening of the 1s band as well as a noticeable loss in intensity. The broadening in the

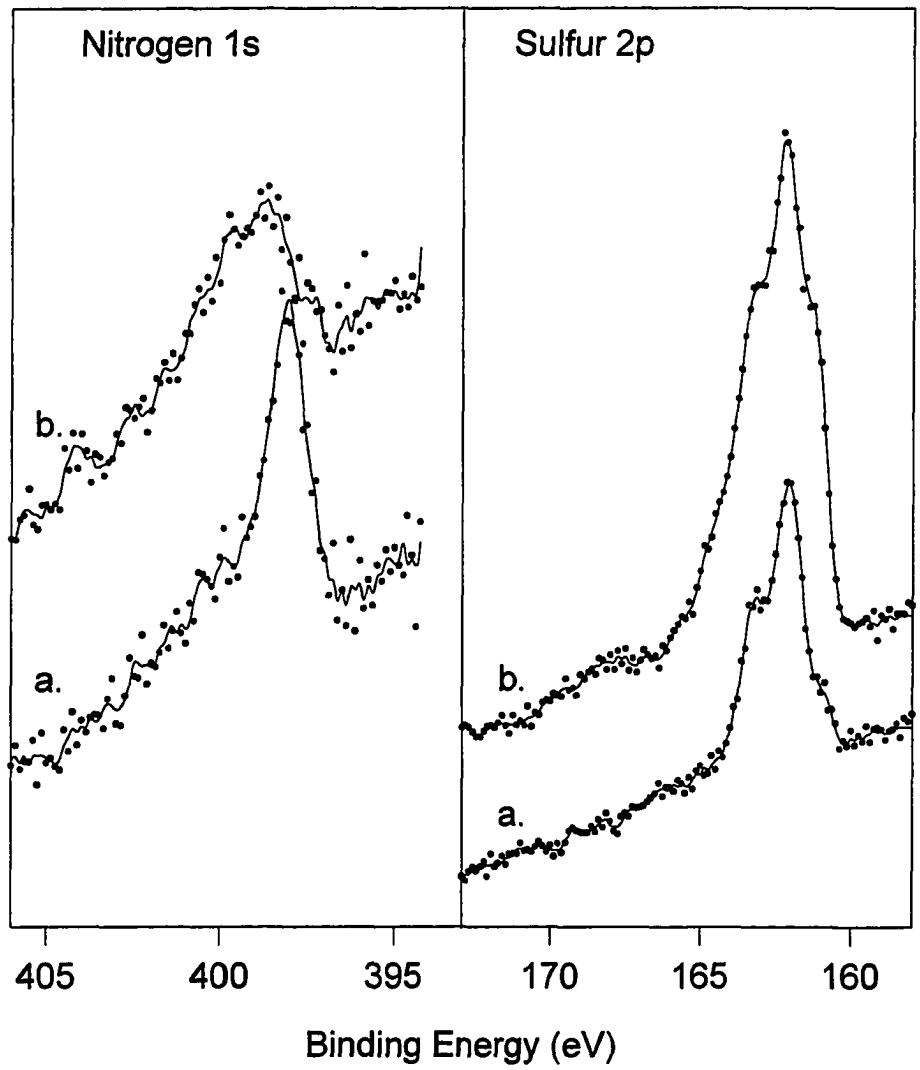

Figure 5.7. Dependence of immersion time in precursor solution on XPS spectra in the Nitrogen 1s and Sulfur 2p regions. Immersion time in 1 mM PySH solution: a. 1 min, b. 24 hr.

nitrogen case is much less reproducible in terms of peak shape and integrated area. There is typically a detectable nitrogen signal, but the sulfur to nitrogen ratio increases from 1:1 to at least 2.5 or 3:1.

The general broadening and decrease of the nitrogen signal indicates a loss and/or conversion of the nitrogen in the pyridyl ring which leads to a change in charge on the nitrogen in at least some of the adsorbates. The decrease in intensity is also consistent with the overall decrease in IR intensity for the long immersion time samples.

Scanning tunneling microscopy. The immersion time dependence on the microstructure of the PyS/Au electrodes was examined using scanning tunneling microscopy (STM). The evolution of the STM images as a function of immersion time in PyS solution is presented in Figure 5.8. The 100 nm x 100 nm image of a bare Au/mica electrode (Figure 5.8a) shows the typical flat terraces observed for these samples. Of particular note is the lack of noticeable structure in the interior of the flat terraces. An image of a sample immersed for 1 min in PySH solution is presented on the same lateral scale in Figure 5.8b. Present in this image are a number of depressions which have been previously observed for alkanethiolate monolayers at gold electrodes [30]. These depressions correspond to single gold atom deep pits in the electrode surface. For the 1 min immersion sample, the size and distribution of the depressions are consistent with that seen for alkanethiolate films.

For long immersion samples, as in Figure 5.8c, images reveal a large degree of structural change at the electrode surface. In general, the size and density of the depressions increases dramatically, resulting in a severely corroded surface.

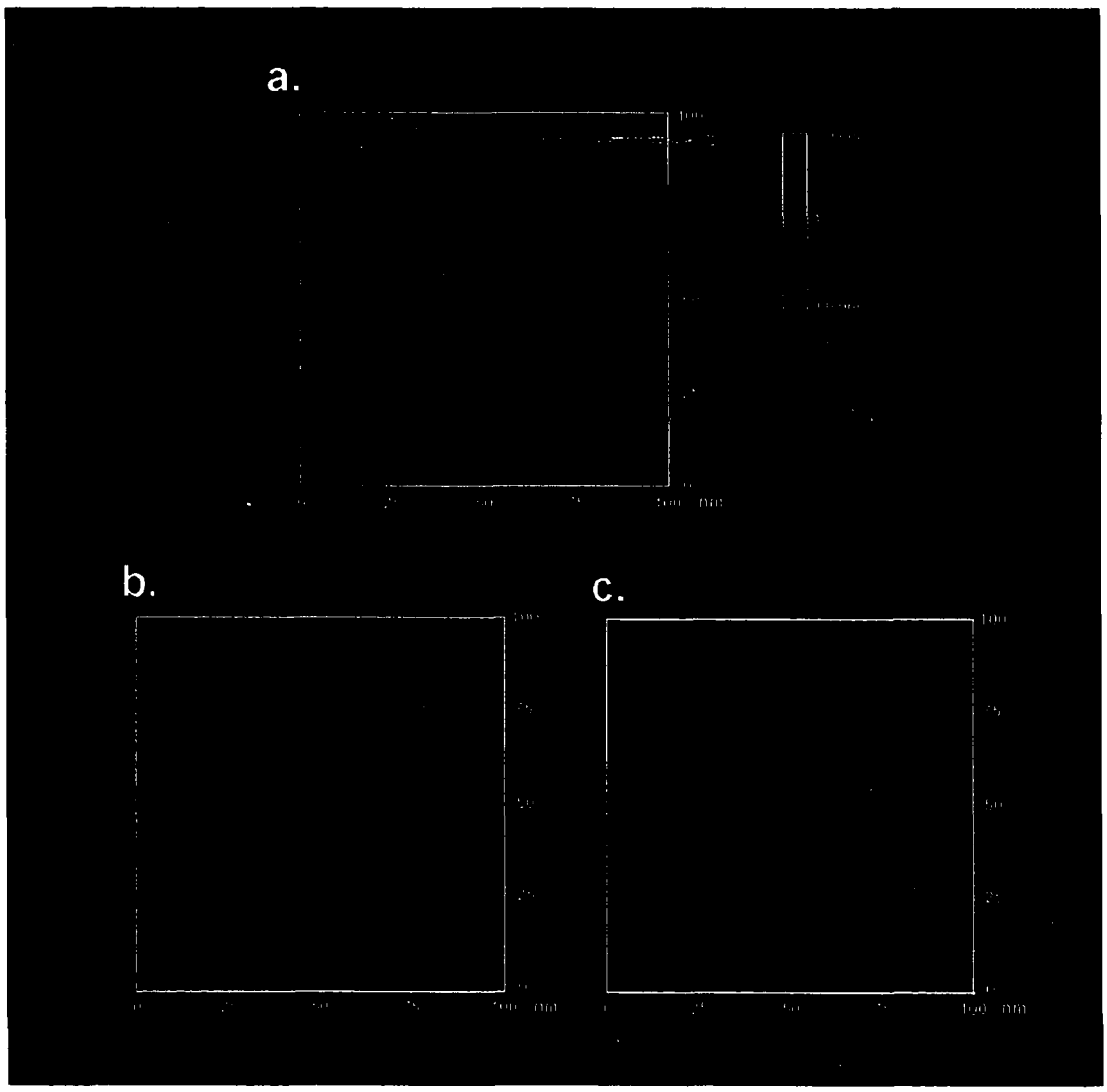

Figure 5.8. STM images. a. bare Au. b. 1 min immersion in PySH solution. c. 24 hr immersion in PySH solution. Vertical scale is identical for all images.

Comparison with monolayers assembled from sulfide. As previously stated, earlier experiments in our group with short chain hydroxy- and acid- terminated thiols revealed a similar trend in the desorption data which corresponds to the oxidative cleavage of the C-S bond, resulting in the formation of a sulfur-like adlayer [17]. To determine if a similar process is occurring with the PyS monolayers, comparisons with electrodes immersed in sulfide solutions were made.

The results of an electrochemical desorption experiment at an electrode which had been immersed in sodium sulfide solution for 30 min are presented in Figure 5.9a. Longer immersion times do not effect the voltammetric response, and generally result in delamination of the gold from the mica support. Evident in this voltammogram is a single cathodic wave at -0.90 V, having a charge density of 150 $\mu C/cm^2$, consistent with the voltammetry for long immersion PyS, and previous experiments with Na_2S at gold [31].

X-Ray photoelectron spectra of S/Au samples also correlate well with those for long immersion PyS samples, as shown in Figure 5.9b. Characteristic of these spectra are large, relatively broad features centered at ~162 eV. The broad nature of the wave is most likely due to a combination of a relatively broad range of oxidation states of the sulfur and an increased heterogeneity in the character of sulfur binding sites [6].

Conversion of the films to a more sulfur-like species is also consistent with the trends in the cytochrome c facilitation data. Gold electrodes treated with sulfide have been shown to be far less effective as facilitators for the electrode reaction of cytochrome c than pyridinethiolate modified electrodes [5b]. The gradual decrease in the ability of the

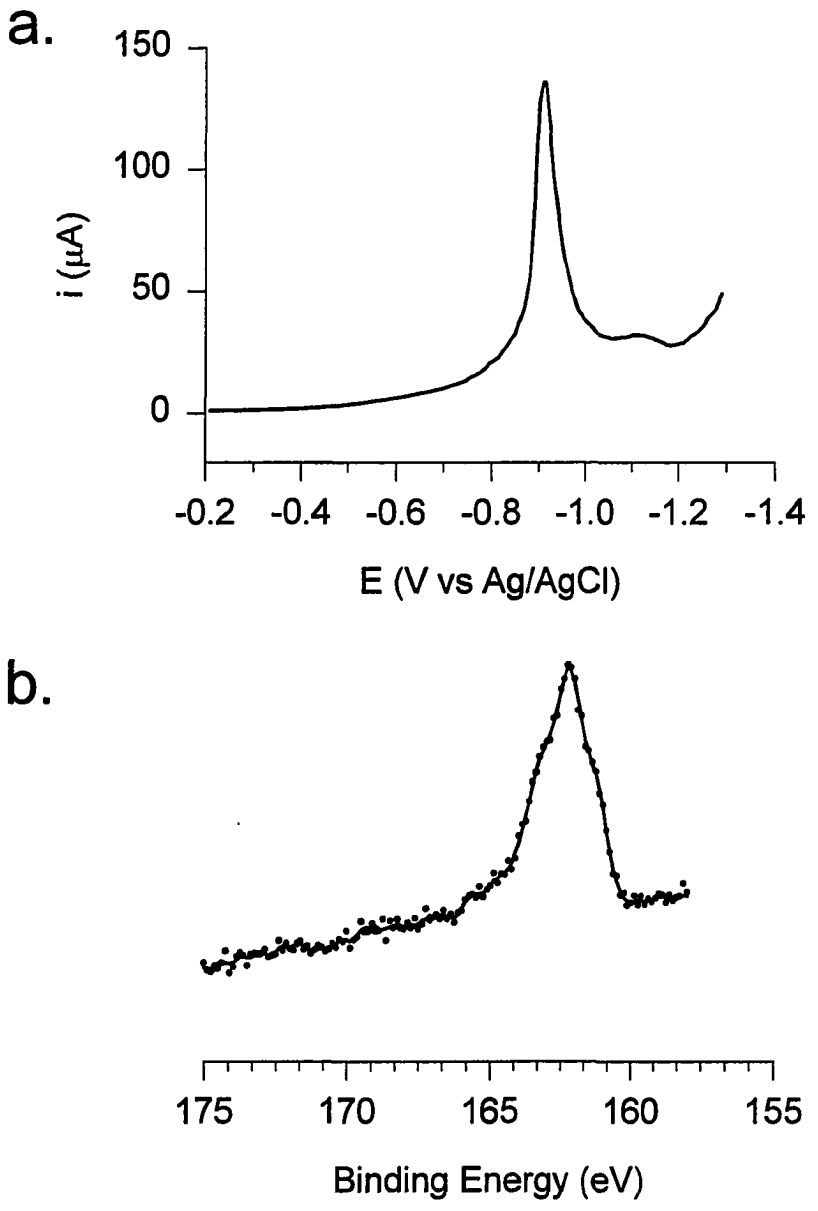

Figure 5.9. Characterization of electrodes immersed for 30 min in 1 mM Na_2S (aq). a. Electrochemical desorption, conditions are as in Figure 5.2. b. XPS spectrum in the sulfur 2p region.

electrodes to facilitate the electrode process can then be ascribed to the increased sulfur character at the pyridinethiolate modified electrode which accompanies increased immersion time in the precursor solution.

Sample and solution treatments. The effect of the presence of oxygen in the precursor solution was investigated by comparing samples immersed in argon purged solutions with those assembled from air saturated counterparts. As shown in Figure 5.10, the presence (or absence) of oxygen appears to have little effect on the stability of the pyridinethiolate monolayer films at gold. Also, the presence of the pyridyl precursorappears critical for the conversion process to occur. Samples immersed for 1 min in the precursor solution and emmersed, rinsed, and immersed in neat, air saturated water do not undergo the same conversion as the samples maintained in the pyridyl precursor. The same is true for samples subsequently immersed for 24 hr in 1 mM aqueous pyridine solution.

Prolonged exposure to the laboratory ambient has a similar effect on the stability of short immersion time samples, as evidenced by Figure 5.11. However, even after over 20 days in the laboratory ambient, an obvious wave at -0.55 V is present, indicating incomplete conversion of the PyS/Au to the sulfur-like product. Also, the charge density for the wave at -0.90 V is much less than that observed for the 24 hr immersion time samples shown in Figure 5.3.

Comparisons to other heteroaromatic monolayers. To examine the breadth of this instability in pyridyl-functionalized thiolates, monolayers of related pyridyl-functionalized compounds were also investigated. The results of desorption voltammetry for short and long

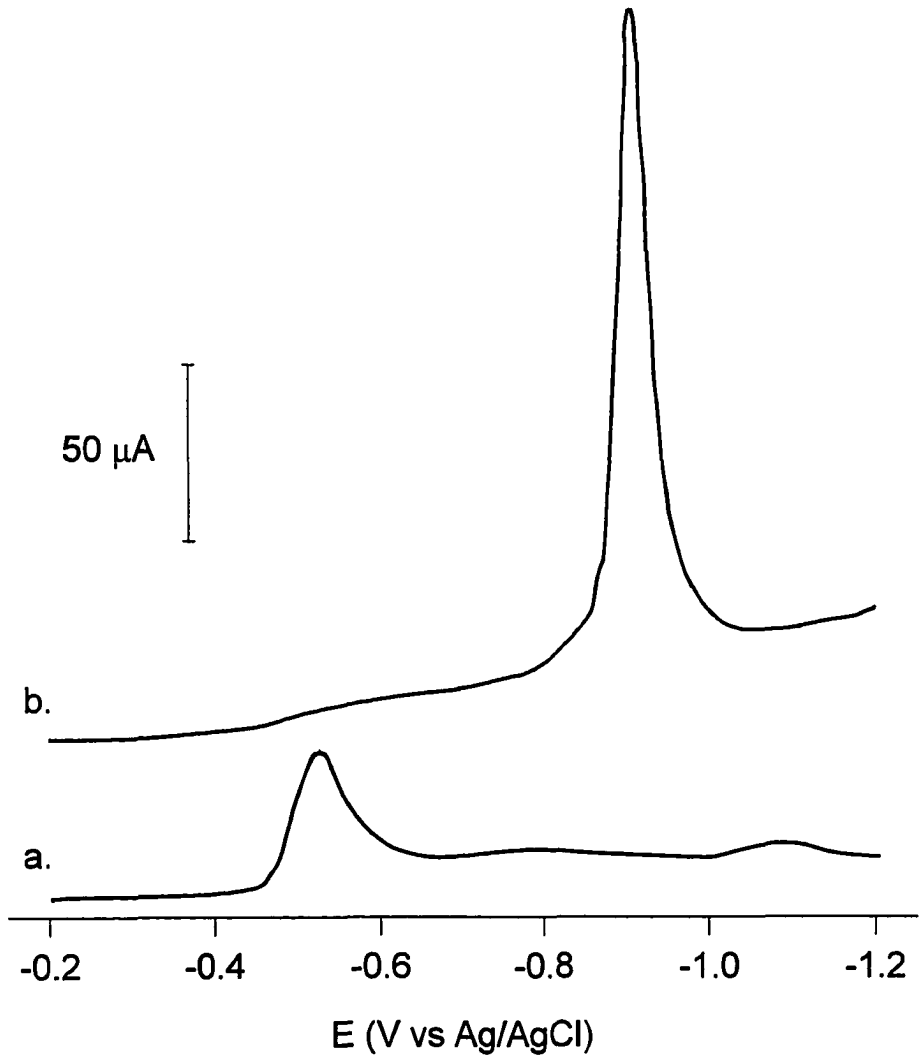

Figure 5.10. Effect of oxygen in precursor solution. a. 1 minute immersion in argon purged solution, b. 24 hr immersion in argon purged solution

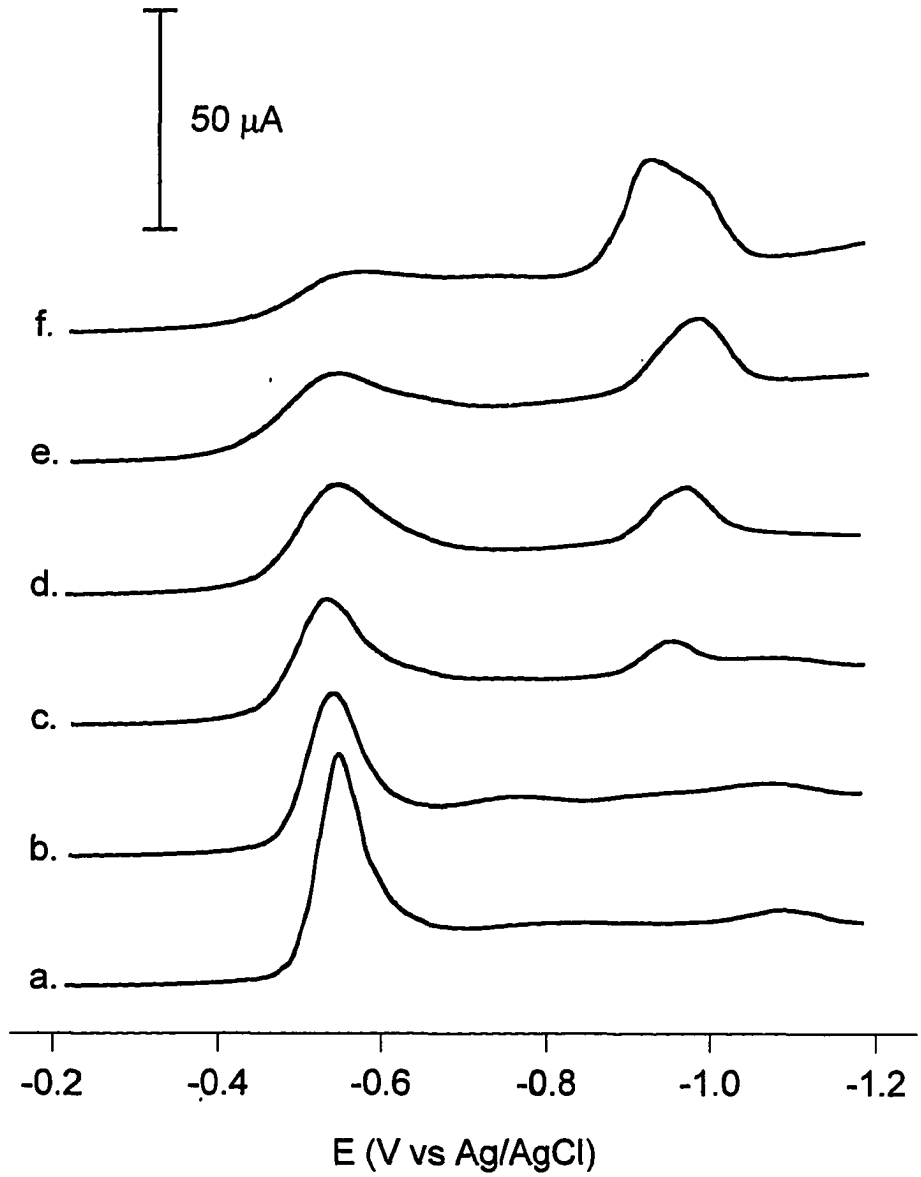

Figure 5.11. Effect of exposure to the laboratory ambient on the electrochemical desorption of PyS/Au modified electrodes. Exposure time: a. 0 min, b. 1 hr, c. 12 hr, d. 3 days, e. 8 days, f. 22 days.

immersion time samples in 1 mM solutions of 2-mercaptopyridine (2-PySH), and 2,2'-mercaptopyrimidine (2-PyR) are presented in Figure 5.12. In the 2-PySH case, prolonged immersion in the precursor solution results in a similar conversion seen for the 4-substituted compounds. Samples immersed in 2-PyR, however, do not appear to be susceptible to the same conversion as in the pyridine derivatized films, even after four days immersion in the precursor solution.

Conclusions

Pyridinethiolate monolayers adsorbed at gold undergo a structural conversion from a film consisting of intact pyridinethiolate to a film which is characteristic of adsorbed sulfur. This conversion occurs both in ambient and in solutions containing the pyridyl precursor. The result of this conversion is decreased ability of the electrode to facilitate the electrode reaction cytochrome c in solution.

At present, the reaction products of this conversion of the pyridinethiolate monolayers at gold electrodes have not been defined, although their elucidation would provide interesting information into the factors which influence instability in these monolayer systems.

Acknowledgments

The expert assistance of Jim Anderegg in the collection and analysis of the XPS data is gratefully acknowledged. KN and DH acknowledge the Japan Society for Promotion of Science (US-Japan Cooperative Science Program).

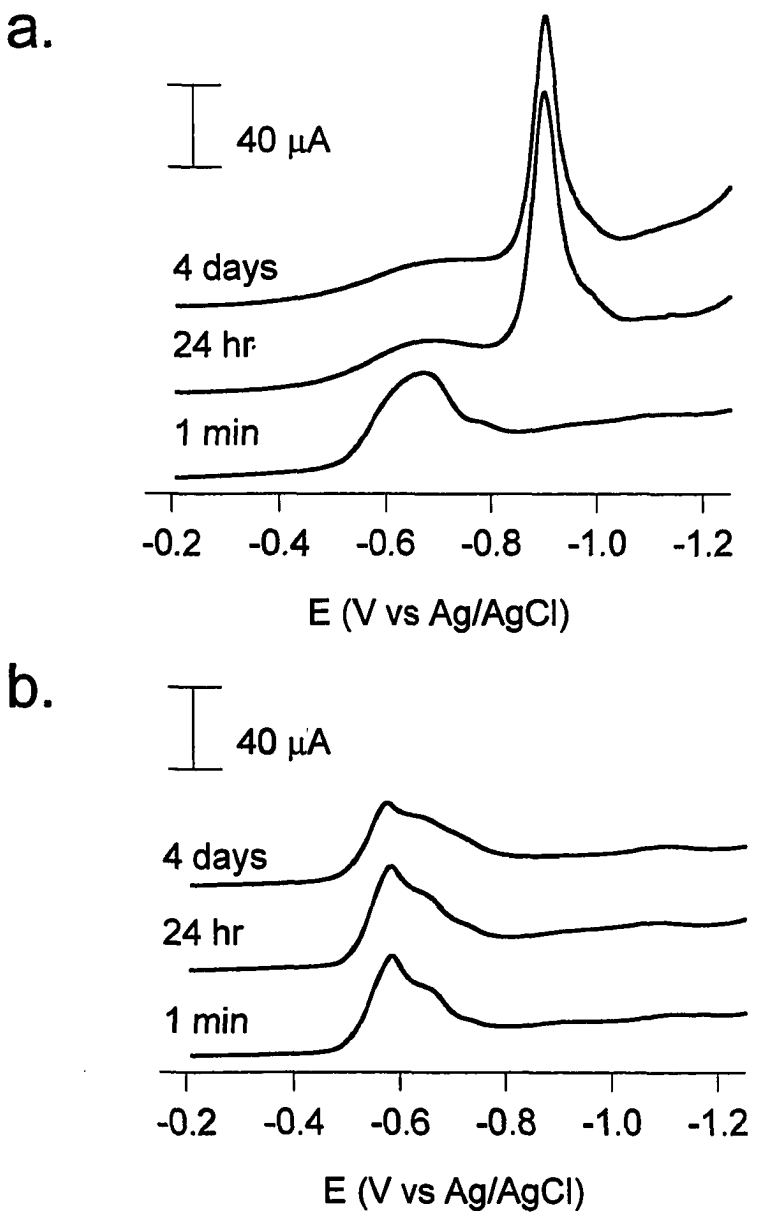

Figure 5.12. Electrochemical desorption for samples immersed for 1 min, 24 hr, and 4 days in 1 mM 2-PySH or 2-PyR solutions. a. 2-PySH, b. 2-PyR. All conditions as in Figure 5.2.

References

1 . Ames Lab-USDOE and Department of Chemistry, Iowa State University, Ames, IA, 50011

2 . Department of Physical Chemistry, Yokohama National University, Yokohama, Japan.

3 . (a) Taniguchi, I.; Toyosawa, K.; Yamaguchi, H.; Yasukouchi, K. *J. Electroanal. Chem.* **1982**, *140*, 187-193. (b) Armstrong, F.A. *Struct. Bonding (Berlin)* **1990**, *72*, 137-221. (c) Zhang, D.; Wilson, G. S.; Niki, K. *Anal. Chem.* **1994**, *66*, 3873-3881. (d)Tarlov, M. J.; Bowden, E. F. *J. Am. Chem. Soc.* **1991**, *113*, 1847-1849. (e)Song, S.; Clark, R. A.; Bowden, E. F.; Tarlov, M. *J. Phys. Chem.* **1993**, *97*, 6564-6572. (f)Cullison, J. K.; Hawkridge, F. M.; Nakashima, N.; Yoshikawa, S. *Langmuir* **1994**, *10*, 877-882.

4 . (a) Hobara, D.; Niki, K.; Chumanov, G.; Cotton, T. M. *Colloids and Surfaces* **1994**, *93*, 241-250. (b) Kuznetsov, B. A.; Mestechkina, N. M.; Shumakovich, G. P. *Bioelectrochem. and Bioenerg.* **1977**, *4*, 1-17. (c) Kuznetsov, B. A.; Shumakovich, G. P.; Mestechkina, N. M. *Bioelectrochem. and Bioenerg.* **1977**, *4*, 512-521.

5 . (a) Allen, P. M.; Hill, A. O.; Walton, N. J. *J. Electroanal. Chem.* **1984**, *178*, 69-86. (b) Niwa, K.; Furuwakawa, M.; Niki, K. *J. Electroanal. Chem.* **1988**, *245*, 275-285. (c) Hinnen, C.; Niki, K. *J. Electroanal. Chem.* **1989**, *264*, 157-165. (d) Sagara, T.; Niwa, K.; Sone, A.; Hinnen, C.; Niki, K. *Langmuir* **1990**, *6*, 254-262. (e) Bond, A. M.; Hill, H. A. O.; Komorsky-Lovric, S.; Lovric, M.; McCarthy, M. E.; Psalti, I. S. M.; Walton, N. J. *J. Phys. Chem.* **1992**, *96*, 8100-8105.

6 . Walczak, M. M.; Alves, C. A.; Lamp, B. D.; Porter, M. D. *J. Electroanal. Chem.* **1995**, *396*, 103-114.

7 . Widrig, C. A.; Chung, C.; Porter, M. D. *J. Electroanal. Chem.* **1991**, *310*, 335-359.

8 . Walczak, M.M.; Popenoe, D.D.; Deinhammer, R.S.; Lamp, B.D.; Chung, C.; Porter, M.D. *Langmuir*, **1991**, *7*, 2687-2693.

9 . Weisshaar, D. E.; Lamp, B. D.; Porter, M. D. *J. Am. Chem. Soc.*, **1992**, *114*, 5860-5862.

10 . Zhong, C. J.; Porter, M. D. *J. Am. Chem. Soc.*, **1994**, *116*, 11616-11617.

11 . After correction for surface roughness factor of 1.1.

12 . Gui, J. Y.; Stern, D. A.; Frank, D. G.; Lu, F.; Zapien, D. C.; Hubbard, A. T. *Langmuir* **1991**, *7*, 955-963.

13 . Gui, J. Y.; Stern, D. A.; Lin, C.-H.; Gao, P.; Hubbard, A. T. *Langmuir* **1991**, *7*, 3183-3189.

14 . Sabatini, E.; Cohen-Boulakia, J.; Bruening, M.; Rubinstein, I. *Langmuir* **1993**, *9*, 2974-2981.

15 . Voltammograms at intermediate times are less reproducible than those at each time extreme, most likely a result of variable solution concentration and electrode activity.

16 . To confirm the desorption potential, experiments were condicted using 1 mM PySH in the electrolyte solution. Primarily a single redox couple is evident in these voltammograms. These waves are characteristic of the reversible adsorption/desorption of thiolate from the electrode surface [9]. The couple present in these data is centered at -0.53 V and has a charge for both the anodic adsorption and cathofdic desorption of 50 $\mu C/cm^2$

17 . Weisshaar, D. E.; Walczak, M. M., Porter, M. D. *Langmuir* **1993**, *9*, 323-329.

18 . Katritzky, A. R.; Gardner, J. N. *J. Chem. Soc.* **1958**, 2198-2204.

19 . Katritzky, A. R. *Quarterly Reviews* **1959**, *13*, 353-373.

20 . Kline, C. H., Jr.; Turkevich, J. *J. Chem. Phys.* **1944**, *12*, 300-309.

21 . Christensen, P. A.; Hamnett, A.; Blackham, I. *J. Electroanal. Chem.* **1991**, *318*, 407-410.

22 . Precise orientational determination was precluded by unreliable thickness measurements from optical ellipsometry.

23 . Carron, K. T.; Hurley, L. G. *J. Phys. Chem.* **1991**, *95*, 9979-9984.

24 . Joo, T. H.; Kim, M. S.; Kim, K. *Journal of Raman Spectroscopy* **1987**, *18*, 57-60.

25 . Nordberg, R.; Albridge, R.G.; Bergmark, T.; Ericson, U.; Hedman, J.; Nordling, C.; Siegbahn, K.; Lindberg, B.J. *Arkiv för Kemi* **1967**, *28*, 257-278.

26 . Lamp, B. D.; Alves, C. A.; Franek, J. E.; Porter, M. D. Manuscript in preparation.

27 . Bain, C. D.; Biebuyck, H. A.; Whitesides, G. M. *Langmuir* **1989**, *5*, 723-727.

28 . Nuzzo, R. G.; Zegarski, B. R.; Dubois, L. H. *J. Am. Chem. Soc.* **1987**, *109*, 733-740.

29 . Nuzzo, R. G.; Fusco, F. A.; Allara, D. L. *J. Am. Chem. Soc.* **1987**, *109*, 2358-2368.

30 . (a) Edinger, K.; Golzhauser, A.; Demota, K.; Woll, C.; Grunze, M. *Langmuir* **1993**, *9*, 4-8. (b) Dürig, U.; Züger, O.; Michel, B.; Häussling, L.; Ringsdorf, H. *Phys. Rev. B* **1993**, *48*, 1711-1717. (c) Chailapakul, O.; Sun, L.; Xu, C.; Crooks, R. M. *J. Am. Chem. Soc.* **1993**, *115*, 12459-12467.(d) Schonenberger, C.; Sondag-Huethorst, J. A. M.; Jorritsma, J.; Fokkink, L. G. J. *Langmuir* **1994**, *10*, 611-614. (e) Schonenberger, C.; Sondag-Huethorst, J. A. M.; Jorritsma, J.; Fokkink, L. G. J. *Langmuir* **1994**, *10*, 611-614. (f) Schonenberger, C.; Jorritsma, J.; Sondag-Huethorst, J. A. M.; Fokkink, L. G. J. *J. Phys. Chem.* **1995**, *99*, 3259.

31 . (a) Wierse, D. G.; Lohrengel, M. M.; Schultze, J. W. *J. Electroanal. Chem.* **1978**, *92*, 121-131. (b) Baltruschat, H.; Staud, N.; Heitbaum, J. *J. Electroanal. Chem.* **1988**, *239*, 361-374. (c) Buckley, A. N.; Hamilton, I. C.; Woods, R. *J. Electroanal. Chem.* **1987**, *216*, 213-227. (d) Lezna, R. O.; de Tacconi, N. R.; Arvia, A. J. *J. Electroanal. Chem.* **1990**, *283*, 319-336.

6. GENERAL CONCLUSIONS

This dissertation has presented several results which add to the base of knowledge which relates to organosulfur monolayers adsorbed at gold electrodes. Common to several of the conclusions is the interplay between intermolecular interactions within the monolayer film and the nature of sulfur-gold bonding.

In situations where the interactions between neighboring adsorbates can be minimized, such as in monolayers assembled from short-chain alkanethiols and disulfides, or in the case of pyridinethiolate films, head group chemistry plays the major role in monolayer formation. However, as chain length increases, the cohesive interactions in the film reinforce the stability of the assembly, as shown by the structural integrity of the film in the in situ infrared experiments.

Aside from these more general conclusions, this dissertation has also provided information relating to the more intricate aspects of the organosulfur monolayer system. For instance, while organosulfur monolayers are generally considered to be quite stable in a wide variety of situations, care must be taken to examine the limits of this assumption when utilizing films which have not been extensively characterized.

Also, considerations of substrate morphology must be sufficiently weighed in all studies regarding these types of materials. Given the infancy of studies which relate microscopic morphology to more macroscopic characteristics of these films, care must be

taken not to exclude these considerations from discussions of film properties and characteristics.

As discussed in the general introduction, there remains a large amount of information to unravel regarding the characterization and applications of organosulfur monolayers. Fundamental studies regarding the nature of sulfur binding at metal surfaces will continue to be an important issue, with particular emphasis placed on unraveling the identity of the byproducts of the spontaneous adsorption reaction.

Also of continuing interest will be the delineation of defect structures in the film and their effects on film properties. Film defects are the defining factor in many of the properties of the monolayer film. Methods which characterize, and perhaps manipulate the type and density of defects will afford a higher degree of control of overall monolayer properties and may aid in the analytical applications of these materials.

Along the lines of applications, continued efforts will be aimed at preparing and characterizing more complicated film structures which may eventually lead to chemical sensors or molecular recognition devices. Special emphasis will be on films which furnish the selectivity and specificity for various electrochemical or optical transduction mechanisms. These studies, combined with ongoing efforts to create microscopically small structures through lithographic techniques provide a host of interesting possibilities for miniaturized analytical instrumentation in the near future.

Common to all studies involving organosulfur monolayers will be the improvement of existing techniques as well as the development of new methods which will provide the

requisite sensitivity to answer the number of questions still remaining regarding these films. The continued development of techniques which provide macroscopic and microscopic information about these systems, both ex situ and in situ, is critical for the further understanding of these materials.

Organosulfur monolayer films promise to continue to be useful materials in the study of interfacial processes for some time. With increased study and the investigation of several key issues, their utility will only grow. The tremendous expansion of interest in the field will serve as an important catalyst in this growth.